NASA-CR-192632

Georgia Institute of Technology
Atlanta, Georgia 30332-0420

FINAL REPORT

ANALYSIS OF DELAMINATION RELATED FRACTURE PROCESSES IN COMPOSITES

NASA GRANT NAG-1-637
GEORGIA TECH PROJECT E16-654

PRINCIPAL INVESTIGATOR
Erian A. Armanios

FINAL REPORT

ANALYSIS OF DELAMINATION RELATED FRACTURE PROCESSES IN COMPOSITES

NASA GRANT NAG-1-637
GEORGIA TECH PROJECT E16-654

PRINCIPAL INVESTIGATOR
Erian A. Armanios

This is a final report that summarizes the results achieved under this grant. The first major accomplishment is the development of the sublaminate modeling approach and shear deformation theory. The sublaminate approach allows the flexibility of considering one ply or groups of plies as a single laminated unit with effective properties. This approach is valid when the characteristic length of the response is small compared to the sublaminate thickness. The sublaminate approach was validated comparing its predictions with a finite element solution [*1*]. A shear deformation theory represents an optimum compromise between accuracy and computational effort in delamination analysis of laminated composites [*2*]. This conclusion was reached by applying several theories with increasing level of complexity to the prediction of interlaminar stresses and strain energy release rate in a double cracked-lap-shear configuration.

The shear deformation theory and sublaminate approach was applied to the free-edge delamination[*1,3*] and internal delamination analysis [*4*] of laminated plates including the influence of hygrothermal stresses [*5,6*] and combined loading [*7*]. the analysis was also applied to tapered laminates subjected to tensile loading [*8,9*].

The second accomplishment is the development of the variationally asymptotical analysis for thin-walled anisotropic beams with closed cross sections [*10-12*]. The theory is a prerequisite for isolating the influence of damage by comparing predictions with an reference undamaged configuration. Existing composite beam theories have significant differences in the derived expressions for the stiffness coefficients. The variationally asymptotical analysis was developed in order to isolate the effects contributing to these differences. The major advantage of this approach lies in the fact that the displacement field is not assumed *a priori* as is the case for the existing theories and emerges as a result of the analysis. Moreover, the assumed displacement fields in the existing theories follow the classical isotropic formulation. However, no proof is provided with regard to the validity of such a displacement field for anisotropic materials.

The displacement field which resulted from the theory showed two new contributions which were identified as out-of-plane warping due to axial strain and bending. These contributions emerge in addition to the classical out-of-plane torsional warping and are significantly influenced by the material's anisotropy. However, they vanish for materials that are orthotropic or whose properties are antisymmetric relative to the beam middle surface. These configurations coincide with the cases where the predictions of the existing theories are in agreement with test results and numerical simulations. For generally anisotropic materials the error associated with the existing theory predictions correspond to the neglect axial strain and bending related out-of-plane warping.

In addition to providing a definitive answer to the reasons for the disparity in existing theories predictions, the variationally aymptotical theory provides a consistent approach to deriving the displacement field in anisotropic structures. A number of investigators have now adopted this approach for the modeling of initially curved and twisted composite beams and laminated composite plates[13, 14]. Moreover, the closed

form expressions indicate that the new contributions are proportional to the extensional strain and bending curvature. This provides a proof for the work of Kosmatka [15] where an improvement to the displacement field was proposed by adding two terms which are proportional to the extensional strain and bending curvatures. However, their contributions were determined using a finite element simulation.

The details of the sublaminate and Variationally asymptotical analyses are provided by the work of Ref. 12 which is provided in Appendix A for convenience. A list of the publications and presentations related to the Grant is provided in Appendix B.

REFERENCES

[*1*]. Armanios, E. A. Rehfield, L. W., Raju, I. S., and O'Brien, T. K. "Sublaminate Analysis of Interlaminar Fracture in Composites: Part II--Applications," *Journal of Composites Technology & Research*, Vol. 11, No. 4, Winter 1989, pp. 147-153.

[2]. Rehfield, L. W., Armanios, E. A. and Weinstein, F., "Analytical Modeling of Interlaminar Fracture in Laminated Composites," Composites '86: Recent Advances in Japan and the United States, Proceedings of the Third Japan-U.S. Conference on Composite Materials, K. Kawata, S. Umekawa, and A. Kobayashi, Eds., pp. 331-340, 1986.

[*3*]. Armanios, E. A. and Rehfield, L. W., "Sublaminate Analysis of Interlaminar Fracture in Composites: Part I - Analytical Model," *Journal of Composites Technology & Research*, Vol. 11, No. 4, Winter 1989, pp. 135-146.

[*4*]. Armanios, E. A., Sriram, P., and Badir, A.M., "Fracture Analysis of Transverse Crack-Tip and Free Edge Delamination in Laminated Composites," *Composite Materials: Fatigue and Fracture (Third Volume), ASTM STP 1110*, T. K. O'Brien, Ed., American Society for Testing and Materials, Philadelphia, 1991, pp. 269-286.

[*5*]. Armanios, E.A. and Mahler, M.A., "Residual Thermal and Moisture Influences on the Free-Edge Delamination of Laminated Composites," *Proceedings of the AIAA/ASME/ASCE/AHS 19th Structures, Structural Dynamics and Materials (SDM) Conference*, Part 1, pp. 371-381, 1988.

[*6*]. Armanios, E.A. and Badir, A.M., "Hygrothermal Influence on Mode I Edge Delamination in Composites," *Journal of Composite Structures*, Vol. 15, No. 4, 1990, pp. 323-342.

[*7*]. Armanios, E.A. and Rehfield, L.W., "Interlaminar Fracture Analysis of Composite Laminates Under Bending and Combined Bending and Extension," *Composite Materials: Testing and Design (Eight Conference), ASTM STP 972*, J.D. Whitcomb, Ed., American Society for Testing and Materials, Philadelphia, 1988, pp. 81-94.

[*8*]. Armanios, E.A., and Parnas, L., "Delamination Analysis of Tapered Laminated Composites Under Tensile Loading," *Composite Materials: Fatigue and Fracture (Third Volume), ASTM STP 1110*, T. K. O'Brien, Ed., American Society for Testing and Materials, Philadelphia, 1991, pp. 340-358.

[*9*]. Parnas, L., "Failure Mechanisms and Prediction in Advanced Composite Materials," Ph.D Thesis, School of Aerospace Engineering, Georgia Institute of Technology, March 1991.

[*10*] Armanios, E.A., Badir, A. and Berdichevsky, V., "Effect of Damage on Elastically Tailored Composite Laminates," Proceedings of the AHS International Technical Specialists' Meeting on Rotorcraft Basic Research, Atlanta, Georgia, March 25-27, 1991, pp. (48-1)-(48-11).

[*11*]. Berdichevsky, V., Armanios, E. A. and Badir, A., "Theory of Anisotropic Thin-walled Closed-cross-section Beams," *Composites Engineering*, Vol. 2, Nos. 5-7, pp. 411-432, 1992.

[*12*] Badir, A. M., "Analysis of Advanced Thin-Walled Composite Structures". Ph.D. Thesis, Georgia Institute of Technology, February 1992.

[13] Hodges, D. W., Lee, B. K. and Atilgan, A. R., " Applicatiopn of the Variational-Asymptotical Method to Laminated Composite Plates," AIAA Paper 92-2357, *Proceedings of the 33rd Structures, Structural Dynamics, and Materials Conference*, Dallas, Texas, April 13-15, 1992, pp. 514 - 524.

[14] Cesnik, C. E., Hodges, D. W. and Atilgan, A. R., " Variational-Asymptotical Analysis of Initially Twisted and Curved Composite Beams," Developments in Theoretical and Applied Mechanics, vol. 16, Proceedings of the Sixteenth Southeastern Conference on Theoretical and Applied Mechanics, Nashville, Tennessee, April 12-14, 1992, pp. II.3.29-II.3.36.

[*15*] Kosmatka, J. B., "Extension-bend-Twist Coupling Behavior of Thin-walled Advanced Composite Beams with Initial Twist," *Proceedings of the 32nd AIAA/ASME/AHS/ASC Structures, Structural Dynamics and Materials Conference*, 1991, pp. 1037-1049.

APPENDIX A

ANALYSIS OF ADVANCED THIN-WALLED COMPOSITE STRUCTURES

Erian A. Armanios, Chairman

Victor L. Berdichevsky

George A. Kardomateas

Dewey H. Hodges

James T. Wang

Date Approved by Chairman 2/13/92

ANALYSIS OF ADVANCED THIN-WALLED COMPOSITE STRUCTURES

A THESIS
Presented to
The Academic Faculty

by

Ashraf M. Badir

In Partial Fulfillment
of the Requirements for the Degree
Doctor of Philosophy in Aerospace Engineering

Georgia Institute of Technology
February, 1992

ACKNOWLEDGEMENTS

I wish to express my sincere appreciation to my thesis advisor, Dr. Erian A. Armanios, for the guidance, assistance, and encouragement which he has generously provided throughout the preparation of this work and his high confidence in me.

I also wish to express my sincere gratitude to Dr. Victor L. Berdichevsky for his advise, assistance and patience throughout the last two years. I am indebted to him for many enlightening discussions.

I wish to thank Drs. G. Kardomateas, D. Hodges, and J. Wang for serving on the thesis committee and for their useful comments.

I wish to extend my special thanks to the members of the advanced structures group and my colleagues, Dr. P. Sriram, Dr. Ali Atilgan, Dr. Levend Parnas, Dr. Brian Fortson, Dr. Y. Song, Jian Li, Carlos Bezzeril, Dr. Bob Bless, Mahera Philobos, David Palmer, and Allen Siu.

My profound appreciation goes to my parents for their constant encouragement and lifelong care and devotion.

The author gratefully acknowledges the financial support provided by NASA under Grant NAG-1-637 and the U.S. Army Research Office under Grant DAAL03-88-C-0003 for performing this research.

TABLE OF CONTENTS

To my parents...

LIST OF TABLES

LIST OF ILLUSTRATIONS

CHAPTER I

INTRODUCTION

1.1 Background

The use of fiber reinforced composites is increasing in engineering applications. One of the major issues in composite structures is the understanding of the role of the material's anisotropy on the deformation modes, damage modes and failure mechanisms. This research work addresses these stiffness and strength related issues by developing analytical models for the prediction of deformation modes and their coupling effects and damage onset and growth in laminated composites. Accurate prediction of stiffness, response, damage modes and failure mechanisms is bound to lead to the design of efficient and damage tolerant composite structures.

Delamination is a predominant failure mode in continuous fiber reinforced laminated composite structures. Based on the location and direction of growth, there are two distinct types of delamination, namely, free edge delamination and local or transverse crack tip delamination. In many cases, both types occur concurrently with varying levels of interaction.

In the first part of this work shear deformation models including hygrothermal effects are developed for the analysis of mid-plane edge delamination and local delamination originating from transverse cracks in 90° plies. The results of these models are combined with a previously developed shear deformation model for mixed-mode edge delamination to yield a unified analysis of delamination and the ability to iden-

tify the critical failure modes and loads.

Elastically tailored composite design are being used to achieve favorable deformation modes under a given loading environment. Coupling between deformation modes such as extension-twist or bending-twist is created by an appropriate selection of fiber orientation, stacking sequence and materials. An example is the X-29 swept forward wing aircraft where a laminated composite skin is used to create the bending-twist coupling required to handle divergence. This design uses AS-1/3501-5A graphite/epoxy wing covers with $-45°$ outboard plies 9° forward of the wing's 40 % chord line. Elastically tailored composite rotor blades have the potential to be used in rotorcraft structures in order to control flapping and twisting motions at different rotor speeds. This concept can be utilized in tilt rotor aircraft in order to achieve a compromise between hover performance and forward flight propulsive efficiency. A change in the blade twist between flight modes can be developed through the use of extension-twist coupling as implemented in the XV-15 tilt rotor aircraft. Twist control is achieved by assuming a 15 percent change in operating rpm between hover and forward flight regimes.

The coupling of deformation modes provides a flexibility to meet design requirements on the aeroelastic behavior, dynamic response and stability of structures and results in improved fatigue life and durability.

A prerequisite for the implementation of an elastically tailored concept, is the development of an analytical model which accurately predicts the various stiffness components and isolate the material and geometrical parameters controlling the behavior.

In the second part, a variationally and asymptotically consistent theory for thin-walled beams that incorporates the anisotropy associated with laminated composites is developed. The theory is based on an asymptotical analysis of $2D$ shell energy.

The major advantage of this approach lies in the fact that the displacement function is not assumed a priori and is determined as a result of the minimization of the energy functional. As a result, two nonclassical contributions to the warping emerge. While these new contributions vanish for isotropic and orthotropic materials, they have a significant influence on the response of generally anisotropic materials. The accuracy of previously developed theories is assessed by comparing the resulting displacement fields and an assessment of the significance of shear deformation is presented. Comparison of predictions with finite element simulation and test results illustrate the consistency and accuracy of the developed theory.

The delamination analysis model is presented in the first part of this work. this is followed by the development of the thin-walled anisotropic beam theory. Each part includes a literature survey in order to place the present work in proper prospective. A comparison of prediction is presented in order to validate the developed theories and assess their accuracy.

CHAPTER II

DELAMINATION ANALYSIS

This chapter addresses damage modeling in laminated composite plates. A review of previous work is presented first, this is followed by a development of the analytical model.

2.1 Review of Previous Work

Failure in laminated composite materials often initiates in the form of matrix fractures, namely, transverse matrix cracks and delaminations. Based on the location and direction of growth, two distinct types of delamination can be discerned. These two types are called edge delamination and local or transverse crack tip delamination, as shown in Fig. 2.1. Edge delaminations initiate at the load free edges of the laminate whereas local delaminations start from a transverse matrix crack. Transverse matrix cracks refer to intralaminar failures whereas delaminations refer to interlaminar failures. Transverse cracks usually occur within laminates where the fibers run at an angle to the primary load direction and hence the name. In many cases, both types occur concurrently with varying levels of interaction.

It has been observed [1] in simple tension tests of uniform rectangular cross section specimen (Edge Delamination tests) that delaminations initiate along the load free edges and propagate normal to the load direction as shown in Fig. 2.1. Transverse matrix cracks running parallel to the fibers have also been observed in off-axis and 90° plies. Such transverse cracks extend through the thickness of similarly oriented

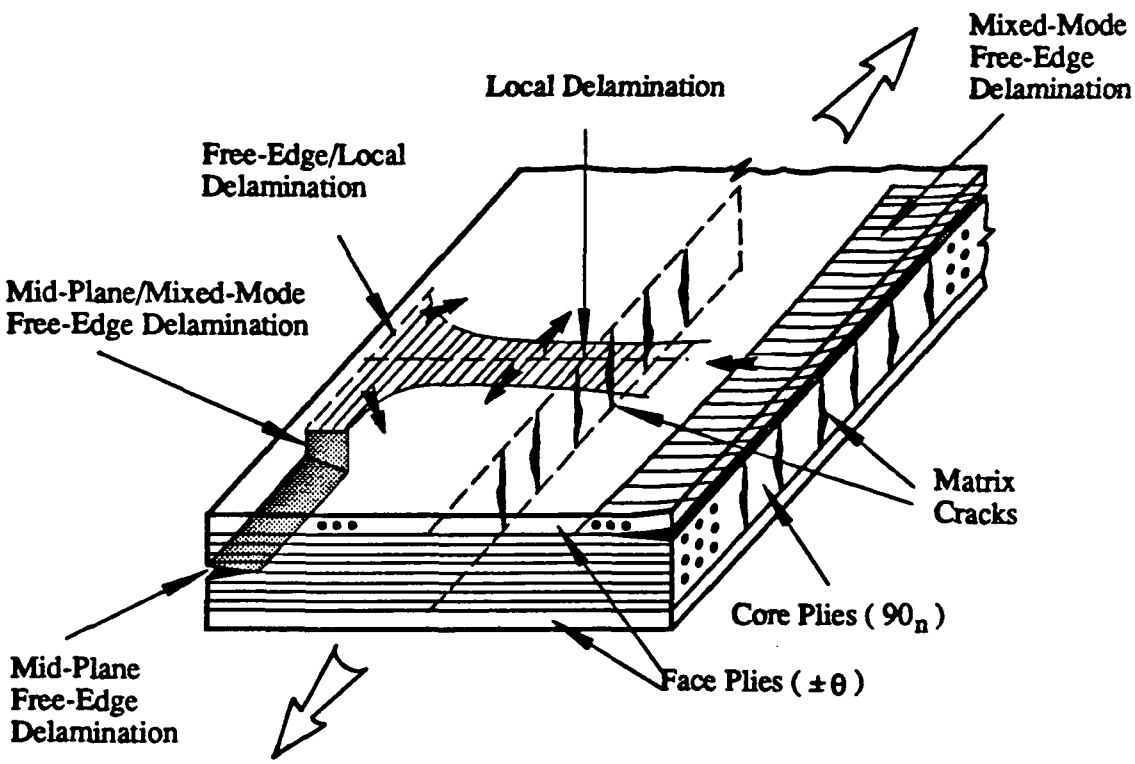

Figure 2.1: Damage Modes

plies and terminate where the ply orientation changes. Delaminations can also originate at the interfaces where transverse cracks terminate. These transverse crack tip delaminations or local delaminations, grow normal to the transverse crack from which they originate. In the case of 90° plies, the growth direction is parallel to the load.

The growth process of edge delaminations and local delaminations is often modeled using a fracture mechanics approach leading to the calculation of a strain energy release rate. This is because the strain energy release rate can correlate delamination behavior from different loading conditions and can account for geometric dependencies. The strain energy release rate associated with a particular growth configuration is a measure of the driving force behind that failure mode. In combination with appropriate failure criteria, the strain energy release rate provides a means of predicting the failure loads of the structure.

Several methods are available in the literature for analyzing edge delaminations. These include finite element modeling as in [2], [3], and [4], the complex variable stress potential approach [5], a simple technique based on classical laminate theory [1] and a higher order laminate theory including shear deformations [6]. Finite element models provide accurate solutions but involve intensive computational effort. Classical laminate theory (CLT) provides simple closed form solutions and is thus well suited for preliminary design evaluation. However, CLT provides only the total energy release rate, and thus, in a mixed mode situation, there is insufficient information to completely assess the delamination growth tendency. A higher order laminate theory including shear deformations has the ability to provide the individual contributions of the three fracture modes while retaining the simplicity of a closed form solution. A shear deformation model is available for off-mid-plane edge delamination and has been shown to agree well with finite element predictions [7].

Crossman and Wang [8] have tested T300/934 graphite/epoxy $[\pm 25/90_n]_s$ speci-

mens in simple tension and reported a range of behavior including transverse cracking, edge delamination and local delamination. O'Brien [9] has presented classical laminate theory solutions for these specimens, demonstrating reasonable agreement in the case of edge delamination but with some discrepancies in the local delamination predictions. The local delamination model overestimates the failure strains for $[\pm 25/90_n]_s$ specimens for small values of n mainly due to the implicit critical strain energy matching used.

A finite element model combining edge and local delaminations has been proposed by Law [10]. His predictions, however, do not fully explain the dependency of the critical strain on the number of 90° plies. A similar three-dimensional finite element analysis including hygrothermal effects has been performed by Wang *et al.* [11] to determine the delamination onset load for combined delamination, qualitatively demonstrating stable crack growth.

A three-dimensional finite element analysis of delamination from matrix cracks has been developed by Fish and O'Brien[12]. They conducted an experimental and analytical study on the influence of matrix cracking on delamination in $[+15/-90_n/-15]_s$ glass-epoxy laminates subjected to monotonically increasing tension loads. Experimental results showed that local delaminations form at the intersection of matrix cracks in the +15° plies and the free-edge. Comparison of a Quasi-three-dimensional (Q3D) finite element results with a three-dimensional (3D) finite element analysis showed significant differences in the relative and absolute magnitudes of the interlaminar stress components. Thus, discrepancies in failure predictions may exist between Q3D and 3D analysis. The results of this study emphasized the importance of incorporating the various damage mechanisms that influence subsequent damage development in the failure analysis.

Thermal and moisture effects on the strain energy release rates for interlaminar

fracture of unidirectional graphite/epoxy have been investigated by Russell and Street [13]. This investigation also included a study of the effects of shear loading through the use of various test configurations (Double Cantilever Beam, Cracked Lap Shear etc.). Initiation energies for delamination were found to increase as the proportion of shear loading increased and as the temperature was lowered, but no significant moisture influence was observed. The fracture resistance to crack extension was found to increase under tensile dominated loadings with both temperature and moisture content, but for high shear loading, the resistance was insensitive to the hygrothermal conditions.

O'Brien, Raju and Garber have presented a CLT based analysis of mixed mode edge delamination specimens including hygrothermal effects [14]. They have used finite element modeling to determine the strain energy release rate components. Their results indicate total strain energy release rate increases of as much as 170% due to thermal effects for some T300/5208 graphite/epoxy laminates. However, a moisture content of 0.75% has been shown to totally alleviate this increase. According to this analysis, in general, the consideration of thermal effects increases the energy release rate whereas moisture effects have the opposite influence. These results have been confirmed using shear deformation models in the case of off-mid-plane edge delaminations [15]. It was found that the interlaminar stresses follow the same trend as the energy release rate, with increase due to thermal effects and alleviation due to hygroscopic effects.

Aoki and Kondo calculated the strain energy release rate under thermal loading for mixed mode edge delamination. They used conventional finite element method [16] and a simplified method [16, 17] based on the classical lamination theory in combination with the J-integral for mechanical loading. Two types of axial constraint conditions were considered : (1) constant strain or fixed-grip and (2) constant load.

Numerical examples for cross-ply and angle-ply laminates showed that in angle-ply laminate, the energy release rate under free axial elongation increased constantly with delamination growth, while it remained constant under fixed-grip conditions. A higher order plate theory including transverse normal strain and thermal effects has been developed by Whitney [18] for the analysis of mid-plane edge delaminations. This approach provides the interlaminar stresses also, in addition to the strain energy release rate. A $[0_3/90_3]_s$ graphite/epoxy mode I specimen was analyzed and the maximum interlaminar normal stress was shown to increase by a factor of 2.7 due to thermal effects, when compared with the pure mechanical strain reference configuration.

From this summary it is found that there is a need for a unified approach that includes the analysis of free edge as well as local delamination and their interaction. In practical composite configuration free edge delamination does not occur in isolation, it is accompanied by other damage modes. Developing an analysis methodology that includes the interaction of delamination with other damage modes is essential for designing damage tolerant structures.

The study of delamination consists of two main sections. These are the analysis of mid-plane edge delamination and local delamination in laminated composite plates.

2.2 Mid-Plane Edge Delamination

A mid-plane edge delamination specimen is shown in Fig. 2.2. A uniform axial strain ϵ is applied in the x direction. From symmetry only one quarter of the specimen is considered. The sublaminate scheme and the choice of coordinate axes are illustrated in Fig. 2.3.

Sublaminates 1 and 2 in Fig. 2.3 represent the uncracked and the cracked regions,

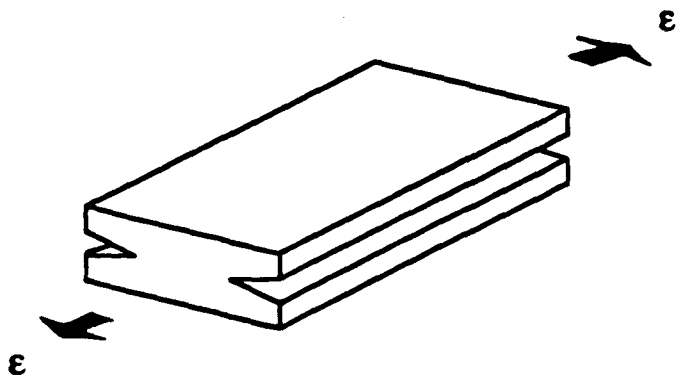

Figure 2.2: Mid-Plane Edge Delamination

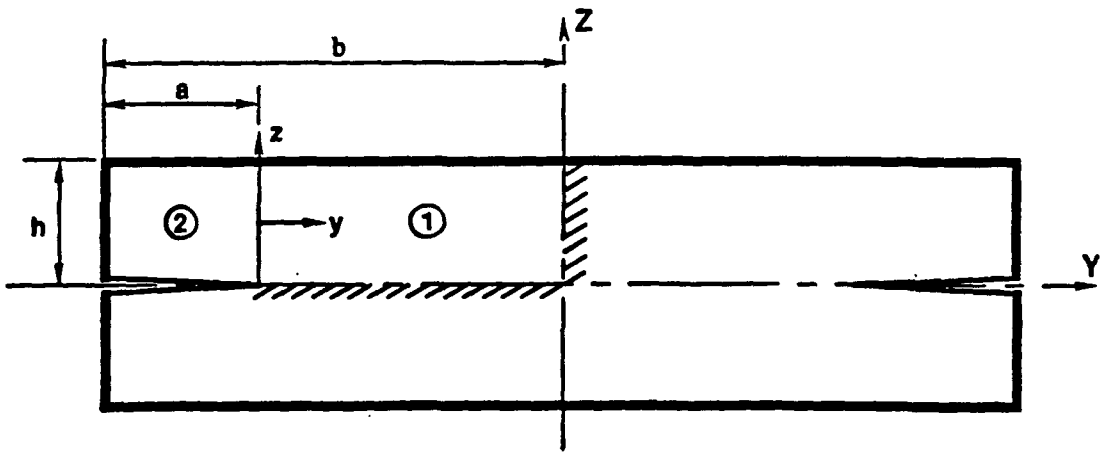

Figure 2.3: Sublaminate Modeling Scheme (Mid-Plane Edge Delamination)

respectively. The analysis is based on the following displacement fields within each sublaminate

$$u = x\varepsilon + U(y) + z\beta_x(y)$$

$$v = V(y) + z\beta_y(y) \tag{2.1}$$

$$w = W(y)$$

where u, v, and w denote the displacements relative to the x, y, and z axes, respectively. Shear deformation is recognized through the rotations β_x and β_y. In the present formulation thickness strain is neglected, and consequently inaccurate values of interlaminar peel stress, σ_{zz}, are expected. However, the peel stress can be modified by enforcing the free edge boundary condition associated with the transverse shear stress resultant.

A generic sublaminate along with the applied forces and moments is shown in Fig. 2.4. The force and moment resultants are denoted by N_i, Q_i, and M_i, respectively. The constitutive relationships in terms of these force and moment resultants can be written as

$$N_i = A_{ij}\varepsilon_j + B_{ik}\kappa_k - N_i^{nm} \qquad (i,j,k = 1,2,6)$$

$$M_i = B_{ij}\varepsilon_j + D_{ik}\kappa_k - M_i^{nm} \qquad (i,j,k = 1,2,6) \tag{2.2}$$

$$Q_i = A_{ij}\varepsilon_j \qquad (i,j = 4,5)$$

The subscripts x, y, z, yz, xz, and xy are replaced by the subscripts 1-6, respectively. The non-mechanical forces and moments resulting from hygrothermal effects are labeled with superscript nm for non-mechanical. They are defined as

$$(N_i^{nm}, M_i^{nm}) = \int_{-\frac{h}{2}}^{+\frac{h}{2}} \left\{\Delta T\overline{\alpha}_j + \Delta H\overline{\beta}_j\right\} \overline{Q}_{ij}(1,z)dz \tag{2.3}$$

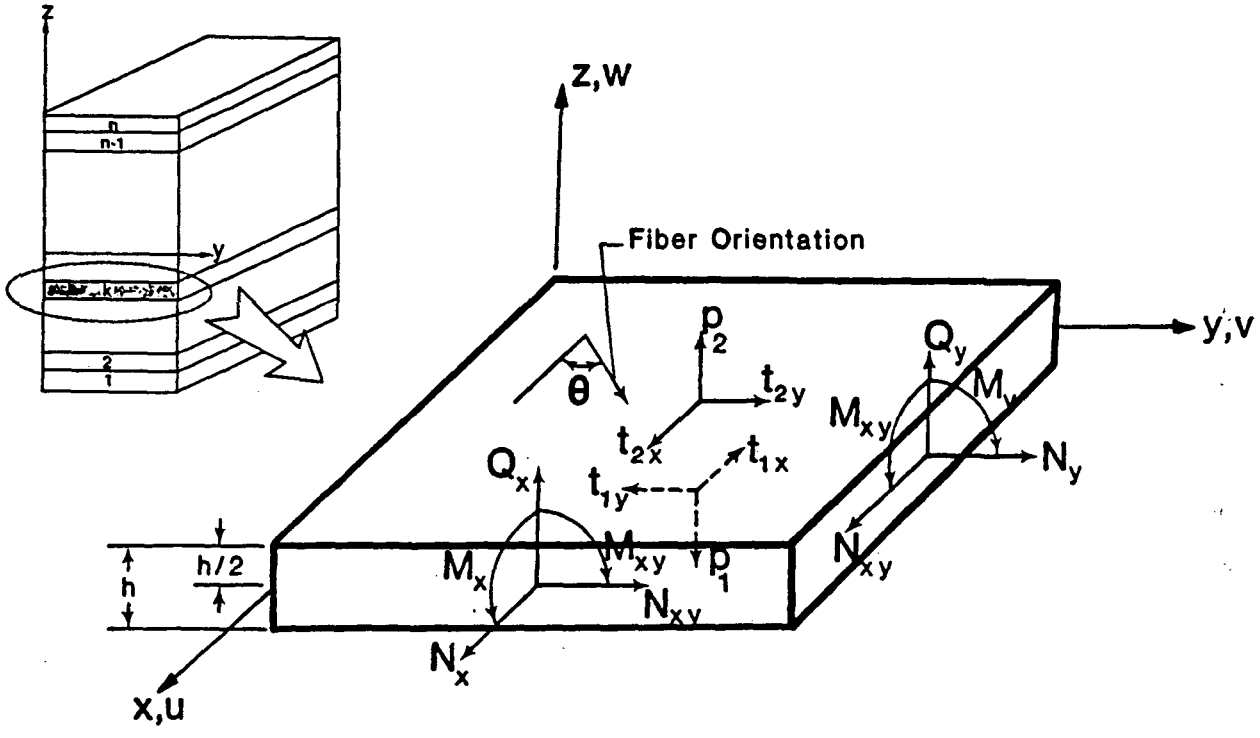

Figure 2.4: Notation and Sign Convention for a Generic Sublaminate

The thermal coefficient is denoted by $\overline{\alpha}_j$ in Eq. (2.3), while the swelling coefficient by $\overline{\beta}_j$. The $\overline{Q}_{ij}$ are the plane stress sublaminate reduced stiffnesses [19]. The bars on α_j, β_j and Q_{ij} indicate that theses quantities are to be obtained through appropriate coordinate transformations. The change in temperature between the ambient and the stress free temperature is denoted by ΔT. The percentage moisture weight gain is represented by ΔH.

For a sublaminate of thickness h, the elastic stiffnesses A_{ij}, B_{ij}, and D_{ij} in Eqs. (2.2) are defined as

$$(A_{ij}, B_{ij}, D_{ij}) = \int_{-\frac{h}{2}}^{+\frac{h}{2}} \overline{Q}_{ij}(1, z, z^2)dz \tag{2.4}$$

The equilibrium equations can be written as follows

$$\begin{aligned} N_{xy,y} + t_{2x} - t_{1x} &= 0 \\ N_{y,y} + t_{2y} - t_{1y} &= 0 \\ Q_{y,y} + p_2 - p_1 &= 0 \\ M_{xy,y} - Q_x + \tfrac{h}{2}(t_{2x} + t_{1x}) &= 0 \\ M_{y,y} - Q_y + \tfrac{h}{2}(t_{2y} + t_{1y}) &= 0 \end{aligned} \tag{2.5}$$

where t_{2x}, t_{2y}, p_2 and t_{1x}, t_{1y}, p_1 denote the interlaminar stress components at the sublaminate upper and lower surfaces, respectively. These stress components appear in Fig. 2.4. Partial differentiation is denoted by a comma in Eqs. (2.5). Application of the boundary conditions and the governing equations to each of the sublaminates results in a system of differential equations which are solved to obtain the stresses and strain energy release rate. The boundary conditions to be prescribed at constant values of y, the sublaminate sections, are N_{xy} or U, N_y or V, Q_y or W, M_y or β_y and M_{xy} or β_x.

2.2.1 Uncracked Region (Sublaminate 1)

From symmetry conditions at the sublaminate bottom surface, both w and the shearing stresses are zero. Since thickness strain is neglected, this leads to w being zero everywhere in this sublaminate. The equilibrium equations can be written as

$$\begin{aligned} N_{xy_1,y} &= 0 \\ N_{y_1,y} &= 0 \\ Q_{y_1,y} - p_1 &= 0 \\ M_{xy_1,y} - Q_{x_1} &= 0 \\ M_{y_1,y} - Q_{y_1} &= 0 \end{aligned} \tag{2.6}$$

where subscript 1 refers to sublaminate 1. From Eqs. (2.6) and the continuity of axial and in-plane shear stress resultants between sublaminates 1 and 2, we get

$$N_{y_1} = N_{xy_1} = 0 \tag{2.7}$$

By substituting from the constitutive relations into Eqs (2.6) and Eq. (2.7), and assuming an exponential form for the rotations β_{1y} and β_{1x}, we get the following characteristic equation

$$E_4 s^4 - E_2 s^2 + E_0 = 0 \tag{2.8}$$

with

$$E_0 = A_{44}A_{55} - (A_{45})^2$$

$$E_2 = \Omega_{21}A_{55} + \Omega_{32}A_{44} - \Omega_{22}A_{45} - \Omega_{31}A_{45}$$

$$E_4 = \Omega_{21}\Omega_{32} - \Omega_{22}\Omega_{31}$$

where

$$[\Omega]_{3\times 2} = \begin{bmatrix} (A_{12}\xi_{12} + A_{16}\xi_{22} + B_{12}) & (A_{12}\xi_{13} + A_{16}\xi_{23} + B_{16}) \\ (B_{22}\xi_{12} + B_{26}\xi_{22} + D_{22}) & (B_{22}\xi_{13} + B_{26}\xi_{23} + D_{26}) \\ (B_{26}\xi_{12} + B_{66}\xi_{22} + D_{26}) & (B_{26}\xi_{13} + B_{66}\xi_{23} + D_{66}) \end{bmatrix}$$

and

$$[\xi]_{2\times 3} = -\begin{bmatrix} A_{22} & A_{26} \\ A_{26} & A_{66} \end{bmatrix}^{-1} \begin{bmatrix} A_{12} & B_{22} & B_{26} \\ A_{16} & B_{26} & B_{66} \end{bmatrix}$$

Coefficient E_0 depends solely on the sublaminate axial stiffness, while E_4 is predominantly influenced by the bending and coupling coefficients D_{ij} and B_{ij} . The numerical value of E_4 can be orders of magnitude smaller than E_2 and E_0. This results in the presence of a boundary zone in the response. For the material and laminate layups considered, the roots of this characteristic equation are real. Only the negative roots of Eq. (2.8) are considered as they give solutions decaying exponentially from the delamination tip. The solution can be written as

$$\begin{Bmatrix} \beta_{1y} \\ \beta_{1x} \end{Bmatrix} = \begin{Bmatrix} 1 \\ \eta_j \end{Bmatrix} I_j e^{-s_j y} \qquad (0 \le y \le b-a) \tag{2.9}$$

where

$$\eta_j = -\frac{\Omega_{21} s_j^2 - A_{44}}{\Omega_{22} s_j^2 - A_{45}} \qquad (j = 1,2)$$

Parameters I_j are arbitrary constants to be determined from the boundary conditions. By substituting Eq. (2.7) into the constitutive relations and using the assumed displacement fields, we obtain

$$\begin{Bmatrix} V_{1,y} \\ U_{1,y} \end{Bmatrix} = \begin{bmatrix} \xi_{11} \\ \xi_{21} \end{bmatrix} \{\varepsilon\} + \begin{Bmatrix} S_1 \\ S_2 \end{Bmatrix}^{nm} + \begin{bmatrix} \xi_{12} & \xi_{13} \\ \xi_{22} & \xi_{23} \end{bmatrix} \begin{Bmatrix} \beta_{1y,y} \\ \beta_{1x,y} \end{Bmatrix} \tag{2.10}$$

where

$$\begin{Bmatrix} S_1 \\ S_2 \end{Bmatrix}^{nm} = \begin{bmatrix} A_{22} & A_{26} \\ A_{26} & A_{66} \end{bmatrix}^{-1} \begin{Bmatrix} N_y \\ N_{xy} \end{Bmatrix}^{nm}$$

Substitute from Eqs. (2.10) into the constitutive relations to get the resultant forces and moments in terms of the total extensional strain

$$\begin{Bmatrix} N_{x_1} \\ M_{y_1} \\ M_{xy_1} \end{Bmatrix} = \begin{bmatrix} A_{11} + A_{12}\xi_{11} + A_{16}\xi_{21} \\ B_{12} + B_{22}\xi_{11} + B_{26}\xi_{21} \\ B_{16} + B_{26}\xi_{11} + B_{66}\xi_{21} \end{bmatrix} \{\varepsilon\}$$

$$+\begin{bmatrix} A_{12}S_1^{nm} + A_{16}S_2^{nm} - N_x^{nm} \\ B_{22}S_1^{nm} + B_{26}S_2^{nm} - M_y^{nm} \\ B_{26}S_1^{nm} + B_{66}S_2^{nm} - M_{xy}^{nm} \end{bmatrix} + [\Omega]_{3\times 2}\begin{Bmatrix} \beta_{1y,y} \\ \beta_{1x,y} \end{Bmatrix} \tag{2.11}$$

2.2.2 Cracked Region (Sublaminate 2)

From the stress free boundary conditions at the face $y = -a$ of sublaminate 2 and the equilibrium equations, we get

$$N_{y_2} = N_{xy_2} = Q_{y_2} = M_{y_2} = 0$$

The equilibrium equations reduce to

$$M_{xy_2,y} - Q_{x_2} = 0$$

Following a similar procedure as in sublaminate 1, the rotation can be written as

$$\beta_{2x} = H_1 e^{\lambda y} \qquad (-a \leq y \leq 0) \tag{2.12}$$

with

$$\lambda = \sqrt{\frac{A_{44}A_{55} - A_{45}^2}{A_{44}(D_{66} + B_{26}\varphi_{12} + B_{66}\varphi_{22} + D_{26}\varphi_{32})}}$$

where

$$[\varphi]_{3\times 2} = -[\psi]^{-1}\begin{bmatrix} A_{12} & B_{26} \\ A_{16} & B_{66} \\ B_{12} & D_{26} \end{bmatrix}$$

and

$$[\psi] = \begin{bmatrix} A_{22} & A_{26} & B_{22} \\ A_{26} & A_{66} & B_{26} \\ B_{22} & B_{26} & D_{22} \end{bmatrix}$$

H_1 is an arbitrary constant to be determined from the continuity conditions between sublaminates 1 and 2. The force and moment resultants can be expressed in

terms of the total strain

$$\begin{Bmatrix} N_{x_2} \\ M_{xy_2} \end{Bmatrix} = \begin{bmatrix} A_{11} + A_{12}\varphi_{11} + A_{16}\varphi_{21} + B_{12}\varphi_{31} \\ B_{16} + B_{26}\varphi_{11} + B_{66}\varphi_{21} + D_{26}\varphi_{31} \end{bmatrix} \{\varepsilon\} + \begin{bmatrix} A_{12}F_1^{nm} + A_{16}F_2^{nm} + B_{12}F_3^{nm} - N_x^{nm} \\ B_{26}F_1^{nm} + B_{66}F_2^{nm} + D_{26}F_3^{nm} - M_{xy}^{nm} \end{bmatrix} + \begin{bmatrix} B_{16} + A_{12}\varphi_{12} + A_{16}\varphi_{22} + B_{12}\varphi_{32} \\ D_{66} + B_{26}\varphi_{12} + B_{66}\varphi_{22} + D_{26}\varphi_{32} \end{bmatrix} \lambda H_1 \epsilon^{\lambda y} \qquad (2.13)$$

where

$$\begin{Bmatrix} F_1 \\ F_2 \\ F_3 \end{Bmatrix}^{nm} = [\psi]^{-1} \begin{Bmatrix} N_y \\ N_{xy} \\ M_y \end{Bmatrix}^{nm}$$

The response associated with sublaminates 1 and 2 shown in Fig. 2.3 is coupled through the following conditions at $y = 0$,

$$M_{y_1}(0) = M_{y_2}(0) = 0$$

$$M_{xy_1}(0) = M_{xy_2}(0) = 0$$

$$\beta_{1x}(0) = \beta_{2x}(0)$$

The solution for both sublaminates i.e., the values of I_j and H_1 can be obtained by applying these conditions. The final expressions for the sublaminate rotations is given by Eqs. (2.9) and Eq. (2.12) where

$$I_1 = \frac{\left\{-\Theta_1 + (\Theta_4 + \Theta_5\eta_2)(\frac{\Lambda_1}{\Lambda_4})\right\}\varepsilon + \Theta_5\eta_2(\frac{\Lambda_2}{\Lambda_4}) - \Theta_2 + \Theta_4(\frac{\Lambda_2}{\Lambda_4})}{\Theta_3 - (\Theta_4 + \Theta_5\eta_2)\frac{\Lambda_3}{\Lambda_4} + \Theta_5\eta_1}$$

$$I_2 = -\tfrac{1}{\Lambda_4}(\Lambda_1\varepsilon + \Lambda_2 + \Lambda_3 I_1)$$

$$H_1 = \eta_1 I_1 + \eta_2 I_2$$

with

$$\Lambda_1 = B_{12} + B_{22}\xi_{11} + B_{26}\xi_{21}$$

$$\Lambda_2 = B_{22}S_1^{nm} + B_{26}S_2^{nm} - M_y^{nm}$$

$$\Lambda_3 = -(\Omega_{21} + \eta_1 \Omega_{22}) s_1$$

$$\Lambda_4 = -(\Omega_{21} + \eta_2 \Omega_{22}) s_2$$

and

$$\Theta_1 = B_{26}(\xi_{11} - \varphi_{11}) + B_{66}(\xi_{21} - \varphi_{21}) - D_{26}\varphi_{31}$$

$$\Theta_2 = B_{26}(S_1^{nm} - F_1^{nm}) + B_{66}(S_2^{nm} - F_2^{nm}) - D_{26}F_3^{nm}$$

$$\Theta_3 = -(\Omega_{31} + \eta_1 \Omega_{32}) s_1$$

$$\Theta_4 = -(\Omega_{31} + \eta_2 \Omega_{32}) s_2$$

$$\Theta_5 = -(D_{66} + B_{26}\varphi_{12} + B_{66}\varphi_{22} + D_{26}\varphi_{32})\lambda$$

The total strain energy release rate can be calculated by considering the work done by the external forces. This is given by

$$G_T = G_I = -\frac{2}{L} \sum_{i=1}^{2} \frac{dW_i}{da} \tag{2.14}$$

where W_i = work done by the external force in sublaminate i, L = laminate length, and a = crack length.

The work done by the external forces is written in terms of the mechanical strain, ε_i^m, as

$$W_i = \frac{L}{2} \int_{y_i} \varepsilon_i^m N_{x_i} dy \tag{2.15}$$

with

$$\varepsilon_i^m = \varepsilon - \varepsilon_i^{nm} \tag{2.16}$$

The sublaminate free expansion strains, ε_i^{nm} , are calculated by setting the axial force resultant to zero, i.e.

$$\int_{y_i} N_{x_i} dy = 0 \tag{2.17}$$

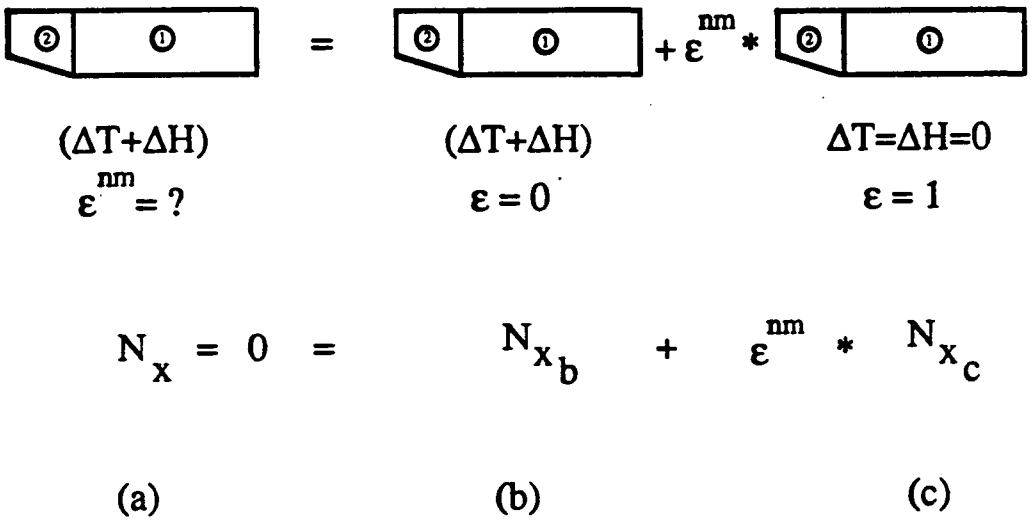

Figure 2.5: Effective non-mechanical free expansion strain across the entire width of the laminate

where N_{x_i} is given in Eq. (2.11) and Eq. (2.13). The expression for each sublaminate is

$$\varepsilon_1^{nm} = -\frac{A_{12}S_1^{nm} + A_{16}S_2^{nm} - N_x^{nm}}{A_{11} + A_{12}\xi_{11} + A_{16}\xi_{21}}$$
$$\varepsilon_2^{nm} = -\frac{A_{12}F_1^{nm} + A_{16}F_2^{nm} + B_{12}F_3^{nm} - N_x^{nm}}{A_{11} + A_{12}\varphi_{11} + A_{16}\varphi_{21} + B_{12}\varphi_{31}} \qquad (2.18)$$

The total strain, ε, is given by

$$\varepsilon = \varepsilon^m + \varepsilon^{nm} \qquad (2.19)$$

where ε^m is the effective mechanical strain and ε^{nm} is the effective free-expansional strain across the entire width of the laminate estimated by decomposing the non-mechanical problem in Fig. 2.5(a) into the superposition of the two cases shown in Fig. 2.5(b) and Fig. 2.5(c). In case (b) the laminate is subjected to a non-mechanical change ($\Delta T + \Delta H$), while the strain is prescribed to be zero. In case (c) a unit axial strain is applied, while no hygrothermal change is considered. Knowing that no axial

force is applied in the main problem, i.e. Fig. 2.5(a), the sum of the axial forces in the two subproblems should be zero, hence

$$N_{x_b} + \varepsilon^{nm} N_{x_c} = 0 \tag{2.20}$$

and

$$\varepsilon^{nm} = -\frac{N_{x_b}}{N_{x_c}} \tag{2.21}$$

where N_{x_b} and N_{x_c} are the axial forces in case (b) and case (c), respectively. These axial forces are computed by substituting the expressions of N_{x_1} and N_{x_2} from Eq. (2.11) and Eq. (2.13) into the relations

$$\begin{aligned} N_{x_b} &= \left[\int_0^{(b-a)} N_{x_1} dy + \int_{-a}^{0} N_{x_2} dy\right]_{\epsilon=0,(\Delta T+\Delta H)} \\ N_{x_c} &= \left[\int_0^{(b-a)} N_{x_1} dy + \int_{-a}^{0} N_{x_2} dy\right]_{\epsilon=1,\Delta T=\Delta H=0} \end{aligned} \tag{2.22}$$

The expressions for N_{x_b} and N_{x_c} are found to be

$$\begin{aligned} N_{x_b} &= (A_{12}S_1^{nm} + A_{16}S_2^{nm} - N_x^{nm})(b-a) \\ &\quad + (A_{12}F_1^{nm} + A_{16}F_2^{nm} + B_{12}F_3^{nm} - N_x^{nm})a \end{aligned} \tag{2.23}$$

and

$$\begin{aligned} N_{x_c} &= (A_{11} + A_{12}\xi_{11} + A_{16}\xi_{21})(b-a) \\ &\quad + (A_{11} + A_{12}\varphi_{11} + A_{16}\varphi_{21} + B_{12}\varphi_{31})a \end{aligned} \tag{2.24}$$

The crack length and half of the total laminate width are denoted by a and b, respectively, as shown in Fig. 2.3.

By combining the expressions of N_{x_i} from Eqs. (2.11) and Eqs. (2.13) with Eqs. (2.14)-(2.24), the total energy release rate for the Mode I case can be written in the form

$$G_I = (G_{IL}) + (G_{IL_a}) + (G_{IR} + G_{IR_a}) \tag{2.25}$$

where

$$
\begin{aligned}
G_{IL} &= (\varepsilon - \varepsilon_1^{nm})\left[(A_{11} + A_{12}\xi_{11} + A_{16}\xi_{21})\,\varepsilon + (A_{12}S_1^{nm} + A_{16}S_2^{nm} - N_x^{nm})\right] \\
&\quad - (\varepsilon - \varepsilon_2^{nm})\left[(A_{11} + A_{12}\varphi_{11} + A_{16}\varphi_{21} + B_{12}\varphi_{31})\,\varepsilon \right. \\
&\qquad \left. + (A_{12}F_1^{nm} + A_{16}F_2^{nm} + B_{12}F_3^{nm} - N_x^{nm})\right]
\end{aligned}
$$

$$
\begin{aligned}
G_{IL_a} &= -\frac{d\varepsilon}{da}(b-a)\left\{(A_{11} + A_{12}\xi_{11} + A_{16}\xi_{21})\left[(2\varepsilon - \varepsilon_1^{nm})\right.\right. \\
&\qquad \left.\left. + (A_{12}S_1^{nm} + A_{16}S_2^{nm} - N_x^{nm})\right]\right\} \\
&\quad - \frac{d\varepsilon}{da}a\left\{(A_{11} + A_{12}\varphi_{11} + A_{16}\varphi_{21} + B_{12}\varphi_{31})(2\varepsilon - \varepsilon_2^{nm})\right. \\
&\qquad \left. + (A_{12}F_1^{nm} + A_{16}F_2^{nm} + B_{12}F_3^{nm} - N_x^{nm})\right\}
\end{aligned}
$$

$$
\begin{aligned}
G_{IR} &= -(\varepsilon - \varepsilon_1^{nm})\left[(\Omega_{11} + \eta_1\Omega_{12})\,I_1 s_1 \epsilon^{-s_1(b-a)} + (\Omega_{11} + \eta_2\Omega_{12})\,I_2 s_2 \epsilon^{-s_2(b-a)}\right] \\
&\quad - (\varepsilon - \varepsilon_2^{nm})\,(B_{16} + A_{12}\varphi_{12} + A_{16}\varphi_{22} + B_{12}\varphi_{32})\,H_1\lambda\epsilon^{-\lambda a}
\end{aligned}
$$

$$
\begin{aligned}
G_{IR_a} &= -\frac{d\varepsilon}{da}\left\{(\Omega_{11} + \eta_1\Omega_{12})\,I_1\left[\epsilon^{-s_1(b-a)} - 1\right] + (\Omega_{11} + \eta_2\Omega_{12})\,I_2\left[\epsilon^{-s_2(b-a)} - 1\right]\right. \\
&\qquad \left. + (B_{16} + A_{12}\varphi_{12} + A_{16}\varphi_{22} + B_{12}\varphi_{32})\,H_1\left(1 - \epsilon^{-\lambda a}\right)\right\}
\end{aligned}
$$

and

$$
\begin{aligned}
\frac{d\varepsilon}{da} &= \frac{d\varepsilon^{nm}}{da} = \frac{A_{12}(S_1^{nm} - F_2^{nm}) + A_{16}(S_2^{nm} - F_2^{nm}) - B_{12}F_3^{nm}}{N_{x_c}} \\
&\quad - \frac{Nx_b\left[A_{12}(\xi_{11} - \varphi_{11}) + A_{16}(\xi_{21} - \varphi_{21}) - B_{12}\varphi_{31}\right]}{N_{x_c}^2}
\end{aligned}
\tag{2.26}
$$

The resulting expression for the total energy release rate G_I is composed of three terms. The first term, denoted by G_{IL} is independent of the delamination length while the second, G_{IL_a}, is a linear function of the crack length. The third term denoted by $(G_{IR} + G_{IR_a})$, is an exponentially decaying function of the delamination length.

In computing the non-mechanical strains, the laminate is assumed to be held at the prescribed temperature and moisture levels. This is followed by testing under

fixed-grip condition, i.e., the constant strain measured in the lab is the mechanical strain ϵ^m. In Refs.[18] and [20], Whitney considered the strain measured in the tests to be the total strain, i.e. $\epsilon = \epsilon^m + \epsilon^{nm} = constant$. The difference between the two interpretations is detected by the terms G_{IL_a} and G_{IR_a} in Eq. (2.25). These two terms are neglected in Refs. [18] and [20] since the total strain ϵ is assumed to be constant.

As mentioned previously, neglecting the thickness strain leads to inaccurate estimates for the peel stress. The peel stress is given by

$$p = Q_{y_1,y} = -(A_{44} + A_{45}\eta_j)I_j s_j \epsilon^{-s_j y} \qquad (j = 1,2) \tag{2.27}$$

The equilibrium of transverse force requires that

$$\int_0^{(b-a)} p dy = 0 \tag{2.28}$$

or from the equilibrium equations (2.6)

$$Q_{y_1}|_{y_1=(b-a)} - Q_{y_1}|_{y_1=0} = 0$$

While for all practical purpose the resultant shear stress $Q_{y_1}|_{y_1=(b-a)}$ vanishes due to the free edge, the resultant shear stress at the delamination front $Q_{y_1}|_{y_1=0} \neq 0$. That is in order for the peel stress to satisfy transverse force equilibrium, the shear force boundary condition at the sublaminate end should be enforced. This is done by adding to the peel stress distribution an appropriate boundary function expressed in terms of the characteristics roots as

$$a_1 e^{-s_1 y} + a_2 e^{-s_2 y}$$

The coefficients a_1 and a_2 are obtained by enforcing equilibrium of transverse force given in Eq. (2.28) and moment given by

$$\int_0^{(b-a)} p y dy + M_{y_1}|_{y_1=(b-a)} = 0$$

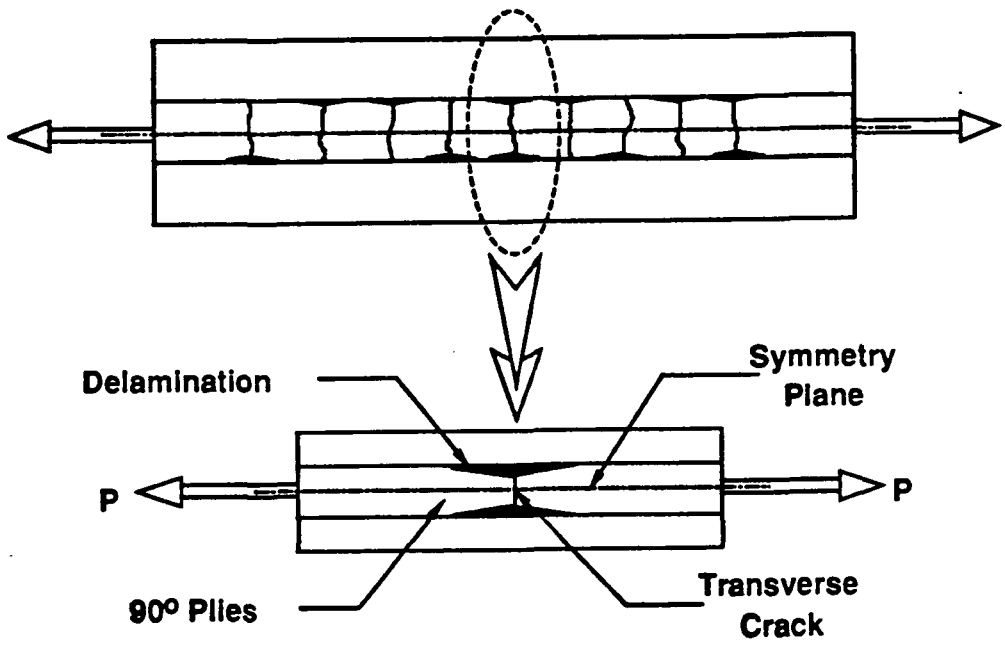

Figure 2.6: Local Delamination Specimen Cross Section

The corrected peel stress distribution is

$$p = \frac{s_1 s_2}{s_1 - s_2} M_{y_1}|_{y_1=(b-a)} \left[s_1 e^{-s_1 y} - s_2 e^{-s_2 y} \right]$$

2.3 Local Delamination

A longitudinal section illustrating the geometry of a generic configuration is shown in Fig. 2.6. The central region is assumed to be made of 90° plies with an isolated transverse crack in the middle. Delaminations are assumed to grow from both ends of the transverse crack, and towards both specimen ends as shown. From symmetry considerations, only one quarter of the configuration is modeled. The modeled portion of length L is divided into four sublaminates as shown in Fig. 2.7. The crack length is denoted by a. The top surface (sublaminates 1 and 4) is stress free. In order to

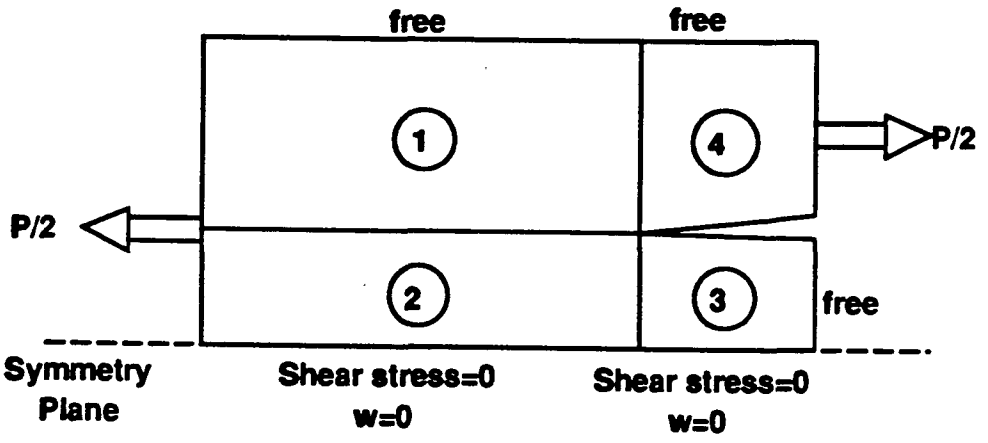

Figure 2.7: Sublaminate Scheme for Local Delamination

simplify the analysis, the thickness strain ε_z is neglected. The consequence of this, combined with the fact that the transverse displacement w is zero along the center line, is that w is zero in sublaminates 1, 2, and 3. Also, this approximation does not allow for the enforcement of boundary conditions on the shear stress resultants, leading to incorrect estimates of the interlaminar normal stresses. The interlaminar shear stress estimates, however, are reliable [6]. These assumptions lead to considerable simplifications in the analysis. In spite of the simplifications, reliable energy release rate components can be estimated based on the interlaminar shear stress distributions [7].

A generic sublaminate is shown in Fig. 2.8 along with the notations and sign conventions. The peel and interlaminar shear stresses are denoted by P and T, respectively, with t and b subscripts for the top and bottom surfaces, respectively.

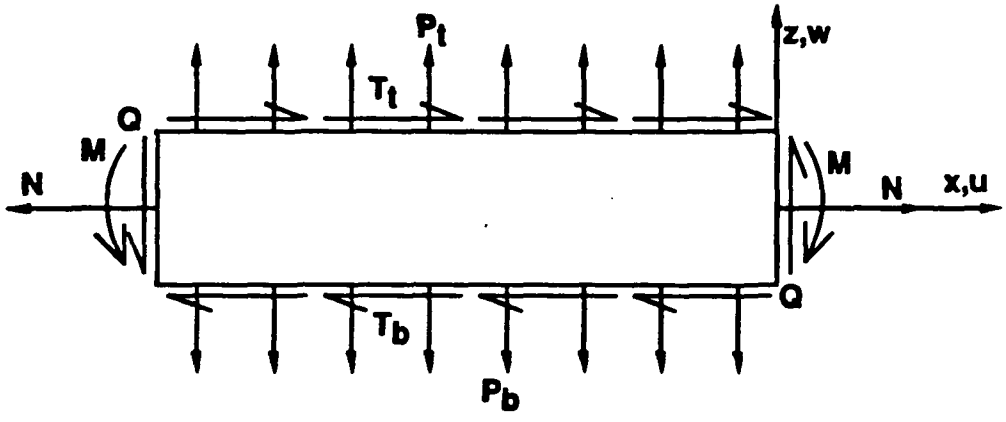

Figure 2.8: Generic Sublaminate for Local Delamination

The axial stress resultant, shear stress resultant, and bending moment resultant are denoted by N, Q, and M, respectively. The governing equations correspond to the one-dimensional form of Eqs. (2.1 - 2.5). These are summarized in the following for convenience.

The x and z displacements within the sublaminate are assumed to be of the form

$$u(x,z) = U(x) + z\beta(x)$$

$$w(x,z) = W(x)$$

Here, U represents the axial mid-plane stretching and W is the transverse displacement. The shear deformation is recognized through the rotation, β. These displacements are the total quantities and include the hygrothermal effects. The origin of the coordinate axes for the sublaminates is taken at the delamination tip as shown in Fig. 2.9 . The equilibrium equations take the form

$$N_{,x} + T_t - T_b = 0$$

$$Q_{,x} + P_t - P_b = 0 \qquad (2.29)$$

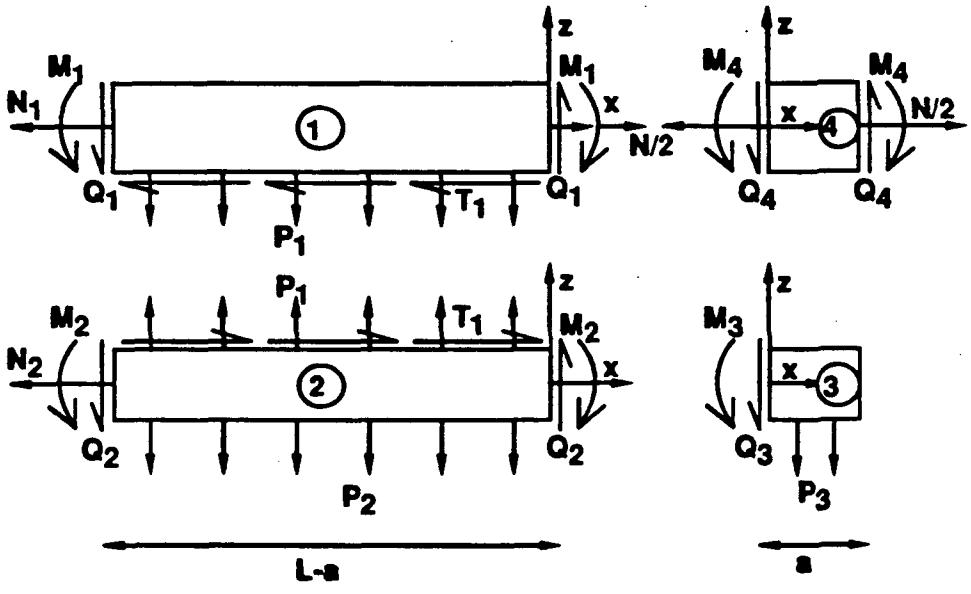

Figure 2.9: Sublaminate Forces and Coordinate Systems

$$M_{,x} - Q + \frac{h}{2}(T_t + T_b) = 0$$

where h is the thickness of the sublaminate. The constitutive relationships in terms of the force and moment resultants are

$$N = A_{11}U_{,x} + B_{11}\beta_{,x}$$

$$Q = A_{55}(\beta + W_{,x}^{0})$$

$$M = B_{11}U_{,x} + D_{11}\beta_{,x}$$

The boundary variables to be prescribed at the sublaminate edges are

$$N \quad or \quad U$$

$$M \quad or \quad \beta$$

$$Q \quad or \quad W$$

Additionally, at the interfaces between sublaminates, reciprocal traction, and displacement matching boundary conditions have to be specified. The stress resultants in these equations include the equivalent hygrothermal loads also.

The solutions in sublaminates 1 and 2 are coupled by the reciprocal interlaminar stresses denoted T_1 and P_1 and by displacement continuity at the common interface. Assuming exponential solutions for the axial force and bending moment resultants leads to an eigenvalue problem involving the exponential parameters. The characteristic equation is of the form

$$s[B_1 s^4 + B_2 s^2 + B_3] = 0$$

where s is the eigenvalue parameter, and the B coefficients are given by

$$B_1 = \left(\frac{1}{A_{11(2)}} + \frac{1}{A_{11(1)}} + \frac{h_1^2}{4D_{11(1)}} + \frac{h_2^2}{4D_{11(2)}}\right)\frac{D_{11(1)}}{A_{55(1)}}\frac{D_{11(2)}}{A_{55(2)}}$$

$$\begin{aligned} B_2 \;=\; & -\frac{D_{11(2)}}{A_{55(2)}}\left(\frac{1}{A_{11(1)}} + \frac{1}{A_{11(2)}} + \frac{h_2^2}{4D_{11(2)}}\right) \\ & -\frac{D_{11(1)}}{A_{55(1)}}\left(\frac{1}{A_{11(1)}} + \frac{1}{A_{11(2)}} + \frac{h_1^2}{4D_{11(1)}}\right) \end{aligned}$$

and

$$B_3 = \frac{1}{A_{11(1)}} + \frac{1}{A_{11(2)}}$$

The eigenvalues turn out to be zero and two nonzero values given by

$$s = \pm\left(\frac{-B_2 \pm (B_2^2 - 4B_1B_3)^{1/2}}{2B_1}\right)^{1/2}$$

For the problem under consideration, all the square roots in this expression lead to real quantities and thus the eigenvalues are real. Since the eigenvalues involve only the stiffness parameters, they are not affected by the inclusion of hygrothermal effects. Further, due to the fact that B_1 has D terms in the numerator, it is much smaller

than B_3. This leads to the boundary layer nature of the solution. Since the response (axial forces, moments) has finite values at large distances from the origin, namely, at the ends of the specimen, only the exponentially decaying and constant solutions are used. Using subscripts to denote the sublaminate of validity, the following boundary conditions from the ends of the modeled region are enforced.

$$N_2(0) = 0$$

$$Q_4(a) = 0$$

$$\beta_4(a) = 0$$

$$N_1 + N_2 = Applied\ \ Load$$

The conditions on N apply only to the mechanical quantities. Further, the following displacement matching conditions are applied.

$$u_1\left(x, -\frac{h_1}{2}\right) = u_2\left(x, \frac{h_2}{2}\right)$$

$$U_1(0) = U_4(0)$$

$$U_2(0) = U_3(0)$$

$$\beta_1(0) = \beta_4(0)$$

It should be noted that a β_2 and β_3 matching condition cannot be applied at this level of modeling since it would amount to specifying both W' and Q. To eliminate rigid body displacements, U_1 is set to zero at the left end. The following solutions can then be obtained for the stress resultants in sublaminates 1 and 2

$$N_1 = a_1 e^{s_1 x} + a_2 e^{s_2 x} + \varepsilon A_{11(1)} - N_1^{nm}$$

$$N_2 = -a_1 e^{s_1 x} - a_2 e^{s_2 x} + \varepsilon A_{11(2)} - N_2^{nm}$$

$$M_1 = a_1 k_1 e^{s_1 x} + a_2 k_2 e^{s_2 x} - M_1^{nm}$$

$$M_2 = a_1 k_3 e^{s_1 x} + a_2 k_4 e^{s_2 x} - M_2^{nm}$$

Here k_1 is defined as

$$k_1 = \frac{\frac{h_1}{2} s_1^2}{\frac{A_{55(1)}}{D_{11(1)}} - s_1^2}$$

The parameter k_2 is defined in a similar manner using the eigenvalue, s_2. The remaining parameters, k_3 and k_4 , are similar to k_1 and k_2 but based on sublaminate 2 properties. The nominal strain, ε, is defined as

$$\varepsilon = \left(\frac{P}{2b} + N_1^{nm} + N_2^{nm}\right) \frac{1}{A_{11(1)} + A_{11(2)}}$$

where P is the applied uniform axial force and b is the specimen width. The $a_j's$ can be derived from the boundary conditions as follows

$$a_1 = \frac{\theta_3 + \theta_4 a}{\theta_d} \frac{1}{A_{11(1)} + A_{11(2)}} \left(\frac{P}{2b} A_{11(2)} + N_1^{nm} A_{11(2)} - N_2^{nm} A_{11(1)}\right)$$

$$a_2 = -\frac{\theta_1 + \theta_2 a}{\theta_d} \frac{1}{A_{11(1)} + A_{11(2)}} \left(\frac{P}{2b} A_{11(2)} + N_1^{nm} A_{11(2)} - N_2^{nm} A_{11(1)}\right)$$

with

$$\theta_1 = \frac{s_1}{A_{55(1)}} \left(k_1 + \frac{h_1}{2}\right)$$

$$\theta_2 = \frac{k_1}{D_{11(1)}}$$

$$\theta_3 = \frac{s_2}{A_{55(1)}} \left(k_2 + \frac{h_1}{2}\right)$$

$$\theta_4 = \frac{k_2}{D_{11(1)}}$$

and

$$\theta_d = \theta_3 - \theta_1 + (\theta_4 - \theta_2) a$$

The interlaminar shear and peel stresses between sublaminates 1 and 2 can be obtained using the equilibrium equations (2.29) as

$$T_1 = a_1 s_1 \epsilon^{s_1 x} + a_2 s_2 \epsilon^{s_2 x}$$

$$P_1 = (k_1 + \frac{h_1}{2}) a_1 s_1 \epsilon^{s_1 x} + (k_2 + \frac{h_1}{2}) a_2 s_2 \epsilon^{s_2 x}$$

As mentioned previously, this peel stress estimate is not accurate because of the inability to apply boundary conditions on shear. Recognizing the fact that there are no applied shear forces, it can be concluded that the peel stress distribution should be self equilibrating. This assumption can be satisfied by including additional exponential terms in the above peel stress expression and determining these additional terms by setting the net force and moment due to the peel stress to zero as shown in section 2.2. The peel stress estimated through this correction process is referred to as the modified peel stress. Proceeding on to sublaminates 3 and 4, the following solutions can be written.

$$N_3 = 0$$

$$M_3 = \varphi_1 \sinh(\omega_3 x) + \varphi_2 \cosh(\omega_3 x)$$

where

$$\varphi_2 = a_1 k_3 + a_2 k_4$$

$$\varphi_1 = -\varphi_2 \coth(\omega_3 a)$$

and

$$\omega_3^2 = \frac{A_{55(2)}}{D_{11(2)}}$$

$$N_4 = \frac{P}{2b}$$

$$M_4 = a_1 k_1 + a_2 k_2$$

The total energy release rate G_T is calculated using $G_T = dW_e/da$ where W_e is the work done per unit width by the external (constant) loads on the specimen displacements. For the case where hygrothermal effects are included, there are additional terms due to the work done by N_i^{nm}. In reality, these N_i^{nm} quantities are not applied loads but correspond to residual stresses. Thus, the additional terms are due to the work done by the applied mechanical strains on these residual stresses. The total energy release including hygrothermal effects is given by

$$\begin{aligned} G_T &= \frac{P}{2b}\left(\frac{P}{b}+N_1^{nm}\right)\left(\frac{1}{A_{11(1)}}-\frac{1}{A_{11(1)}+A_{11(2)}}+I_1-I_2\right) \\ &\quad +\frac{P}{2b}N_2^{nm}\left(-\frac{1}{A_{11(1)}+A_{11(2)}}-I_3+I_2\right) \end{aligned} \tag{2.30}$$

where the I factors are

$$\begin{aligned} I_1 &= \chi\frac{\theta_2\theta_3-\theta_1\theta_4}{\theta_d^2}\left(\frac{1-e^{-s_1(L-a)}}{s_1}-\frac{1-e^{-s_2(L-a)}}{s_2}\right) \\ I_2 &= \chi\frac{(\theta_3+\theta_4 a)e^{-s_1(L-a)}-(\theta_1+\theta_2 a)e^{-s_2(L-a)}}{\theta_d} \end{aligned} \tag{2.31}$$

with

$$\chi = \frac{1}{A_{11(1)}+A_{11(2)}}\frac{A_{11(2)}}{A_{11(1)}}$$

Parameter I_3 is the same as I_1 but with the ratio $A_{11(1)}/A_{11(2)}$ instead of unity in Eq. (2.31). Using the virtual crack closure technique [21], from the relative displacements in the cracked portion and the interlaminar stresses ahead of the crack tip, the mode I and mode II energy release rate contributions can be obtained. The mode III energy release rate is zero from the assumption of plane strain. The mode II energy release rate is given by

$$G_{II} = \lim_{\delta\to 0}\frac{1}{2\delta}\int_0^{\delta} T_1(x-\delta)\Delta u(x)dx$$

where δ is the virtual crack step size and Δu is the differential axial displacement across the crack surface. This calculation can be simplified using only the linear

part of the differential displacement [7]. In a similar fashion, the mode I energy release rate can be obtained based on the normal stress (P) and the differential w displacements near the crack front. Since the unmodified peel stress estimate is inaccurate, an alternate approach was used to estimate G_I, the mode I energy release rate. The total energy release rate for this problem is made up entirely of G_I and G_{II} ($G_{III} = 0$). From an estimate of G_T and G_{II}, an estimate for G_I can be obtained simply as

$$G_I = G_T - G_{II}$$

The critical load for a given specimen can then be evaluated based on an appropriate fracture law. This is illustrated in the next chapter.

CHAPTER III

APPLICATIONS OF DELAMINATION MODELS

3.1 Mode I Edge Delamination

The analytical model is applied to the mid-plane edge delamination specimen shown in Fig. 2.2. The material considered is T300/5208 graphite epoxy. Its properties are listed in Table 3.1.

The difference between the ambient and cure temperature, ΔT, is $-156°C$. The moisture level was allowed to vary from 0 to 1.2 percent of the laminate weight, which reflects feasible conditions. Laminates of the class $[\theta/-\theta_2/\theta/90_2]_s$ and $[0_3/90_3]_s$ have been analyzed.

Normalized values of strain energy release rate are shown in Figs. 3.1-3.6, where the labels $M, M+T$, and $M+T+H$ stand for mechanical, mechanical and thermal, and mechanical, thermal and moisture, respectively. The strain energy release

Table 3.1: ED Specimen Geometry and Material Properties

$E_{11} = 128$ GPa	Thermal Coefficients :	$\alpha_1 = -0.41\mu\varepsilon/°C$
$E_{22} = 8.47$ GPa		$\alpha_2 = 26.8\mu\varepsilon/°C$
$G_{12} = 5.73$ GPa	Swelling Coefficients :	$\beta_1 = 0$
$G_{31} = 3.27$ GPa		$\beta_2 = 5560\mu\varepsilon/\%W$
$G_{23} = 3.27$ GPa	Width $= 2b = 38.4$ mm	
$\nu_{12} = 0.292$	Ply Thickness $= 0.14$ mm	

rate parameter in the figures is defined as the total energy release rate divided by $E_{22}h(\varepsilon^m)^2$.

The strain energy release rate in Figs. 3.1-3.3 is zero at $a = 0$. Residual thermal stresses results in an increase of 275%, 40% and 280% of the energy release rate for the $[15/-15_2/15/90_2]_s$, $[60/-60_2/60/90_2]_s$ and $[0_3/90_3]_s$ laminates, respectively. Residual moisture alleviates this effect as illustrated in Figs. 3.4-3.6. The specific moisture content for total alleviation from the thermal effect is equal to 0.763% irrespective of the layup.

The peel stress distribution, σ_{zz}, appears in Figs. 3.7-3.9. The stress parameter in these figures is defined as the interlaminar stress divided by $E_{22}\varepsilon^m$. The inaccurate peel stress distribution given in Eq. (2.27) is plotted for the case where mechanical loading only is considered. The corrected peel stress distribution is self-equilibrating and yields a tensile peel stress at the delamination front.

The magnitude of the peel stresses shows a strong dependency on the thermal and moisture conditions. The stress increases with thermal effect as compared to pure mechanical loading. The addition of moisture alleviates the thermal effect. Moreover, the distance at which the peel stress reverses its sign is not affected by the residual thermal and moisture strains. It is worth noting that at the specific moisture percent (0.763%) producing complete alleviation of the total energy release rate from the thermal effect, the interlaminar peel stress distribution is identical to the case where only mechanical loading is considered. This is shown in Figs. 3.7-3.9. This finding establishes a similarity in behavior between the energy release rate and the interlaminar stresses.

The analytical model presented herein was applied to the laminates presented in Ref. [18]. The Graphite/Epoxy lamina properties from Ref. [18] are listed in Table 3.2. Similar values of strain energy release rate G_I were calculated for the wide range

Table 3.2: ED Specimen Geometry and Material Properties, Ref. [18]

$E_{11}/E_{22} = 14$	Ply Thickness = 0.1267 mm	
$E_{33}/E_{22} = 1$		
$G_{12}/E_{22} = 0.533$	Thermal Coefficients :	$\alpha_1 = -0.9\mu\varepsilon/°C$
$G_{23}/E_{22} = 0.323$		$\alpha_2 = \alpha_3 = 23.0\mu\varepsilon/°C$
$\nu_{12} = 0.3$		
$\nu_{23} = 0.55$	width = $2b$ = 38.0mm	

of a/h where the G_I remains constant as shown in Figs. 3.10 and 3.11. Negligible change in the G_I value with decreasingly small values of a/h were obtained. This is in contrast with the increase in G_I at small values of a/h reported in Ref. [18]. Although thickness strain is neglected in Eqs. (2.1), the peel stress distribution has been estimated through a modification as described previously, which simplifies considerably the computational effort. A comparison of the peel stress distribution with Ref. [18] is shown in Figs. 3.12 and 3.13.

The peel stress intensity at the delamination front in the $[30/-30_2/30/90_2]_s$ is higher than the $[0_3/90_3]_s$ laminate. This is due to the difference in poisson's ratio between the core plies made of 90° plies and the outer plies. The poisson's ratio mismatch is larger for the case of $[30/-30_2/30/90_2]_s$ compared to the $[0_3/90_3]_s$ layup. The interlaminar peel stress distribution predicted by the present approach is in good agreement with the distribution of Ref. [18] for the case of a $[0_3/90_3]_s$laminate. This is in contrast with the case of a$[30/-30_2/30/90_2]_s$ where the maximum stress intensity as well as the distribution differ from the predictions of Ref. [18]. This difference may be due to the transverse normal strain influence on the analysis of these laminates.

3.2 Edge and Local Delamination

The delamination models have been used to study the behavior of $[\pm 25/90_n]_s$ T300/934 Graphite Epoxy specimen for n values of 0.5, 1, 2, 3, 4, 6, and 8. These correspond to the specimen tested by Crossman and Wang [8]. The specimen width and length were fixed at 0.025m and 0.15m, respectively, as in the tests. In computing the non-mechanical strains, the laminate is assumed to be held at the prescribed temperature and moisture levels. In predicting critical strains, the difference between test and stress free temperatures is assumed to be $-155°C$ and specimen is assumed to be dry. It is assumed that local delamination occurs under fixed load conditions whereas edge delamination occurs under fixed grip conditions. This difference is a consequence of the modeling approaches used in the analyses. The applied uniform load was 100 MPa axial stress for the local delamination analysis and 0.5% strain for the edge delamination analysis. The solutions were generated using simple computer programs based on the closed form expressions for the interlaminar stresses and energy release rates.

3.2.1 Local Delamination

An example of the total energy release rate variation associated with local delamination (neglecting hygrothermal effects) with the crack length is presented in Fig. 3.14. The asymptotic value of G_T is denoted by G_{TO} in the figure. It can be observed that after a certain crack length, the G_T is independent of the crack length. On the basis of curves like the one shown in Fig. 3.14, the crack length was fixed at 10 ply thicknesses for the remainder of the studies. Typical interlaminar shear stress profiles including the hygrothermal effect are presented in Fig. 3.15. The corresponding total strain energy release rates appear in Fig. 3.16. The inclusion of thermal effects increases

the stress and the energy release rate while the inclusion of moisture effects has the opposite effect. In fact a moisture level of about 0.75% almost exactly negates the thermal effects. After some initial dependence on crack length, the mode mix tended to stabilize to a constant value. Using the model developed here, the asymptotic mode II component of the local delamination energy release rate was found to be approximately 30 percent for all n values. In the case of off-mid-plane edge delamination, the mode II contribution was less than 10 percent for the $n = 0.5$ specimen and progressively less for the thicker specimen.

3.2.2 Edge Delamination

As in the case of local delaminations, the interlaminar stress increases with thermal effects and the addition of moisture alleviates this as shown in Fig. 3.17 for the case of mid-plane edge delamination. A moisture level of about 0.75% produces a modified peel stress distribution that is indistinguishable from the case of mechanical loading alone. Moreover, the distance at which the modified peel stress reverses its sign is not affected by the residual hygrothermal strains. The hygrothermal influence on mid-plane delamination strain energy release rate is illustrated in Fig. 3.18 where the strain energy release rate is plotted versus moisture content for a $[\pm 25/90_2]_s$ laminate. The strain energy release rate follows the trend of increasing with residual thermal stress as in the case of peel stress. Further, residual moisture alleviates the thermal effects and a moisture level of about 0.75% results in a total alleviation of thermal effects. Similar behavior is observed in the case of off-mid-plane edge delamination.

3.2.3 Failure Loads and Modes

In order to evaluate the critical loads for local delamination, an appropriate mixed mode fracture law has to be applied, based on the calculated energy release compo-

nents. The following mixed mode criterion [22] has been fitted to the test data of Ref. [23] to calculate the mixed mode G_{Tc} which is then used in the Griffith criterion $G_T = G_{Tc}$ to obtain the critical delamination growth stress σ_c and strain ε_c values.

$$G_{Tc} = \xi^{\eta} G_{Ic} + (1 - \xi)^{\eta} G_{IIc}$$

Here ξ is the mode I fraction (G_I/G_T) and G_{Ic} and G_{IIc} are the critical strain energy release rates for the limiting cases of pure mode I and pure mode II, respectively. The exponential parameter η is a material constant and for the T300/934 system, its value is approximately 0.9. In the case of mid-plane delamination, since only mode I is present, G_{Tc} was taken as $G_{Ic}(125 J/m^2)$. Based on the mixed mode criterion, G_{Tc} was about $400 J/m^2$ for the local delamination case ($\xi = 0.7$). The failure loads for edge delamination at the $-25/90$ interface have also been calculated using a G_{Tc} value of 150 J/m^2. This G_{Tc} value is different from the value used for mid-plane delamination due to the limited (less than 10 percent) presence of mode II.

In order to consider a worst case situation, thermal stresses were included and the moisture level was set at zero. Though the thermal stresses had a significant effect on the calculated peak stresses, the effect on the energy release rate was not significant except in the case of mid-plane edge delamination for the material system and layup considered. The critical strains are plotted against n, the number of 90° plies in Fig. 3.19. The experimental results of Ref. [8] are also presented in the figure for comparison. The results of the model developed in this paper are represented by the solid and dotted lines while the experimental results are shown as filled squares. The CLT based model of Ref. [9] agrees well with the shear deformation model in terms of the total energy release rate. However, the CLT based model does not provide information on the mode split and thus, the value of $G_c(\approx G_{Ic})$ used can lead to bias in the critical strain estimates. In the experiments, the local delamination phenomenon

was observed as the predominant failure mode only for the $n = 4, 6$ and 8 specimens. The shear deformation model presented in this paper provides good agreement with the experimental data in this range. For $n < 4$, edge delamination either in the mid-plane or in the 25/90 interface was observed in the tests, in agreement with the edge delamination models. Further, the relative closeness of the calculated critical strains from the mid-plane and off-mid-plane edge delamination models implies that, in practice, one could have interaction between these two modes. In such cases, one can expect the delamination to wander around the mid-plane and the 25/90 interfaces. This is especially so in the case $n = 0.5$ where mid-plane delamination is not actually between two distinct layers but in the middle of a single layer. Experimental observations [8] are in agreement with this expectation. Thus, it can be seen that the shear deformation models reproduce the observed behavior with reasonable accuracy and can be used to estimate critical loads for a range specimen thicknesses incorporating various delamination modes.

3.3 Conclusions

Shear deformation models including hygrothermal effects have been developed to analyze local delaminations growing from transverse cracks in 90° plies and edge delaminations located around the mid-plane of symmetric laminates. The models have been combined into a unified delamination analysis code in order to predict damage modes and loads in laminated composites. The analytical results of the shear deformation models agree reasonably with critical strain experimental data from $[\pm 25/90_n]_s$ T300/934 graphite epoxy laminates in the range of n from 0.5 to 8. Residual thermal and moisture stresses are found to have only minor effects on the critical strains except in the case of mid-plane edge delamination for the geometry

and material considered. The same failure modes as in the tests are reproduced in the analysis. The integrated delamination code is expected to be of use in design evaluation applications.

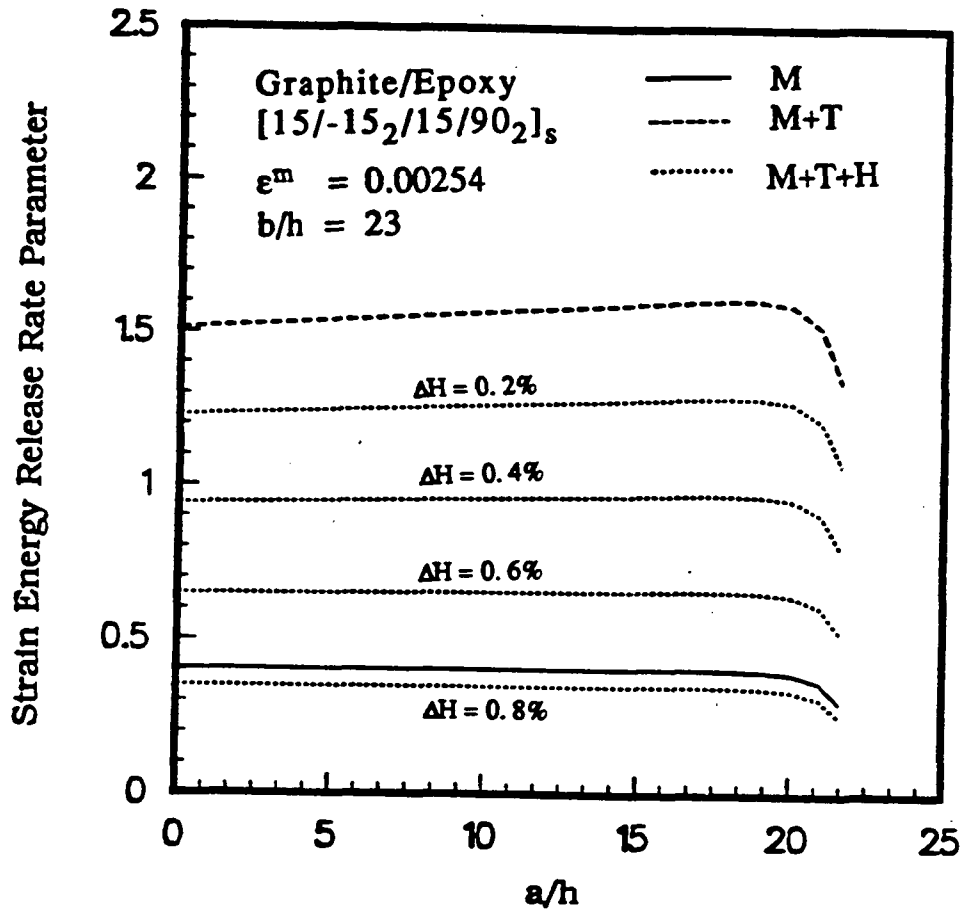

Figure 3.1: Mode I Strain Energy Release Rate in a $[15/-15_2/15/90_2]_s$ Laminate

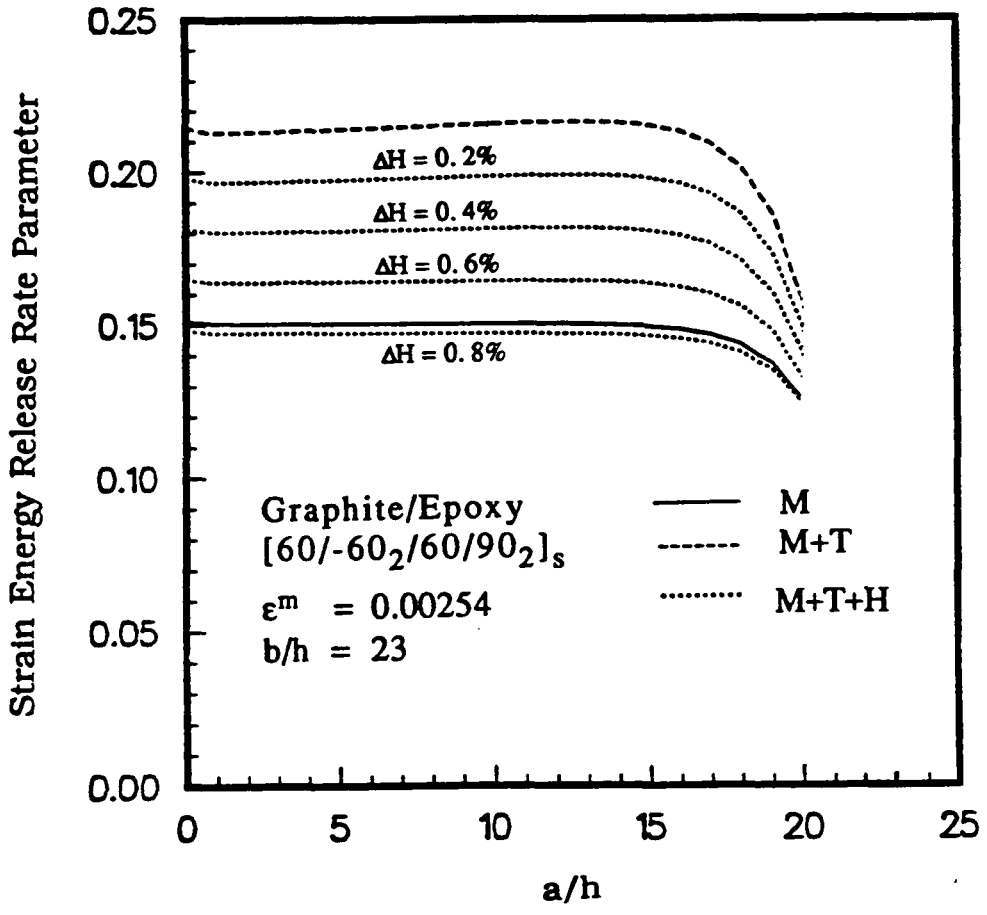

Figure 3.2: Mode I Strain Energy Release Rate in a $[60/-60_2/60/90_2]_s$ Laminate

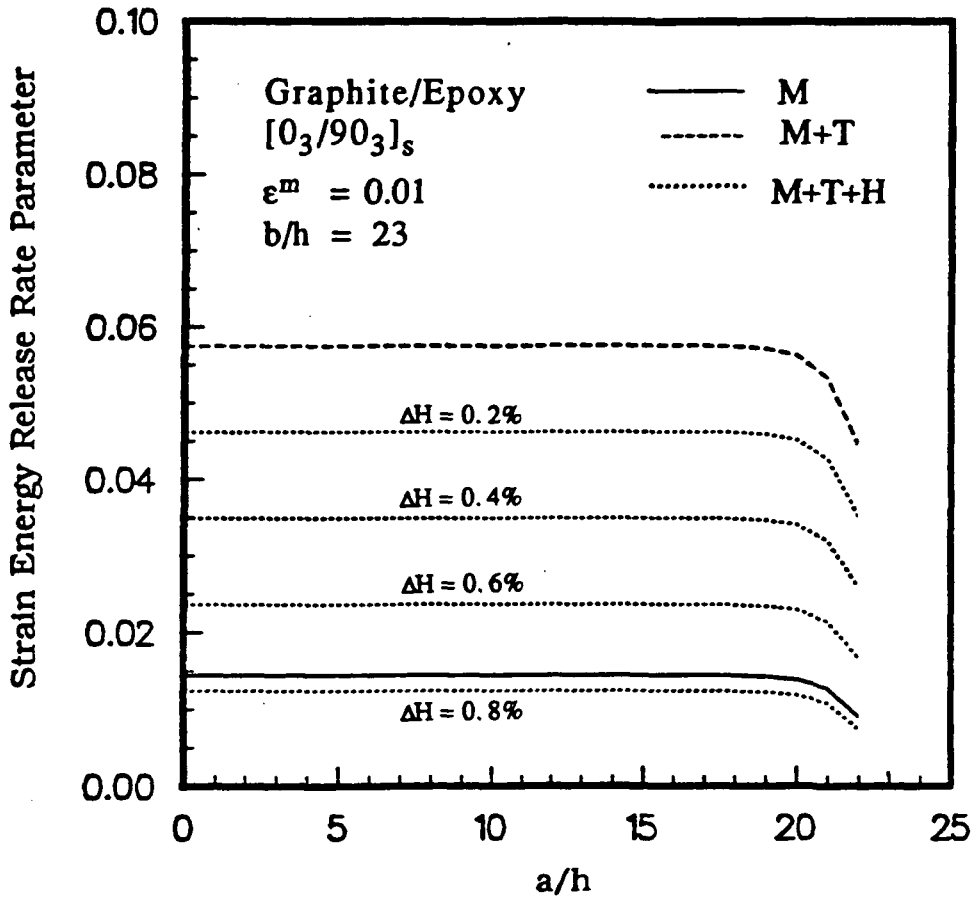

Figure 3.3: Mode I Strain Energy Release Rate in a $[0_3/90_3]_s$ Laminate

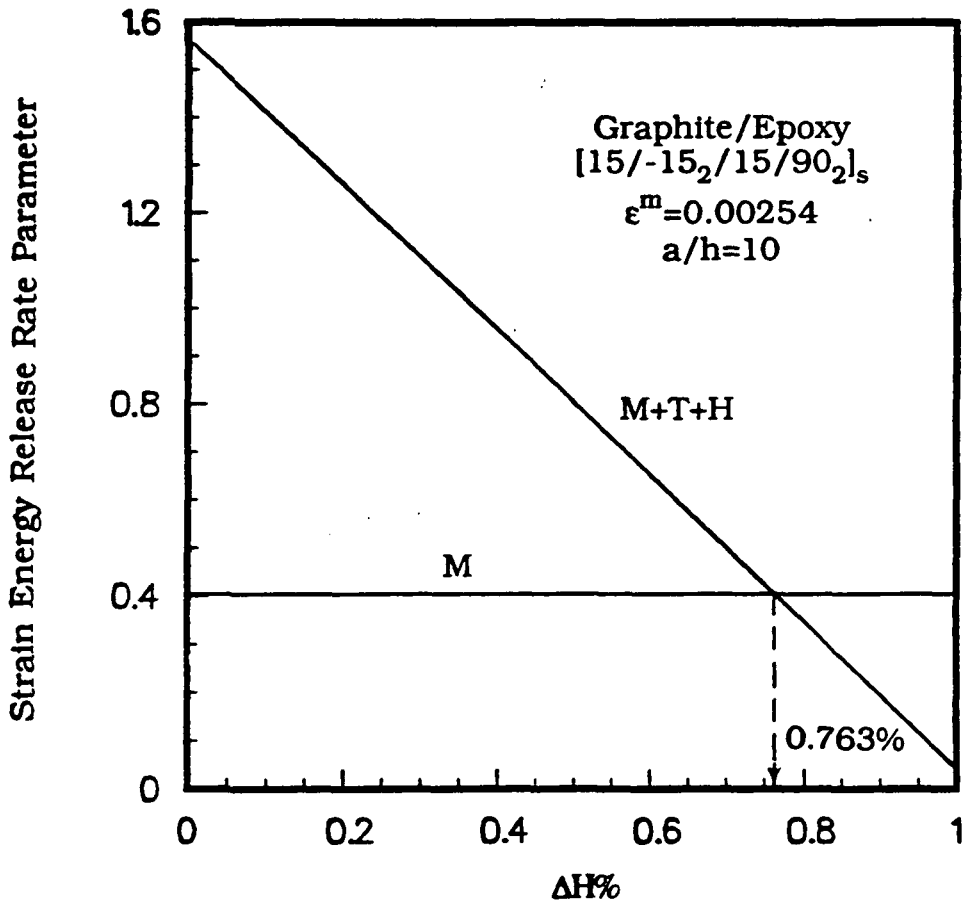

Figure 3.4: Influence of Residual Thermal and Moisture Stresses on Mode I Strain Energy Release Rate in a $[15/-15_2/15/90_2]_s$ Laminate

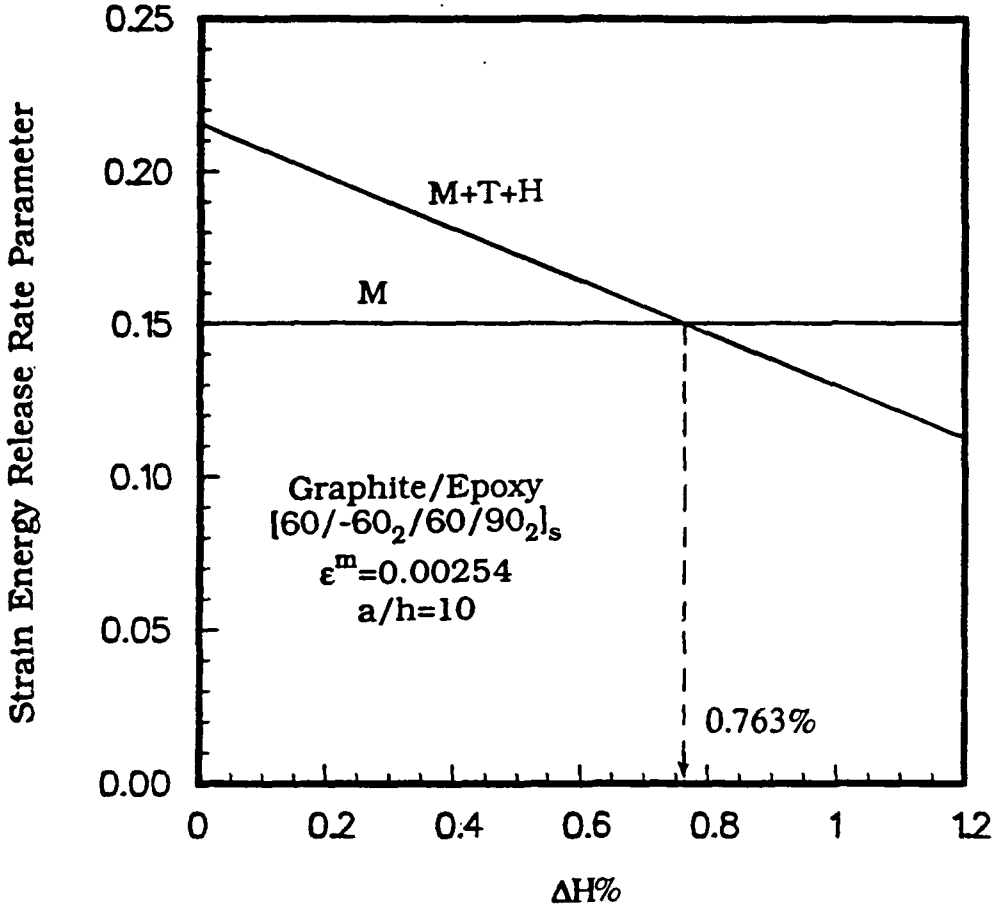

Figure 3.5: Influence of Residual Thermal and Moisture Stresses on Mode I Strain Energy Release Rate in a $[60/-60_2/60/90_2]_s$ Laminate

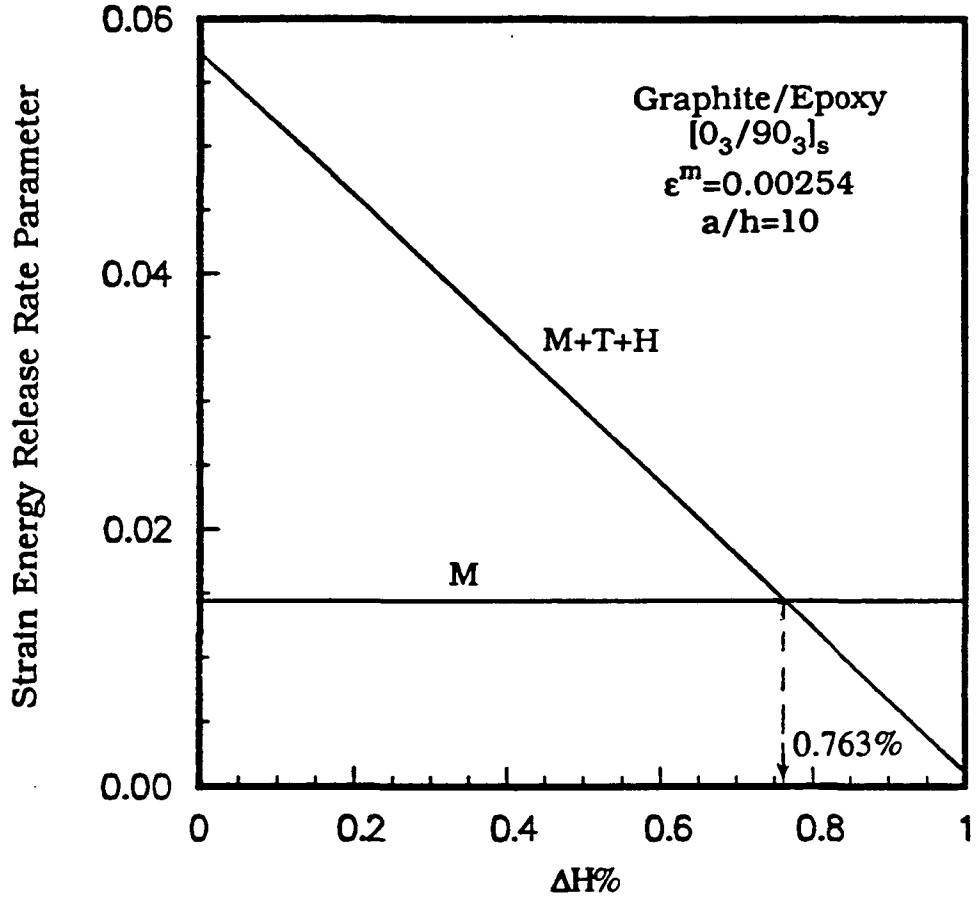

Figure 3.6: Influence of Residual Thermal and Moisture Stresses on Mode I Strain Energy Release Rate in a $[0_3/90_3]_s$ Laminate

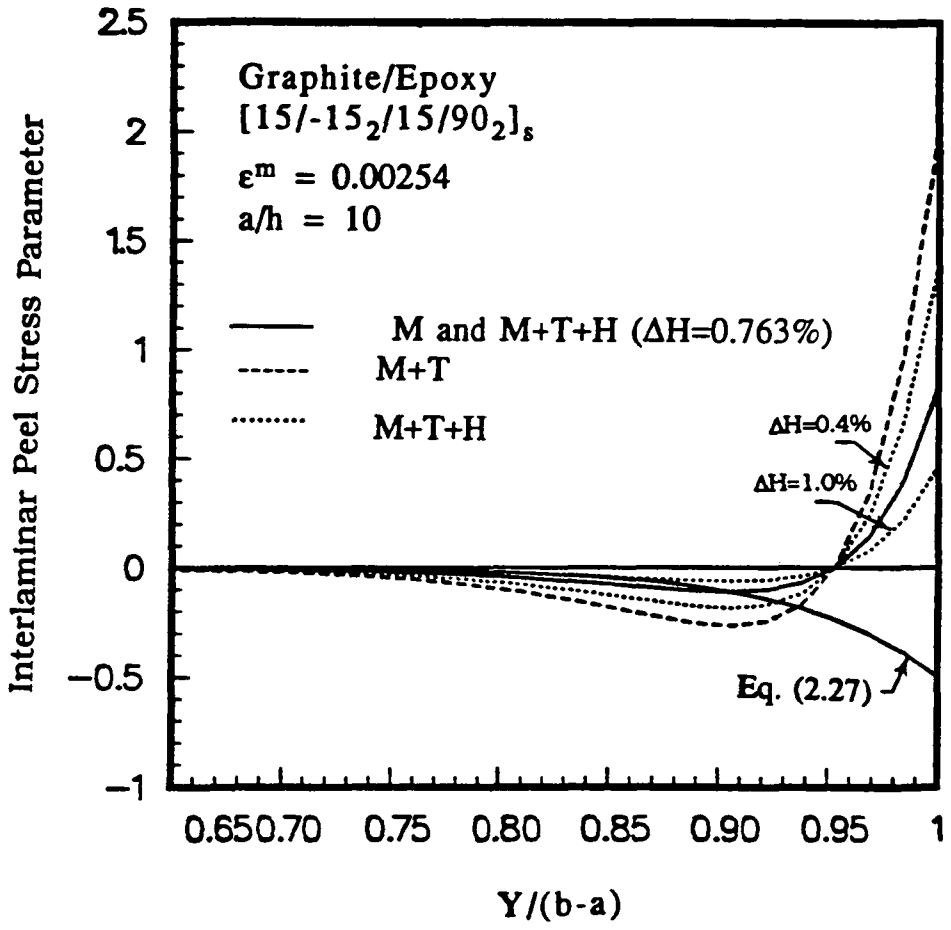

Figure 3.7: Peel Stress Distribution ahead of the Crack in a $[15/-15_2/15/90_2]_s$ Laminate

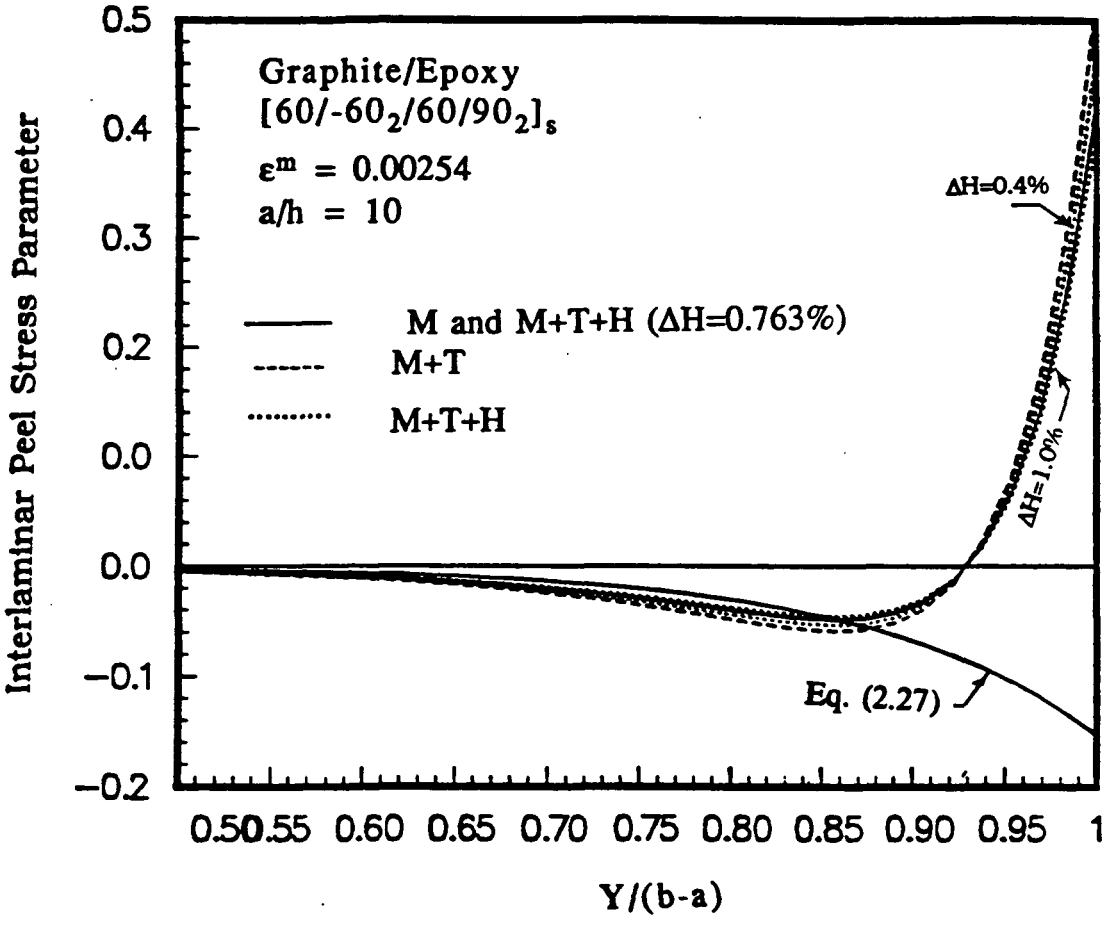

Figure 3.8: Peel Stress Distribution ahead of the Crack in a [60/ − 60$_2$/60/90$_2$]$_s$ Laminate

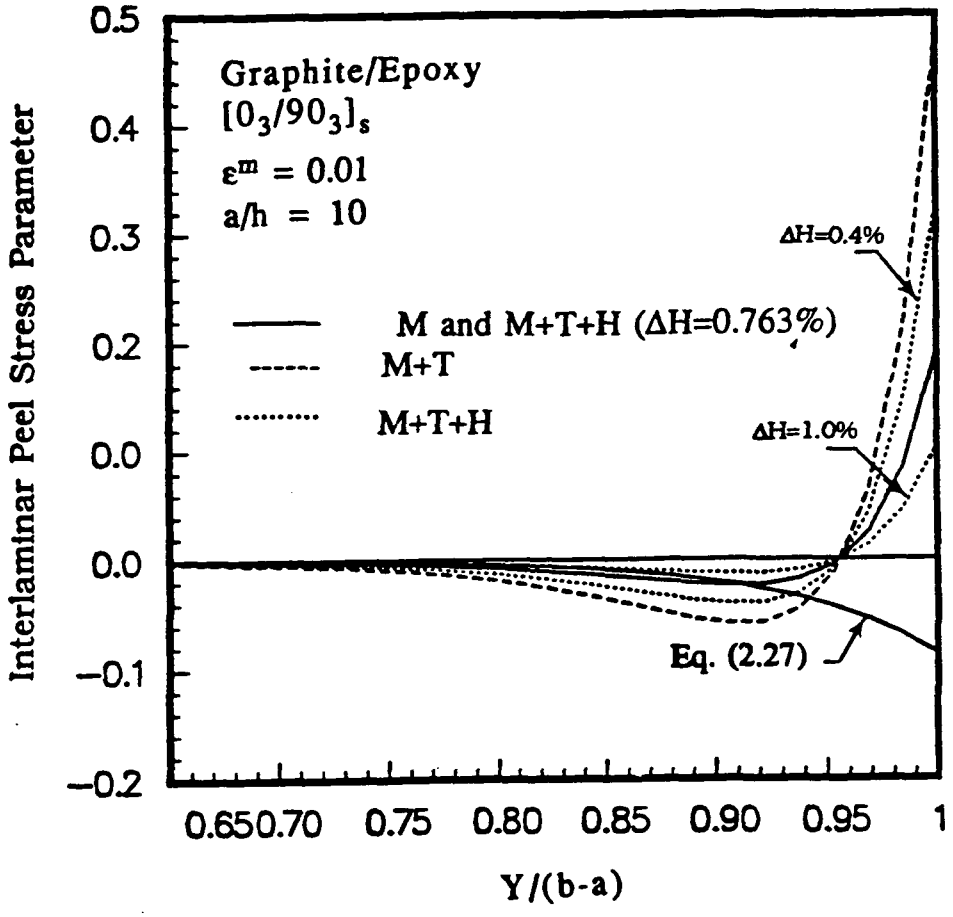

Figure 3.9: Peel Stress Distribution ahead of the Crack in a $[0_3/90_3]_s$ Laminate

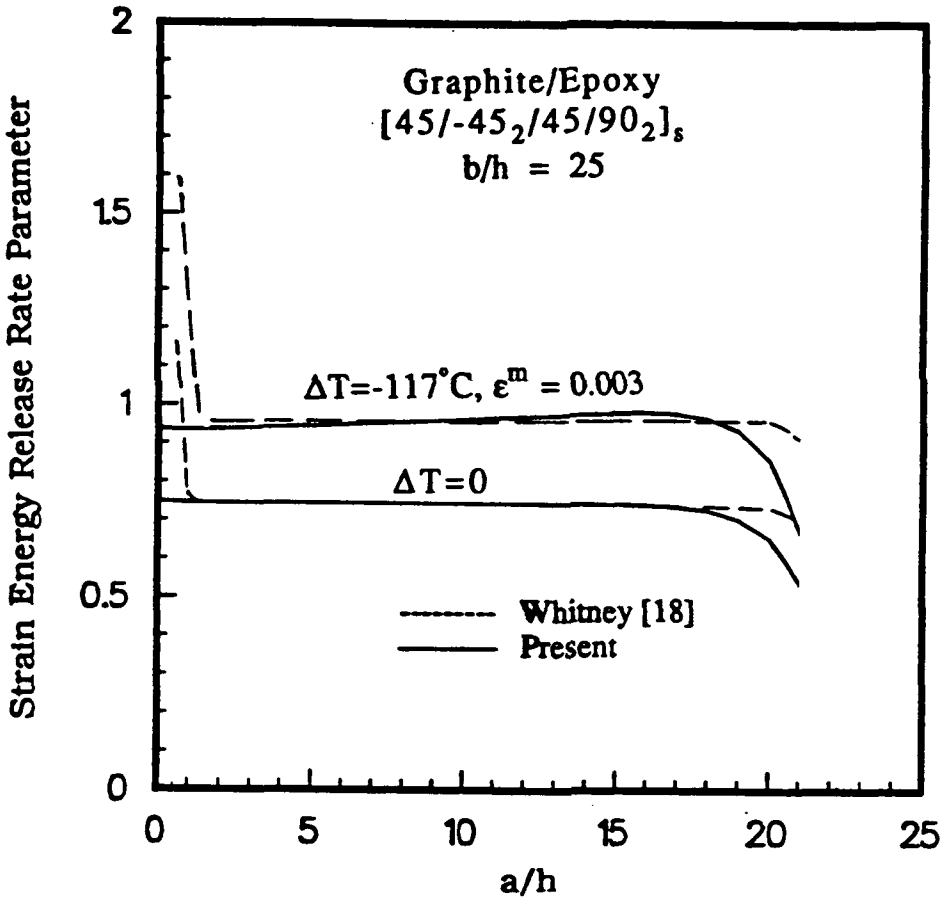

Figure 3.10: Mode I Strain Energy Release Rate in a $[45/-45_2/45/90_2]_s$ Laminate

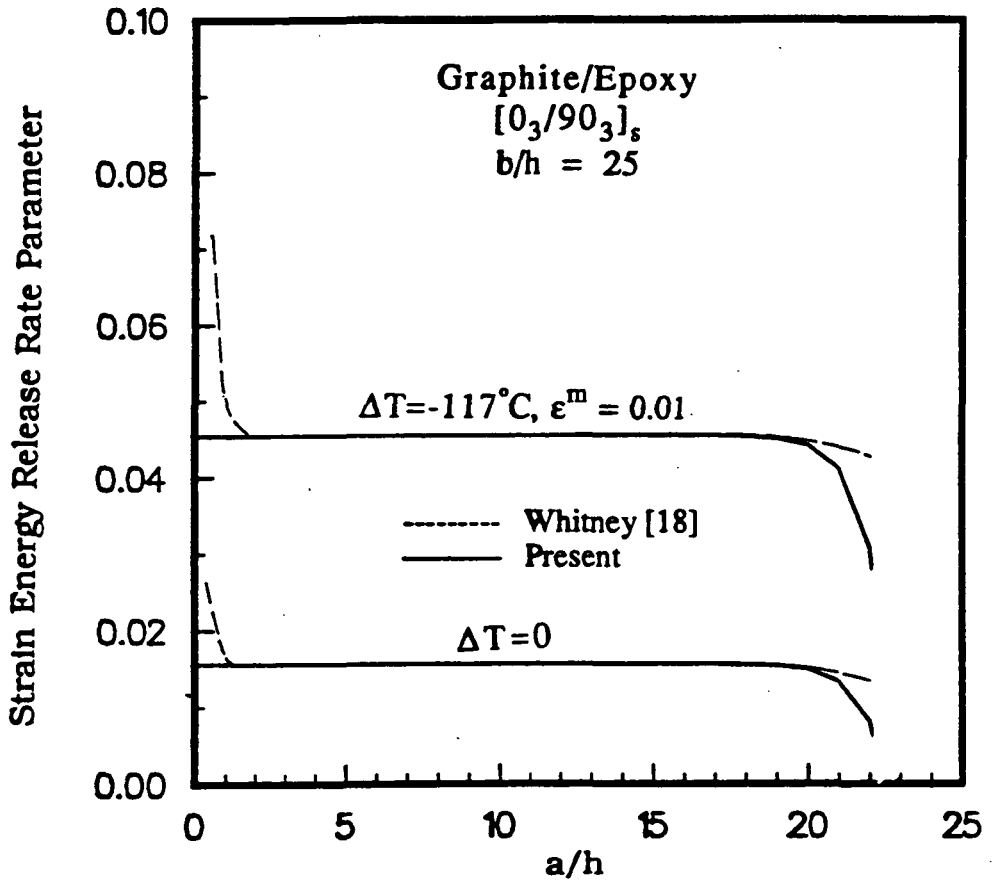

Figure 3.11: Mode I Strain Energy Release Rate in a $[0_3/90_3]_s$ Laminate

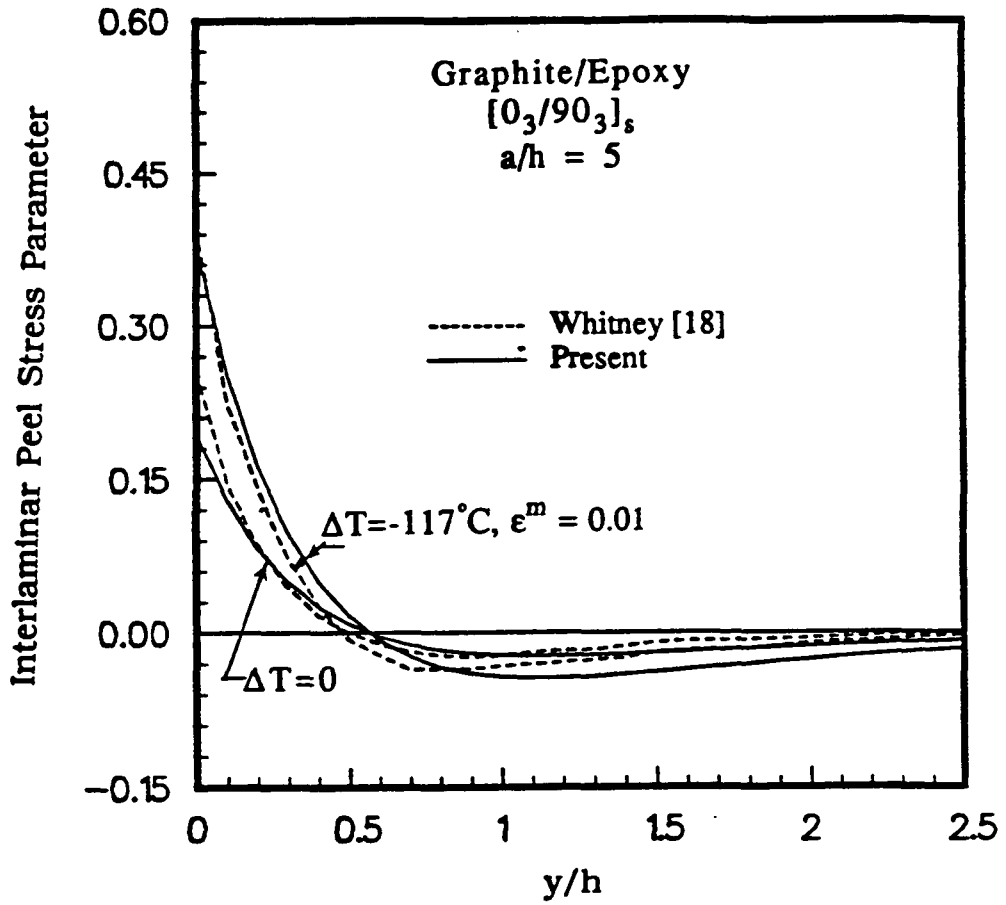

Figure 3.12: Peel Stress Distribution ahead of the Crack in a $[0_3/90_3]_s$ Laminate

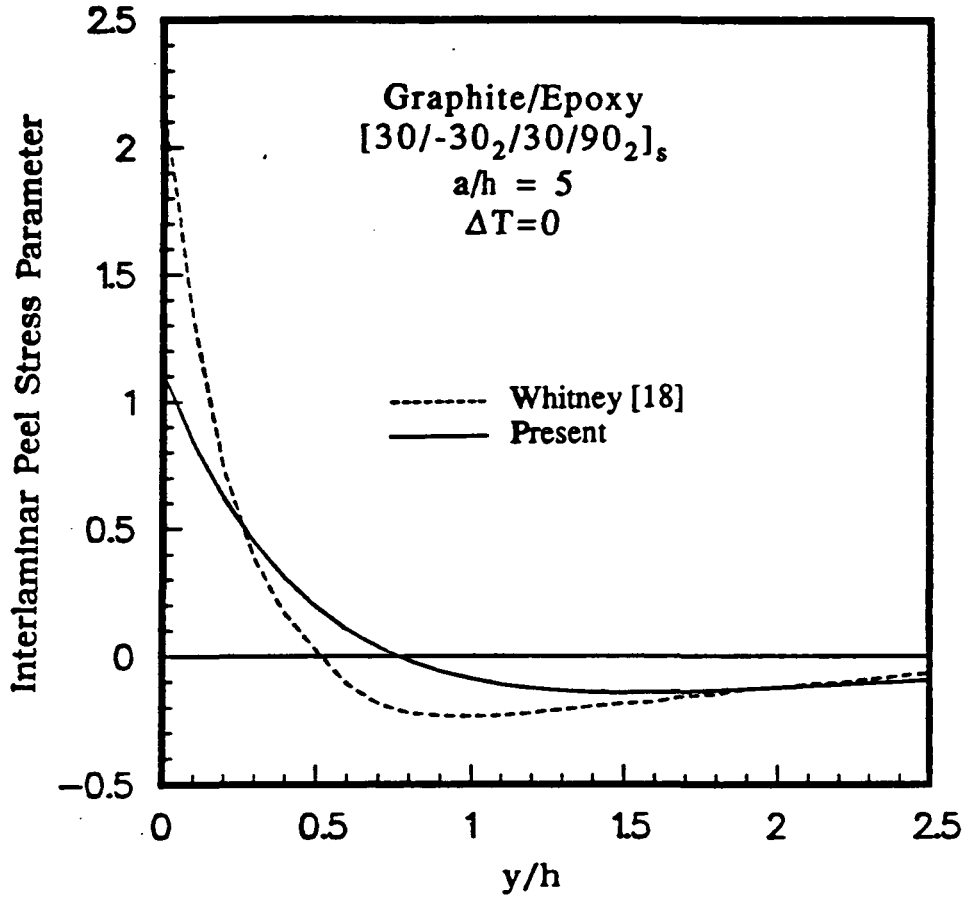

Figure 3.13: Peel Stress Distribution ahead of the Crack in a $[30/-30_2/30/90_2]_s$ Laminate

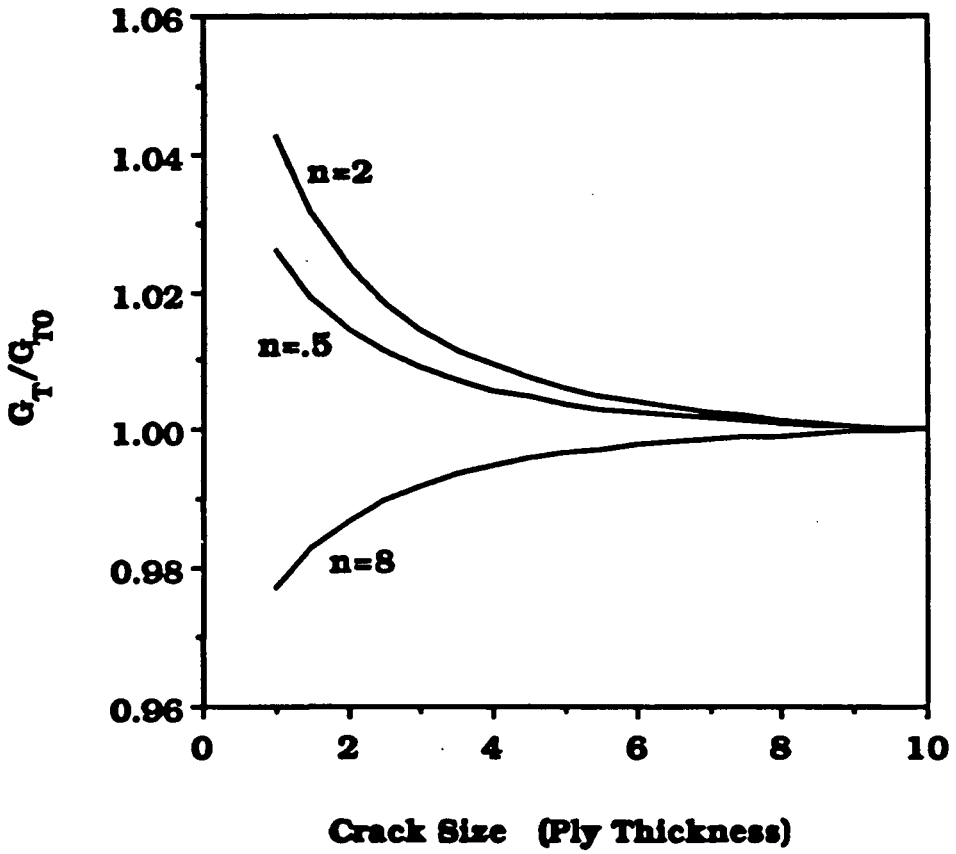

Figure 3.14: Total Local Delamination Energy Release Rate Variation

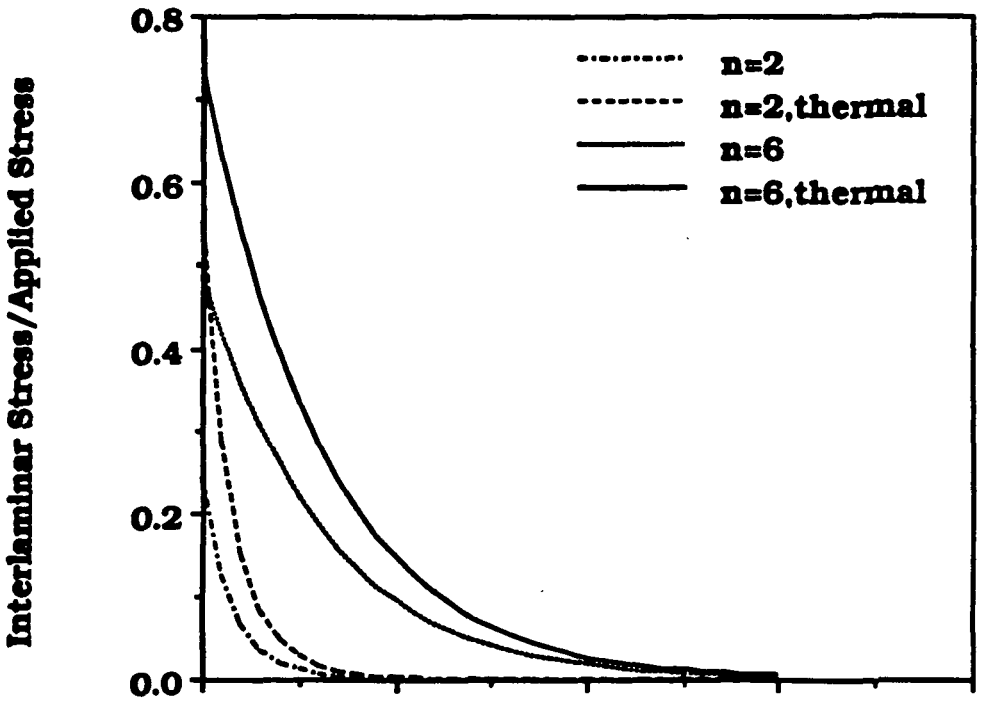

Figure 3.15: Interlaminar Shear Stress Distribution (Local Delamination)

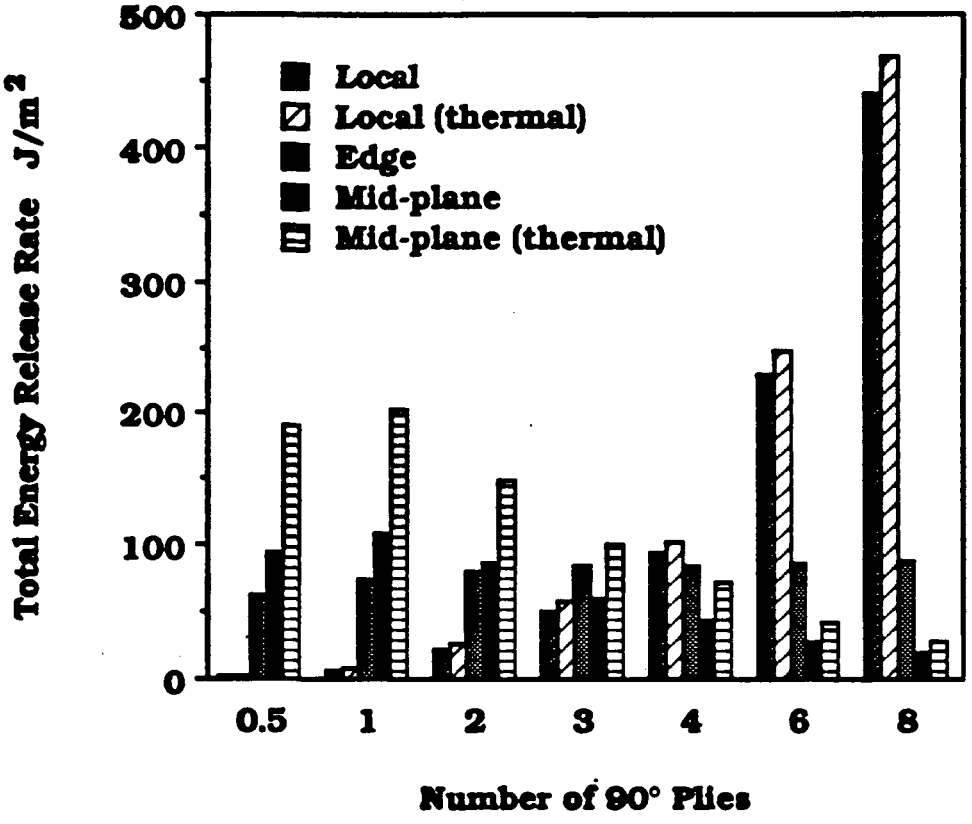

Figure 3.16: Total Energy Release Rate for $[\pm 25/90_n]_s$ Graphite/Epoxy Specimen

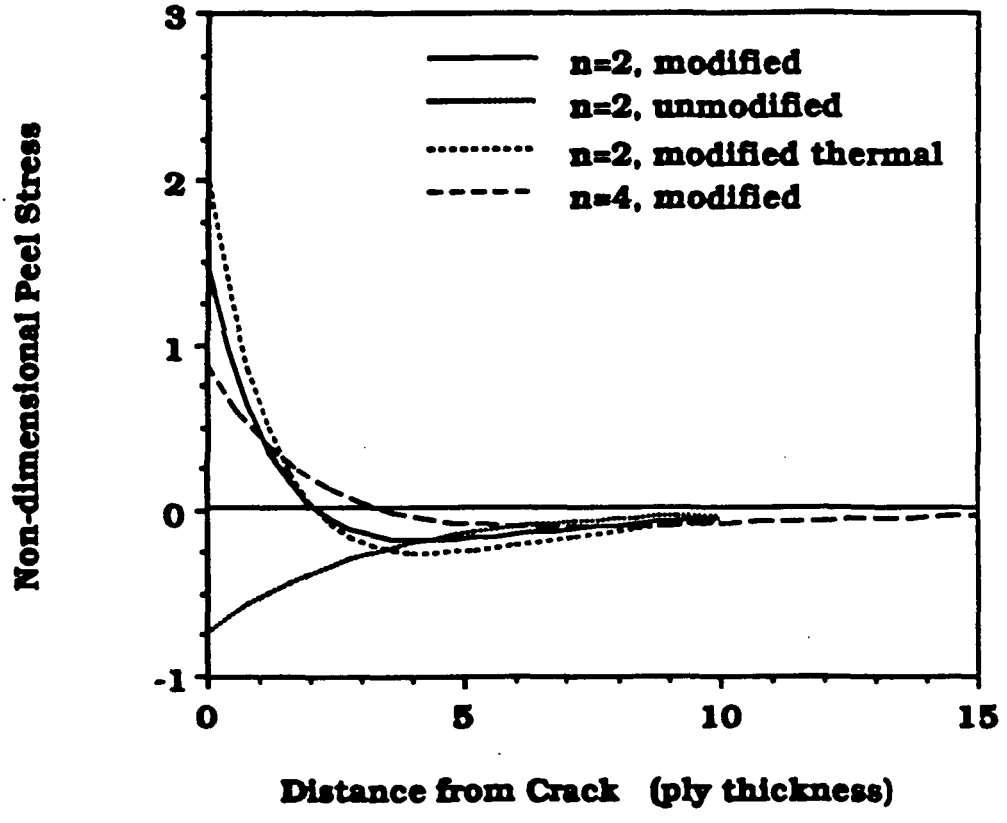

Figure 3.17: Interlaminar Normal Stress (Mid Plane Delamination)

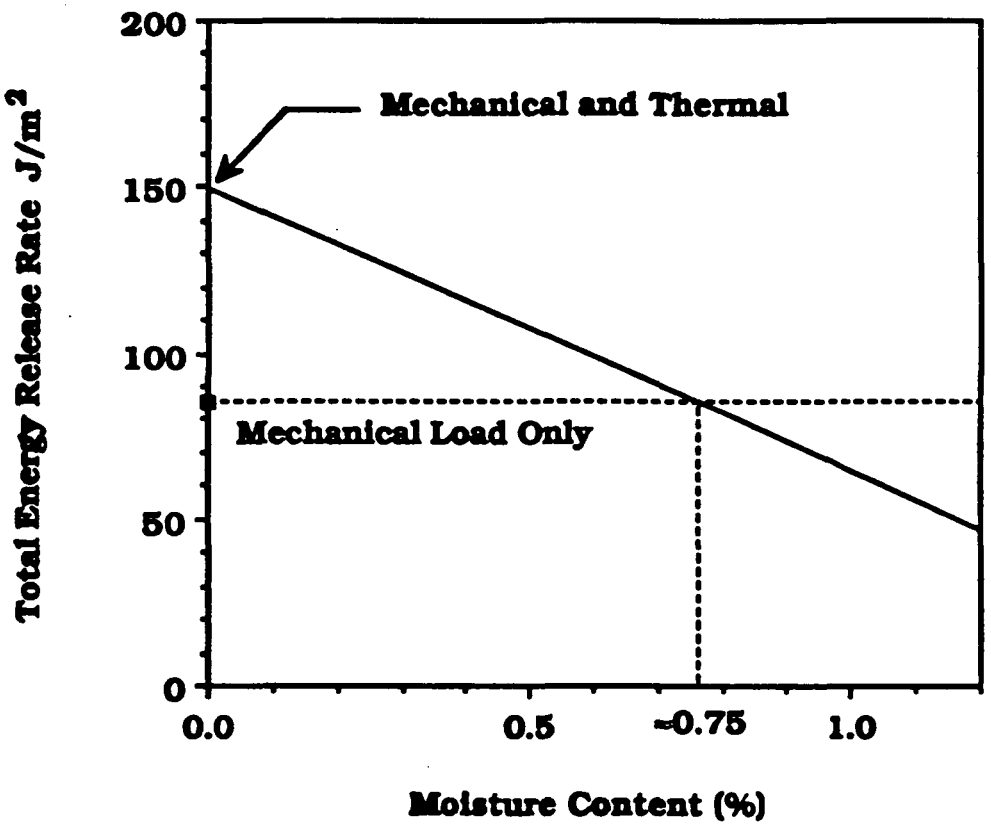

Figure 3.18: Total Energy Release Rate (Mid Plane Delamination) for $[\pm 25/90_2]_s$

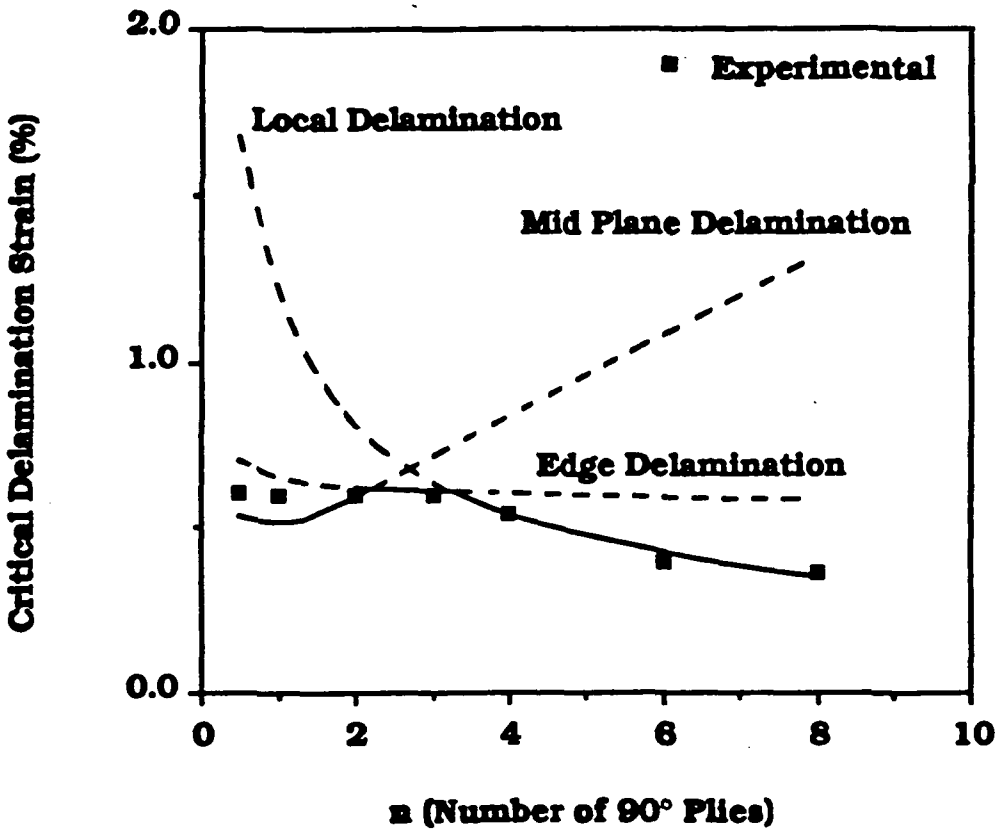

Figure 3.19: Critical Delamination Strain Variation

CHAPTER IV

THEORY OF ANISOTROPIC THIN-WALLED BEAMS

A variationally and asymptotically consistent theory is developed in order to derive the governing equations of anisotropic thin-walled beams with closed cross sections. The theory is based on an asymptotical analysis of two-dimensional shell theory. Closed-form expressions for the beam stiffness coefficients, stress and displacement fields are provided. The influence of material anisotropy on the displacement field is identified. A comparison of results obtained by other analytical developments is performed.

A review of previous work is presented first, this is followed by a detailed development of the theory. Finally an analytical comparison of the displacement field with previously developed theories is provided.

4.1 Review of Previous Work

Elastically tailored composite designs are being used to achieve favorable deformation modes under a given loading environment. Coupling between deformation modes such as extension-twist or bending-twist is created by an appropriate selection of fiber orientation, stacking sequence and materials. The fundamental mechanism producing elastic tailoring in composite beams is a result of their anisotropy. Several theories have been developed for the analysis of thin-walled anisotropic beams. An extensive review is provided in Ref. [26]. A number of issues relevant to the research undertaken in this thesis is highlited in the following.

A basic element in the analytical modeling development is the derivation of the effective stiffness coefficients and governing equations which allows the three-dimensional ($3D$) state of stress to be recovered from a one-dimensional ($1D$) beam formulation. For isotropic or orthotropic materials this is a classical problem, which is considered in a number of text books such as Refs. [52]-[59].

For generally anisotropic materials, a description of the major approaches is provided in Refs. [24]-[49]. A number of $1D$ theories have been developed in Refs. [27], [28], [30], [42], [43], and [46]. A discussion of the displacement provided in these works is presented in the analytical comparison section of this chapter.

Missing from the review of Ref. [26] and all other current publications is the work of Reissner and Tsai in Ref. [27]. It presents an exact solution to the governing equilibrium, compatibility and constitutive relationships of shell theory. Closed as well as open cross-sections were considered. However, the authors left to the reader the derivation of the explicit expressions for the stiffness coefficients. This may be the reason for their work to have been overlooked. These expressions are important in identifying the parameters controlling the behavior and in performing parametric design studies. Furthermore, the explicit form of the displacement field helps evaluate and understand predictions of other analytical and numerical models.

A number of assumptions were adopted in Reissner and Tsai's development regarding material properties such as neglecting the coupling between in-plane strains and curvature which can be significant in anisotropic materials. It is important to assess the influence of these assumptions on the accuracy. This has been done in the present work by using an asymptotical expansion of the shell energy.

Mansfield and Sobey [28] and Libove [29] obtained the beam flexibilities relating the stretching, twisting and bending deformations to the applied axial load, torsional and bending moments for a special origin and axes orientation. Their analyses are

similar. Although they did not refer to the work of Reissner and Tsai [27], surprisingly when their analyses is applied to the special case outlined in Ref. [27], their stiffnesses coincide. However, one has to carry out details to show this fact. They adopted the assumptions of a negligible hoop stress resultant N_{ss} and a membrane state in the thin-walled beam section. The special case in Ref. [27] refers to the one where classical assumption of neglecting shear, hoop stress and constant shear flow is adopted.

A pertinent element in the analytical modeling development is the inclusion of section warping. The major difference among the various theories lies in the methodology used to eliminate warping and consequently obtain a one-dimensional theory. The work of Refs. [30], [41], [42], [43], [44], [45], and [46] use the displacement field of thin-walled isotropic beams with shear deformation as the basis of their analytical development. In Refs. [42] and [46] the torsional rigidity is derived in terms of Classical Lamination Theory in what the author described as a "practical manner". In Refs. [43] and [44] a shear correction factor has been introduced in order to reduce the overestimated bending stiffness. This factor was derived for the case of pure torsion by using the virtual work method and enforcing compatibility. While this approach shows an improvement in predictions, it is problem dependent. Another modification was proposed in the finite element formulation of Ref. [38]. This formulation aims at minimizing the error associated with the neglect of bending-related warping in the theory of Ref. [30]. This modification was based on shear stiffness correction factors determined by numerical comparison of results with an MSC/NASTRAN solution of cantilevered beam configurations loaded transversely at the free end.

This summary points to the necessity of addressing three fundamental issues. The first, is the effect of the material's anisotropy on the displacement field and how to include its contribution in a consistent manner. No rigorous proof is provided to validate the assumed displacement fields in Refs. [30], [42], [43], [44], [45], and

[46] for beams made of anisotropic material as indicated by the various correction factors introduced. The second, is the significance of the shear deformation relative to the other contributions such as section related warping. The last is the accuracy of the membrane stress state assumption in thin-walled anisotropic beam sections. The present work addresses these issues by using an asymptotical expansion of the $2D$ shell energy to derive the $1D$ beam displacement field. As a consequence, the material's anisotropy is accounted for in a consistent manner and the deformation modes that have a lead contribution to the energy emerge naturally.

4.2 Coordinate Systems

Consider the slender thin-walled elastic cylindrical shell shown in Fig. 4.1. The length of the shell is denoted by L, its thickness by h, the radius of curvature of the middle surface by R and the maximum cross sectional dimension by d. It is assumed that

$$d << L \qquad h << d \qquad h << R \tag{4.1}$$

The shell is loaded by external forces applied to the lateral surfaces and at the ends. It is assumed that the variation of the external forces and material properties over distances of order d in the axial direction and over distances of order h in the circumferential direction, is small. The material is anisotropic and its properties can vary circumferentially and in the normal direction to the middle surface as well.

It is convenient to consider two coordinate systems for the description of the state of stress in thin-walled beams. The first one is the Cartesian system x, y and z shown in Fig. 4.1. The axial coordinate is x while y and z are associated with the beam cross section. The second coordinate system, is the curvilinear system x, s and ξ shown in Fig. 4.2. The circumferential coordinate s is measured along the tangent to the middle surface in a counter-clockwise direction whereas ξ is measured along

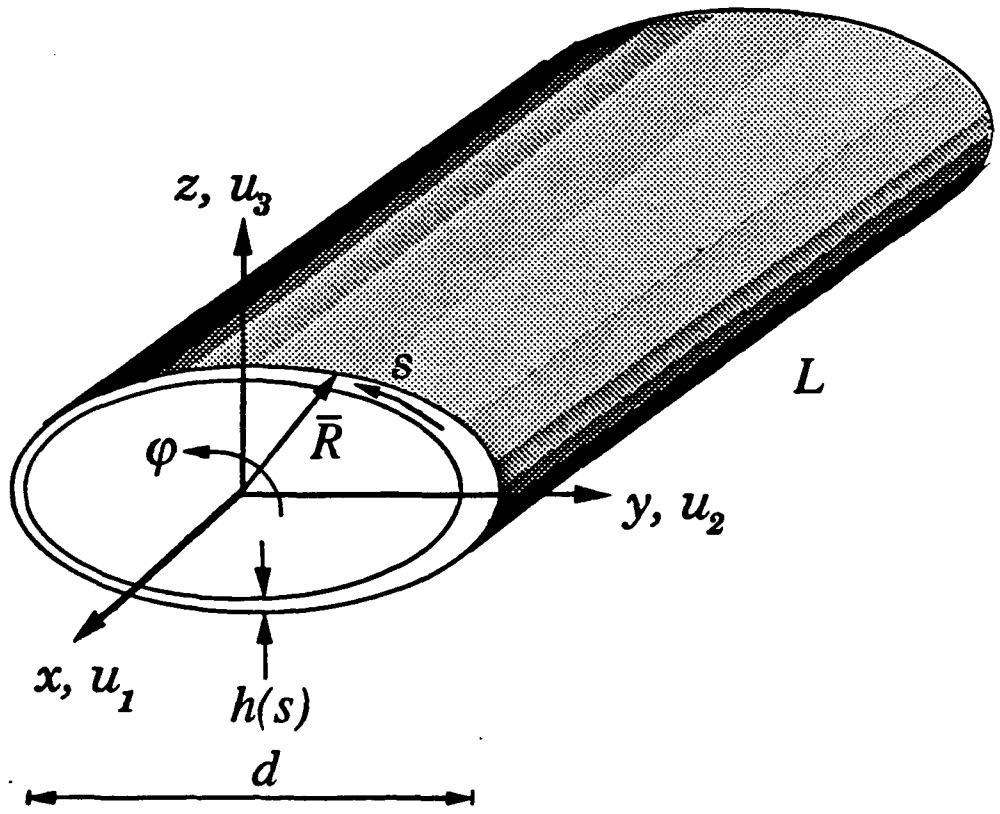

Figure 4.1: Cartesian Coordinate System

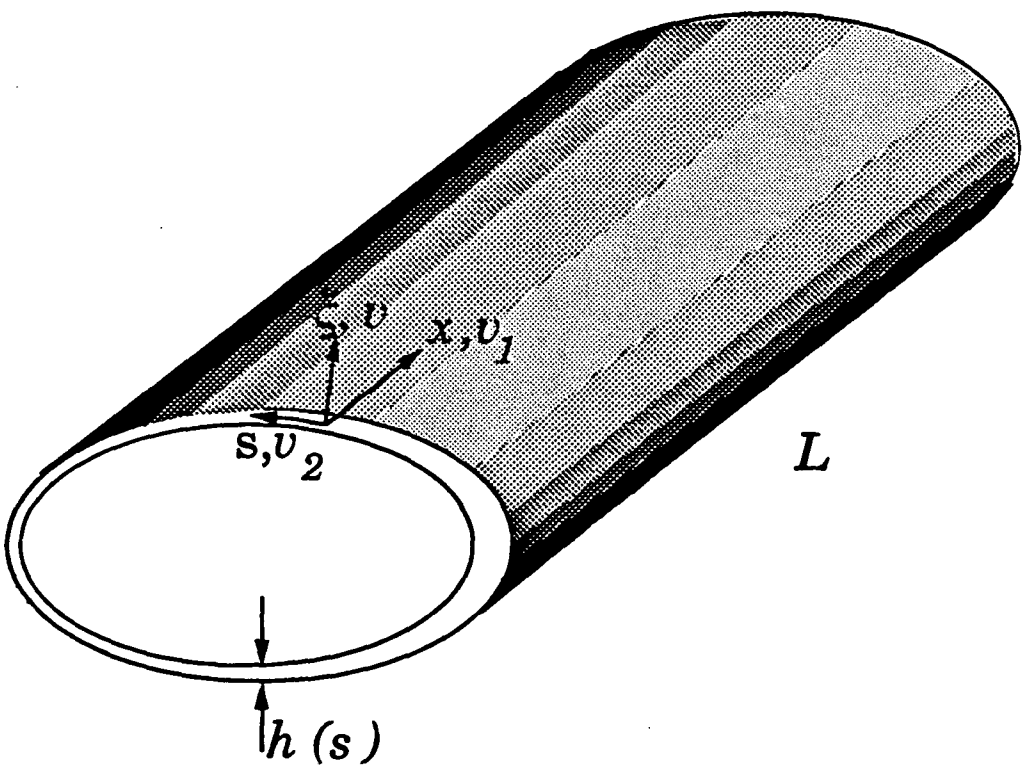

Figure 4.2: Curvilinear Coordinate System

the outward normal to the middle surface. A number of relationships have a simpler form when expressed in terms of curvilinear coordinates. A relationship between the two coordinate systems can be established as follows.

Define the position vector $\vec{r}$ of the shell middle surface as

$$\vec{r} = x\vec{i}_x + y(s)\vec{i}_y + z(s)\vec{i}_z$$

where $\vec{i}_x$, $\vec{i}_y$, $\vec{i}_z$ are unit vectors associated with the cartesian coordinate system x, y and z. Equations $y = y(s)$ and $z = z(s)$ define the closed contour Γ in the y, z plane. The normal vector to the middle surface $\vec{n}$ has two nonzero components

$$\vec{n} = n_y(s)\vec{i}_y + n_z(s)\vec{i}_z \tag{4.2}$$

The position vector $\vec{R}$ of an arbitrary material point can be written in the form

$$\vec{R} = \vec{r} + \xi\vec{n} \tag{4.3}$$

Equations (4.2) and (4.3) establish the relations between the cartesian coordinates x, y, z and the curvilinear coordinates x, s, ξ. The coordinate ξ lies within the limits

$$-\frac{h(s)}{2} \leq \xi \leq \frac{h(s)}{2}$$

The shell thickness varies along the circumferential direction and is denoted by $h(s)$.

The tangent vector $\vec{t}$, the normal vector $\vec{n}$ and the projection of the position vector $\vec{r}$ on $\vec{t}$ and $\vec{n}$ are expressed in terms of the cartesian and curvilinear coordinates as

$$\begin{aligned}
\vec{t} &= \frac{d\vec{r}}{ds} = \frac{dy}{ds}\vec{i}_y + \frac{dz}{ds}\vec{i}_z \\
\vec{n} &= \vec{t} \times \vec{i}_x = \frac{dz}{ds}\vec{i}_y - \frac{dy}{ds}\vec{i}_z \\
r_t &= \vec{r} \cdot \vec{t} = y\frac{dy}{ds} + z\frac{dz}{ds} \\
r_n &= \vec{r} \cdot \vec{n} = y\frac{dz}{ds} - z\frac{dy}{ds}
\end{aligned} \tag{4.4}$$

An asymptotical analysis is used to model the slender thin-walled shell as a beam with effective stiffnesses. The method follows an iterative process. The displacement function corresponding to the zeroth-order approximation is obtained first by keeping the leading order terms in the energy functional. A set of successive corrections is added and the associated energy functional is determined. The process is terminated when the new cycle does not generate any additional terms of the same order in the energy functional.

4.3 Shell Energy Functional

Consider in a $3D$ space the prismatic shell in Fig. 4.2. A curvilinear frame x, s, and ξ is associated with the undeformed shell configuration. Values 1, 2 and 3 denoting x, s, and ξ, respectively are assigned to the curvilinear frame. Throughout this study, Latin superscripts (or subscripts) run from 1 to 3, while Greek superscripts (or subscripts) run from 1 to 2, unless otherwise stated.

The strain energy density of a $3D$ elastic body is a quadratic form of the strains

$$U = \frac{1}{2} E^{ijkl} \varepsilon_{ij} \varepsilon_{kl}$$

The material properties are expressed by the Hookean tensor E^{ijkl}. Following the classical shell formulation of [60], [61], and [62] the through-the-thickness stress components σ^{i3} are considerably smaller than the remaining components $\sigma^{\alpha\beta}$. Therefore we can set

$$\sigma^{i3} = 0 \tag{4.5}$$

so that the strains can be written as

$$\varepsilon_{\alpha\beta} = \gamma_{\alpha\beta} + \xi \rho_{\alpha\beta} \tag{4.6}$$

where $\gamma_{\alpha\beta}$ and $\rho_{\alpha\beta}$ represent the in-plane strain components and the change in the shell middle surface curvatures, respectively. For a cylindrical shell these are related to the displacement variables by

$$\begin{aligned}
\gamma_{11} &= \frac{\partial v_1}{\partial x} \\
2\gamma_{12} &= \frac{\partial v_1}{\partial s} + \frac{\partial v_2}{\partial x} \\
\gamma_{22} &= \frac{\partial v_2}{\partial s} + \frac{v}{R} \\
\rho_{11} &= \frac{\partial^2 v}{\partial x^2} \\
\rho_{12} &= \frac{\partial^2 v}{\partial s \partial x} + \frac{1}{4R}\left(\frac{\partial v_1}{\partial s} - 3\frac{\partial v_2}{\partial x}\right) \\
\rho_{22} &= \frac{\partial^2 v}{\partial s^2} - \frac{\partial}{\partial s}\left(\frac{v_2}{R}\right)
\end{aligned} \tag{4.7}$$

where v_1, v_2 and v represent the middle surface displacements in the axial, tangential and normal directions, respectively as shown in Fig. 4.2. These are related to the displacement components in Cartesian coordinates by

$$\begin{aligned}
v_1 &= u_1 \\
v_2 &= u_2\frac{dy}{ds} + u_3\frac{dz}{ds} \\
v &= u_2\frac{dz}{ds} - u_3\frac{dy}{ds}
\end{aligned} \tag{4.8}$$

where u_1, u_2 and u_3 denote the displacements along the x, y and z coordinates, respectively.

The energy density of the $2D$ elastic body is obtained in terms of $\gamma_{\alpha\beta}$ and $\rho_{\alpha\beta}$ by the following procedure.

The $3D$ energy is first minimized with respect to ε_{i3}. This is equivalent to satisfying Eq. (4.5). The result is

$$\hat{U} = \min_{\varepsilon_{i3}} U = \frac{1}{2} D^{\alpha\beta\gamma\delta}\varepsilon_{\alpha\beta}\varepsilon_{\gamma\delta} \tag{4.9}$$

where $D^{\alpha\beta\gamma\delta}$ represent the component of the $2D$ Young's modulus. The expressions for $D^{\alpha\beta\gamma\delta}$ are given in terms of $E^{\alpha\beta\gamma\delta}$ by

$$D^{\alpha\beta\gamma\delta} = E^{\alpha\beta\gamma\delta} - \frac{E^{\alpha\beta 33}E^{\gamma\delta 33}}{E^{3333}} - H_{\mu\lambda}G^{\alpha\beta\mu}G^{\gamma\delta\lambda} \tag{4.10}$$

where

$$G^{\alpha\beta\mu} = E^{\alpha\beta\mu 3} - \frac{E^{\alpha\beta 33}E^{\mu 333}}{E^{3333}}$$

and $H_{\mu\lambda}$ are components of the inverse of the $2D$ matrix $\left\| E^{\mu 3\lambda 3} - \frac{E^{\mu 333}E^{\lambda 333}}{E^{3333}} \right\|$. The expression for $D^{\alpha\beta\gamma\delta}$ in terms of familiar Classical Lamination Theory (CLT) parameters is provided in Eqs. (4.43) and (4.44).

The strain $\varepsilon_{\alpha\beta}$ from Eq. (4.6) is substituted into Eq. (4.9). After integration of the result over the thickness ξ one obtains the energy of the shell Φ per unit middle surface area

$$2\Phi = hC^{\alpha\beta\gamma\delta}\gamma_{\alpha\beta}\gamma_{\gamma\delta} + h^2C_1^{\alpha\beta\gamma\delta}\gamma_{\alpha\beta}\rho_{\gamma\delta} + \frac{h^3}{12}C_2^{\alpha\beta\gamma\delta}\rho_{\alpha\beta}\rho_{\gamma\delta} \tag{4.11}$$

where

$$C^{\alpha\beta\gamma\delta} = \frac{1}{h} < D^{\alpha\beta\gamma\delta} >$$

$$C_1^{\alpha\beta\gamma\delta} = \frac{2}{h^2} < D^{\alpha\beta\gamma\delta}\xi >$$

$$C_2^{\alpha\beta\gamma\delta} = \frac{12}{h^3} < D^{\alpha\beta\gamma\delta}\xi^2 >$$

and a function of ξ, say $\alpha(\xi)$, between pointed brackets is defined as an integral through the thickness, viz.,

$$< \alpha >= \int_{-h(s)/2}^{+h(s)/2} \alpha(\xi)d\xi \tag{4.12}$$

The first term in Eq. (4.11) represents the in-plane contribution, the second the coupling between in-plane and bending, and the third the bending contribution to the shell energy.

For an applied external loading P_i, the displacement field u_i determining the deformed state are the stationary points of the energy functional

$$I = \int \Phi dx ds - \int P_i u_i dx ds \qquad (4.13)$$

4.4 Asymptotical Analysis of the Shell Energy Functional

4.4.1 Zeroth-Order Approximation

Let Δ and E be the order of displacements and stiffness coefficients $C^{\alpha\beta\gamma\delta}$, respectively. Assume that the order of the external forces is

$$P \sim O\left(\frac{E\Delta h}{L^2}\right) \qquad (4.14)$$

This assumption is shown later to be consistent with the equilibrium equations. An alternative would be to assume the order of the external force as some quantity P and derive the order of the displacements as PL^2/Eh from an asymptotical analysis of the energy functional.

For a thin-walled slender beam whose dimensions satisfy Eq. (4.1) the rate of change of the displacements along the axial direction is much smaller than their rate of change along the circumferential direction. That is, for each displacement component

$$\left|\frac{\partial v_i}{\partial x}\right| << \left|\frac{\partial v_i}{\partial s}\right| \qquad (4.15)$$

Using Eq. (4.7) and assuming that d is smaller or of the same order as R, the order of magnitude of the in-plane strains and curvatures is

$$\gamma_{11} \sim O\left(\frac{\Delta}{L}\right)$$

$$2\gamma_{12} \sim O\left(\frac{\Delta}{d}\right)$$

$$\gamma_{22} \sim O\left(\frac{\Delta}{d}\right)$$

$$\rho_{11} \sim O\left(\frac{\Delta}{L^2}\right)$$

$$\rho_{12} \sim O\left(\frac{\Delta}{d^2}\right)$$

$$\rho_{22} \sim O\left(\frac{\Delta}{d^2}\right)$$

Since γ_{11} and ρ_{11} are much smaller than γ_{12}, γ_{22} and ρ_{12}, ρ_{22}, respectively, their contribution to the elastic energy is neglected.

The order of magnitude of the shell energy per unit area and the work done by external forces is

$$\Phi \sim O\left(\frac{E\Delta^2 h}{d^2}\right)$$

$$P_i u_i \sim O\left(\frac{E\Delta^2 h}{L^2}\right)$$

Since $P_i u_i << \Phi$, the contribution of external forces is neglected. Therefore the energy functional takes the form

$$\begin{aligned} 2I = \int_0^L \oint \{ & 4hC^{1212}(\gamma_{12})^2 + 4hC^{1222}\gamma_{12}\gamma_{22} + hC^{2222}(\gamma_{22})^2 + 4h^2 C_1^{1212}\gamma_{12}\rho_{12} \\ & + 2h^2 C_1^{1222}\gamma_{12}\rho_{22} + 2h^2 C_1^{2212}\gamma_{22}\rho_{12} + h^2 C_1^{2222}\gamma_{22}\rho_{22} \\ & + \frac{h^3}{3}C_2^{1212}(\rho_{12})^2 + \frac{h^3}{3}C_2^{1222}\rho_{12}\rho_{22} + \frac{h^3}{12}C_2^{2222}(\rho_{22})^2\} ds dx \end{aligned} \tag{4.16}$$

Using Eq. (4.15), the strain-displacement relationships in Eq. (4.7) can be written as

$$\begin{aligned} 2\gamma_{12} &= \frac{\partial v_1}{\partial s} \\ \gamma_{22} &= \frac{\partial v_2}{\partial s} + \frac{v}{R} \\ \rho_{12} &= \frac{1}{4R}\frac{\partial v_1}{\partial s} \\ \rho_{22} &= \frac{\partial^2 v}{\partial s^2} - \frac{\partial}{\partial s}\left(\frac{v_2}{R}\right) \end{aligned} \tag{4.17}$$

The integrand in Eq. (4.16) is a positive quadratic form, therefore the minimum of the functional is reached by functions v, v_1, and v_2 for which $\gamma_{12} = \gamma_{22} = \rho_{12} = \rho_{22} = 0$. From Eq. (4.17) this corresponds to

$$\frac{\partial v_1}{\partial s} = 0 \tag{4.18}$$

$$\frac{\partial v_2}{\partial s} + \frac{v}{R} = 0 \tag{4.19}$$

$$\frac{\partial^2 v}{\partial s^2} - \frac{\partial}{\partial s}\left(\frac{v_2}{R}\right) = 0 \tag{4.20}$$

The function v in Eqs. (4.19) and (4.20) should be single valued, i. e.

$$\overline{\left(\frac{\partial v}{\partial s}\right)} \equiv \frac{1}{l}\oint \frac{\partial v}{\partial s} ds = 0 \tag{4.21}$$

The bar in (4.21) and in the subsequent derivation denotes averaging along the closed contour Γ whose length is denoted by l in Eq. (4.21).

Equation (4.18) implies that v_1 is a function of x only, i.e.

$$v_1 = U_1(x) \tag{4.22}$$

Integrate Eq. (4.20) to get

$$\frac{\partial v}{\partial s} - \frac{v_2}{R} = -\varphi(x) \tag{4.23}$$

where $\varphi(x)$ is an arbitrary function which is shown later to represent the cross-sectional twist. From Eq. (4.21) and (4.23), one obtains the relation between $\varphi(x)$ and v_2.

$$\varphi(x) = \overline{\left(\frac{v_2}{R}\right)}$$

Substitute v from Eq. (4.19) into Eq. (4.23), to get the following second-order differential equation for v_2

$$\frac{\partial}{\partial s}\left(R\frac{\partial v_2}{\partial s}\right) + \frac{v_2}{R} = \varphi(x) \tag{4.24}$$

To solve this equation, one has to recall the relations between the radius of curvature R and the components $y(s)$ and $z(s)$ of the position vector associated with contour Γ

$$\frac{d^2z}{ds^2} = \frac{1}{R}\frac{dy}{ds}$$
$$\frac{d^2y}{ds^2} = -\frac{1}{R}\frac{dz}{ds} \tag{4.25}$$

It follows from Eqs. (4.25) and (4.4) that $\frac{dy}{ds}$ and $\frac{dz}{ds}$ are solutions of the homogeneous form of Eq. (4.24) and $v_2 = \varphi(x)r_n$ is its particular solution. The general solution is therefore given by

$$v_2 = U_2(x)\frac{dy}{ds} + U_3(x)\frac{dz}{ds} + \varphi(x)r_n \tag{4.26}$$

where U_2 and U_3 are arbitrary functions of x. Substitute from Eq. (4.26) into Eq. (4.19) to get

$$v = U_2(x)\frac{dz}{ds} - U_3(x)\frac{dy}{ds} - \varphi(x)r_t \tag{4.27}$$

Eqs. (4.22), (4.26) and (4.27) represent the curvilinear displacement field that minimizes the zeroth-order approximation of the shell energy. Using Eq. (4.8) the curvilinear displacement field is written in Cartesian coordinates as

$$u_1 = U_1(x)$$
$$u_2 = U_2(x) - z\varphi(x) \tag{4.28}$$
$$u_3 = U_3(x) + y\varphi(x)$$

The variables $U_1(x), U_2(x)$ and $U_3(x)$ represent the average cross-sectional translation while $\varphi(x)$ the cross-sectional rotation normally referred to in beam theory as the torsional rotation. This displacement field corresponds to the zeroth-order approximation and does not include bending behavior. For a centroidal coordinate system $U_1(x), U_2(x), U_3(x)$ and $\varphi(x)$ can be expressed as

$$U_1(x) = \overline{u_1}$$

$$U_2(x) = \overline{u_2}$$

$$U_3(x) = \overline{u_3} \tag{4.29}$$

$$\varphi(x) = \frac{\overline{(\vec{u} \cdot \vec{t})}}{\overline{r_n}}$$

4.4.2 First-Order Approximation

A first-order approximation can be constructed by rewriting the displacement field in Eqs. (4.22), (4.26) and (4.27) in the form

$$v_1 = U_1(x) + w_1(s,x)$$

$$v_2 = U_2(x)\frac{dy}{ds} + U_3(x)\frac{dz}{ds} + \varphi(x)r_n + w_2(s,x) \tag{4.30}$$

$$v = U_2(x)\frac{dz}{ds} - U_3(x)\frac{dy}{ds} - \varphi(x)r_t + w(s,x)$$

where w_1, w_2 and w can be regarded as correction functions to be determined based on their contributions to the energy functional.

Substitute Eq. (4.30) into (4.7) to obtain the strains and curvatures in terms of the displacement corrections

$$\gamma_{11} = \mathring{\gamma}_{11} + \frac{\partial w_1}{\partial x}$$

$$2\gamma_{12} = 2\mathring{\gamma}_{12} + \frac{\partial w_2}{\partial x} + 2\hat{\gamma}_{12} \quad , \quad 2\hat{\gamma}_{12} = \frac{\partial w_1}{\partial s}$$

$$\gamma_{22} = \mathring{\gamma}_{22} + \hat{\gamma}_{22} \quad , \quad \hat{\gamma}_{22} = \frac{\partial w_2}{\partial s} + \frac{w}{R}$$

$$\rho_{11} = \mathring{\rho}_{11} + \frac{\partial^2 w}{\partial x^2} \tag{4.31}$$

$$\rho_{12} = \mathring{\rho}_{12} + \frac{\partial^2 w}{\partial s \partial x} - \frac{3}{4R}\frac{\partial w_2}{\partial x} + \hat{\rho}_{12} \quad , \quad \hat{\rho}_{12} = \frac{1}{4R}\frac{\partial w_1}{\partial s}$$

$$\rho_{22} = \mathring{\rho}_{22} + \hat{\rho}_{22} \quad , \quad \hat{\rho}_{22} = \frac{\partial^2 w}{\partial s^2} - \frac{\partial}{\partial s}\left(\frac{w_2}{R}\right)$$

where $\gamma^{\circ}_{\alpha\beta}$ and $\rho^{\circ}_{\alpha\beta}$ are the strains and curvatures corresponding to the zeroth-order approximation. These are expressed as

$$\begin{aligned}
\overset{\circ}{\gamma}_{11} &= U_1'(x) \sim O\left(\frac{\Delta}{L}\right) \\
2\overset{\circ}{\gamma}_{12} &= U_2'(x)\frac{dy}{ds} + U_3'(x)\frac{dz}{ds} + \varphi'(x)r_n \sim O\left(\frac{\Delta}{L}\right) \\
\overset{\circ}{\gamma}_{22} &= 0 \\
\overset{\circ}{\rho}_{11} &= U_2''(x)\frac{dz}{ds} - U_3''(x)\frac{dy}{ds} - \varphi''(x)r_t \sim O\left(\frac{\Delta}{L^2}\right) \\
\overset{\circ}{\rho}_{12} &= \frac{1}{4R}\left[U_2'(x)\frac{dy}{ds} + U_3'(x)\frac{dz}{ds} + \varphi'(x)r_n\right] - \varphi'(x) \sim O\left(\frac{\Delta}{dL}\right) \\
\overset{\circ}{\rho}_{22} &= 0
\end{aligned} \tag{4.32}$$

The prime in Eq. (4.32) denotes differentiation with respect to x. Among the new terms introduced by the function w_i the leading ones are denoted by superscript $\hat{}$ in Eq. (4.31). The order of w_i is $(\frac{\Delta d}{L})$, this is derived from Eqs. (4.31) and (4.32) where it is seen that the leading terms $2\hat{\gamma}_{12}$ and $\hat{\rho}_{12}$ are of the same order of magnitude as $2\gamma^{\circ}_{12}$ and ρ°_{12} , respectively, i.e.

$$\begin{aligned}
2\hat{\gamma}_{12} &= \frac{\partial w_1}{\partial s} \sim O\left(\frac{\Delta}{L}\right) \\
\hat{\rho}_{12} &= \frac{1}{4R}\frac{\partial w_1}{\partial s} \sim O\left(\frac{\Delta}{dL}\right)
\end{aligned} \tag{4.33}$$

Therefore,

$$w_1 \sim O\left(\frac{\Delta d}{L}\right) \tag{4.34}$$

An alternative approach is to assume the order of w_i as $\left(\frac{\Delta d}{L}\right)$ and verify this assumption, as shown later, once w_i is determined. The order of magnitude of the remaining leading terms in Eq. (4.31) is as follows

$$\hat{\gamma}_{22} \sim O\left(\frac{\Delta}{L}\right)$$

$$\hat{\rho}_{22} \sim O\left(\frac{\Delta}{dL}\right) \tag{4.35}$$

The energy functional can be represented by $\Phi(\gamma_{11}, 2\gamma_{12}, \gamma_{22}, \rho_{11}, \rho_{12}, \rho_{22})$. By keeping the strains and curvature associated with the zeroth-order approximation and the leading terms contribution over the other terms (i.e., by dropping the terms $\frac{\partial w_1}{\partial x}$, $\frac{\partial w_2}{\partial x}$, $\frac{\partial^2 w}{\partial x^2}$, and $\frac{\partial^2 w}{\partial s \partial x} - \frac{1}{4R}\frac{\partial w_2}{\partial x}$ in Eq. (4.31)) the energy function can be written as

$$\Phi(\overset{\circ}{\gamma}_{11}, 2\overset{\circ}{\gamma}_{12} + 2\hat{\gamma}_{12}, 0 + \hat{\gamma}_{22}, \overset{\circ}{\rho}_{11}, \overset{\circ}{\rho}_{12} + \hat{\rho}_{12}, 0 + \hat{\rho}_{22})$$

The interaction terms associated with $\rho^{\circ}{}_{11}$ and $\rho^{\circ}{}_{12}$, namely

$$h\overset{\circ}{\rho}_{11}\hat{\gamma}_{12}\,,\; h\overset{\circ}{\rho}_{11}\hat{\gamma}_{22}\,,\; h^2\overset{\circ}{\rho}_{11}\hat{\rho}_{12}\,,\; h^2\overset{\circ}{\rho}_{11}\hat{\rho}_{22}$$

$$h\overset{\circ}{\rho}_{12}\hat{\gamma}_{12}\,,\; h\overset{\circ}{\rho}_{12}\hat{\gamma}_{22}\,,\; h^2\overset{\circ}{\rho}_{12}\hat{\rho}_{12}\,,\; h^2\overset{\circ}{\rho}_{12}\hat{\rho}_{22}$$

are of order $\left(\frac{\Delta^2 h}{L^2 d}\right)$ or smaller. They are neglected in comparison with the following terms

$$\overset{\circ}{\gamma}_{11}\hat{\gamma}_{12}\,,\; \overset{\circ}{\gamma}_{11}\hat{\gamma}_{22}\,,\; \overset{\circ}{\gamma}_{12}\hat{\gamma}_{12}\,,\; \overset{\circ}{\gamma}_{12}\hat{\gamma}_{22} \tag{4.36}$$

of order $(\frac{\Delta^2}{L^2})$. Similarly, the contribution of the work done by external forces, $P_i w_i$, is neglected since its order is $\left(Eh\frac{\Delta^2}{L^2}(\frac{d}{L})\right)$ in comparison with the order of the remaining terms in the energy functional $\left(Eh\frac{\Delta^2}{L^2}\right)$. Therefore in order to determine the functions w_i one has to minimize the functional

$$\oint \Phi(\overset{\circ}{\gamma}_{11}, 2\overset{\circ}{\gamma}_{12} + 2\hat{\gamma}_{12}, \hat{\gamma}_{22}, 0, \hat{\rho}_{12}, \hat{\rho}_{22})\, ds$$

If the rigid body motion is suppressed the solution is unique. The terms $\hat{\rho}_{12}$, $\hat{\rho}_{22}$ are essential to the uniqueness of the solution; however, their contribution to the energy, expressed by the interaction terms

$$h\hat{\rho}_{12}\overset{\circ}{\gamma}_{11}, h\hat{\rho}_{12}\overset{\circ}{\gamma}_{12}, h\hat{\rho}_{22}\overset{\circ}{\gamma}_{11}, h\hat{\rho}_{22}\overset{\circ}{\gamma}_{12}$$

is of order $\left(\frac{\Delta^2}{L^2}(\frac{h}{d})\right)$ or smaller, and is consequently dropped in comparison with the membrane contribution listed in (4.36). This aspect is discussed by Berdichevsky and Misiura [63], with regard to the accuracy of classical shell theory. Therefore, the shell energy can be represented by

$$I = \int_0^L \oint \Phi(\mathring{\gamma}_{11}, 2\mathring{\gamma}_{12} + 2\hat{\gamma}_{12}, \hat{\gamma}_{22}, 0, 0, 0)\, ds dx \tag{4.37}$$

It is worth noting that the bending contribution does not appear in Eq. (4.37). That is, to the first-order approximation the shell energy corresponds to a membrane state.

The first variation of the energy functional is

$$\delta I = \int_0^L \oint \left\{ \frac{\partial \Phi}{\partial(2\gamma_{12})} \delta\left(\frac{\partial w_1}{\partial s}\right) + \frac{\partial \Phi}{\partial \gamma_{22}} \delta\left(\frac{\partial w_2}{\partial s} + \frac{w}{R}\right) \right\} ds dx \tag{4.38}$$

Recall that $\frac{\partial \Phi}{\partial(2\gamma_{12})} = N_{12}$ and $\frac{\partial \Phi}{\partial \gamma_{22}} = N_{22}$, Eq. (4.38) takes the form

$$\delta I = \int_0^L \oint \left\{ N_{12} \frac{\partial(\delta w_1)}{\partial s} + N_{22}\left(\frac{\partial(\delta w_2)}{\partial s} + \frac{1}{R}\delta w\right) \right\} ds dx$$

Set the first variation of the energy to zero, to obtain the following

$$\frac{\partial N_{12}}{\partial s} = 0$$

$$\frac{\partial N_{22}}{\partial s} = 0$$

$$\frac{N_{22}}{R} = 0$$

which result in

$$N_{12} = \text{constant} \tag{4.39}$$

and

$$N_{22} = 0 \tag{4.40}$$

This is similar to the classical solution of constant shear flow and vanishing hoop stress resultant. By setting N_{22} to zero the energy density is expressed in terms of

γ_{11} and γ_{12} only

$$2\Phi_1 = \min_{\gamma_{22}} 2\Phi = \min_{\gamma_{22}} hC^{\alpha\beta\gamma\delta}\gamma_{\alpha\beta}\gamma_{\gamma\delta} = A(s)(\gamma_{11})^2 + 2B(s)\gamma_{11}\gamma_{12} + C(s)(\gamma_{12})^2 \quad (4.41)$$

The variables $A(s)$, $B(s)$ and $C(s)$ represent the axial, coupling and shear stiffnesses, respectively. They are defined in terms of the $D^{\alpha\beta\gamma\delta}$ as follows

$$\begin{aligned} A(s) &= < D^{1111} > - \frac{(< D^{1122} >)^2}{< D^{2222} >} \sim O(Eh) \\ B(s) &= 2\left[< D^{1112} > - \frac{< D^{1122} >< D^{1222} >}{< D^{2222} >}\right] \sim O(Eh) \\ C(s) &= 4\left[< D^{1212} > - \frac{(< D^{1222} >)^2}{< D^{2222} >}\right] \sim O(Eh) \end{aligned} \quad (4.42)$$

where the $2D$ Young's modulus $D^{\alpha\beta\gamma\delta}$ are expressed in terms of the Hookean tensor $E^{\alpha\beta\gamma\delta}$ in Eq. (4.10). The pointed brackets denote integration over the thickness as defined in Eq. (4.12).

For convenience, $D^{\alpha\beta\gamma\delta}$ is given in matrix form as

$$[D] = \left[Q^1\right] - 2\left[Q^2\right]\left[Q^3\right]^{-1}\left[Q^4\right] + \left[Q^4\right]^T\left[Q^3\right]^{-1}\left[Q^4\right] \quad (4.43)$$

where

$$\begin{aligned} [D] &= \begin{bmatrix} D^{1111} & D^{1122} & D^{1112} \\ D^{1122} & D^{2222} & D^{1222} \\ D^{1112} & D^{1222} & D^{1212} \end{bmatrix} \\ \left[Q^1\right] &= \begin{bmatrix} \overline{Q}_{11} & \overline{Q}_{12} & \overline{Q}_{16} \\ \overline{Q}_{12} & \overline{Q}_{22} & \overline{Q}_{26} \\ \overline{Q}_{16} & \overline{Q}_{26} & \overline{Q}_{66} \end{bmatrix} \\ \left[Q^2\right] &= \begin{bmatrix} \overline{Q}_{13} & \overline{Q}_{15} & \overline{Q}_{14} \\ \overline{Q}_{23} & \overline{Q}_{25} & \overline{Q}_{24} \\ \overline{Q}_{36} & \overline{Q}_{56} & \overline{Q}_{46} \end{bmatrix} \\ \left[Q^3\right] &= \begin{bmatrix} \overline{Q}_{33} & \overline{Q}_{35} & \overline{Q}_{36} \\ \overline{Q}_{35} & \overline{Q}_{55} & \overline{Q}_{45} \\ \overline{Q}_{36} & \overline{Q}_{45} & \overline{Q}_{44} \end{bmatrix} \end{aligned} \quad (4.44)$$

$$[Q^4] = \begin{bmatrix} \overline{Q}_{13} & \overline{Q}_{23} & \overline{Q}_{36} \\ \overline{Q}_{15} & \overline{Q}_{25} & \overline{Q}_{56} \\ \overline{Q}_{14} & \overline{Q}_{24} & \overline{Q}_{46} \end{bmatrix}$$

The indices adopted in Eq. (4.44) follow the convention of Ref. [50]. The bars over the reduced stiffness coefficients Q_{ij} of Classical Laminate Theory, Refs. [19] and [50], indicate that these quantities are to be obtained through appropriate coordinate transformations.

Equation (4.41) indicates that, to the first-order, the energy density function is independent of functions w_2 and w. That is, the in-plane warping contribution to the shell energy is negligible. The function w_1 however, can be determined from Eq. (4.39) and (4.41) and by enforcing the condition on w_1 to be single valued as follows

$$N_{12} = \frac{\partial \Phi_1}{\partial (2\gamma_{12})} = \frac{1}{2}(B(s)\gamma_{11} + C(s)\gamma_{12}) = \text{constant} \tag{4.45}$$

Substitute from Eqs. (4.31) and (4.32) into (4.45) to get

$$\frac{1}{2}B\left(U_1'(x) + \frac{\partial w_1}{\partial x}\right) + \frac{1}{4}C\left(U_2'(x)\frac{dy}{ds} + U_3'(x)\frac{dz}{dx} + \varphi'(x)r_n(s) + \frac{\partial w_2}{\partial x} + \frac{\partial w_1}{\partial s}\right) = \text{constant} \tag{4.46}$$

Following the relations in Eq. (4.15), the term $\frac{\partial w_2}{\partial x}$ is neglected in comparison with $\frac{\partial w_1}{\partial s}$. Moreover, the term $\frac{1}{2}B\frac{\partial w_1}{\partial x}$ in Eq. (4.46) may be neglected in comparison with $\frac{1}{4}C\frac{\partial w_1}{\partial s}$. This is possible, if $|B|$ is less or of the same order of magnitude as C. For the case when $|B| >> C$ additional investigation is needed. Since the elastic energy is positive definite, $B^2 \leq AC$, and B could be greater than C only if $A >> C$. In practical laminated composite designs $|B| < C$ as the shear stiffness is greater than the extension-shear coupling. Therefore, Eq. (4.46) becomes

$$\frac{1}{2}BU_1'(x) + \frac{1}{4}C\left(U_2'(x)\frac{dy}{ds} + U_3'(x)\frac{dz}{dx} + \varphi'(x)r_n(s) + \frac{\partial w_1}{\partial s}\right) = \text{constant} \tag{4.47}$$

Equation (4.47) is a first order ordinary differential equation in w_1. The value of the constant in the right hand side of (4.47) can be found from the single value condition of the function w_1:

$$\overline{\left(\frac{\partial w_1}{\partial s}\right)} \equiv \frac{1}{l}\oint \frac{\partial w_1}{\partial s} ds = 0 \tag{4.48}$$

The solution of Eq. (4.47) is determined within an arbitrary function of x. This function can be specified from various conditions. Each one yields a specific interpretation of the variable U_1. For example if $\overline{w_1} = 0$ the variable $U_1 = \overline{v_1}$ according to Eq. (4.30). The choice of these conditions does not affect the final form of the $1D$ beam theory and therefore will not be specified in this formulation. The result is the following simple analytical solution of Eq. (4.47)

$$w_1 = -yU_2'(x) - zU_3'(x) + G(s)\varphi'(x) + g_1(s)U_1'(x) \tag{4.49}$$

where

$$G(s) = \int_0^s \left[\frac{2A_\epsilon}{l\,\bar{c}} c(\tau) - r_n(\tau)\right] d\tau \sim O\left(d^2\right)$$

$$g_1(s) = \int_0^s \left[b(\tau) - \frac{\bar{b}}{\bar{c}} c(\tau)\right] d\tau \sim O(d)$$

$$b(s) = -2\frac{B(s)}{C(s)} \qquad c(s) = \frac{1}{C(s)} \qquad A_\epsilon = \frac{l}{2}\overline{r_n} \tag{4.50}$$

The area enclosed by contour Γ is denoted by A_ϵ in Eq. (4.50). It is seen from expression (4.49) that w_1 is of order $\left(\frac{\Delta d}{L}\right)$ and relation (4.34) is justified. The displacement field corresponding to the first correction is obtained by substituting Eq. (4.49) into Eq. (4.30) and dropping w_2 and w since their contribution to the shell energy is negligible compared to w_1. The result referred to as the first-order approximation is given by

$$v_1 = U_1(x) - y(s)U_2'(x) - z(s)U_3'(x) + G(s)\varphi'(x) + g_1(s)U_1'(x)$$

$$v_2 = U_2(x)\frac{dy}{ds} + U_3(x)\frac{dz}{ds} + \varphi(x)r_n \tag{4.51}$$

$$v = U_2(x)\frac{dz}{ds} - U_3(x)\frac{dy}{ds} - \varphi(x)r_t$$

4.4.3 Second-Order Approximation

Following a similar procedure to the one described in section 4.4.2, a second-order approximation can be constructed by rewriting the displacement field in Eq. (4.51) in the form

$$\begin{aligned} v_1 &= U_1(x) - yU_2'(x) - zU_3'(x) + G(s)\varphi'(x) + g_1(s)U_1'(x) + \tilde{w}_1(s,x) \\ v_2 &= U_2(x)\frac{dy}{ds} + U_3(x)\frac{dz}{ds} + \varphi(x)r_n + \tilde{w}_2(s,x) \\ v &= U_2(x)\frac{dz}{ds} - U_3(x)\frac{dy}{ds} - \varphi(x)r_t + \tilde{w}(s,x) \end{aligned} \tag{4.52}$$

where $\tilde{w}_1, \tilde{w}_2$ and $\tilde{w}$ can be regarded as correction functions to be determined based on their contributions to the energy functional.

Substitute Eq. (4.52) into (4.7) to obtain the strains and curvatures in terms of the displacement corrections

$$\begin{aligned} \gamma_{11} &= \check{\gamma}_{11} + \frac{\partial \tilde{w}_1}{\partial x} \\ 2\gamma_{12} &= 2\check{\gamma}_{12} + \frac{\partial \tilde{w}_2}{\partial x} + 2\hat{\check{\gamma}}_{12} \quad , \quad 2\hat{\check{\gamma}}_{12} = \frac{\partial \tilde{w}_1}{\partial s} \\ \gamma_{22} &= \check{\gamma}_{22} + \hat{\check{\gamma}}_{22} \quad , \quad \hat{\check{\gamma}}_{22} = \frac{\partial \tilde{w}_2}{\partial s} + \frac{\tilde{w}}{R} \\ \rho_{11} &= \check{\rho}_{11} + \frac{\partial^2 \tilde{w}}{\partial x^2} \\ \rho_{12} &= \check{\rho}_{12} + \frac{\partial^2 \tilde{w}}{\partial s \partial x} - \frac{3}{4R}\frac{\partial \tilde{w}_2}{\partial x} + \hat{\check{\rho}}_{12} \quad , \quad \hat{\check{\rho}}_{12} = \frac{1}{4R}\frac{\partial \tilde{w}_1}{\partial s} \\ \rho_{22} &= \check{\rho}_{22} + \hat{\check{\rho}}_{22} \quad , \quad \hat{\check{\rho}}_{22} = \frac{\partial^2 \tilde{w}}{\partial s^2} - \frac{\partial}{\partial s}\left(\frac{\tilde{w}_2}{R}\right) \end{aligned} \tag{4.53}$$

where $\check{\gamma}_{\alpha\beta}$ and $\check{\rho}_{\alpha\beta}$ are the strains and curvatures corresponding to the first-order approximation. These are expressed as

$$\check{\gamma}_{11} = \overbrace{U_1'(x)}^{\left(\frac{\Delta}{L}\right)} - \overbrace{yU_2''(x)}^{\left(\frac{\Delta d}{L^2}\right)} - \overbrace{zU_3''(x)}^{\left(\frac{\Delta d}{L^2}\right)} + G(s)\varphi''(x) + g_1(s)U_1''(x)$$

$$
\begin{aligned}
2\check{\gamma}_{12} &= \frac{2A_\epsilon}{l\bar{c}} c\varphi'(x) + \frac{dg_1}{ds} U_1'(x) \sim O\left(\frac{\Delta}{L}\right) \\
\check{\gamma}_{22} &= 0 \\
\check{\rho}_{11} &= U_2''(x)\frac{dz}{ds} - U_3''(x)\frac{dy}{ds} - \varphi''(x) r_t \sim O\left(\frac{\Delta}{L^2}\right) \\
\check{\rho}_{12} &= \frac{1}{4R}\frac{dg_1}{ds} U_1'(x) + \left(\frac{1}{4R}\frac{2A_\epsilon}{l\bar{c}} c - 1\right)\varphi'(x) \sim \left(\frac{\Delta}{dL}\right) \\
\check{\rho}_{22} &= 0
\end{aligned}
\tag{4.54}
$$

The terms written over the overbraced expressions in Eq. (4.54) denote their order. Among the new terms introduced by the function $\tilde{w}_i$ the leading ones are denoted by superscript $\hat{}$ in Eq. (4.53). The order of $\tilde{w}_i$ is assumed to be

$$
\tilde{w}_i \sim O\left(\frac{\Delta d^2}{L^2}\right) \tag{4.55}
$$

Such an assumption will be justified later. Therefore, the order of magnitude of the leading terms, Eq. (4.53), is as follows

$$
\begin{aligned}
\hat{\check{\gamma}}_{12} \sim \hat{\check{\gamma}}_{22} &\sim O\left(\frac{\Delta d}{L^2}\right) \\
\hat{\check{\rho}}_{12} \sim \hat{\check{\rho}}_{22} &\sim O\left(\frac{\Delta}{L^2}\right)
\end{aligned}
\tag{4.56}
$$

The energy functional can be represented by $\Phi(\gamma_{11}, 2\gamma_{12}, \gamma_{22}, \rho_{11}, \rho_{12}, \rho_{22})$. By keeping the strains and curvature associated with the first-order approximation and the leading terms contribution over the other terms (i.e., by dropping the terms $\frac{\partial \tilde{w}_1}{\partial x}$, $\frac{\partial \tilde{w}_2}{\partial x}$, $\frac{\partial^2 \tilde{w}}{\partial x^2}$, and $\frac{\partial^2 \tilde{w}}{\partial s \partial x} - \frac{1}{4R}\frac{\partial \tilde{w}_2}{\partial x}$ in Eq. (4.53)) the energy function can be written as

$$
\Phi(\check{\gamma}_{11}, 2\check{\gamma}_{12} + 2\hat{\check{\gamma}}_{12}, 0 + \hat{\check{\gamma}}_{22}, \check{\rho}_{11}, \check{\rho}_{12} + \hat{\check{\rho}}_{12}, 0 + \hat{\check{\rho}}_{22}) \tag{4.57}
$$

In the following, the order of magnitude of the energy due to bending, i.e. due to $\check{\rho}_{11}$, $\check{\rho}_{12}$, $\hat{\check{\rho}}_{12}$, and $\hat{\check{\rho}}_{22}$, is investigated.

The interaction terms associated with $\check{\rho}_{11}$, namely

$$h\check{\rho}_{11}\hat{\check{\gamma}}_{12}\,,\; h\check{\rho}_{11}\hat{\check{\gamma}}_{22}\,,\; h^2\check{\rho}_{11}\hat{\rho}_{12}\,,\; h^2\check{\rho}_{11}\hat{\rho}_{22}$$

are of order $\left(\frac{\Delta^2 hd}{L^4}\right)$ or smaller. They are neglected in comparison with the following membrane contribution to the energy

$$\check{\gamma}_{11}\hat{\check{\gamma}}_{12}\,,\; \check{\gamma}_{11}\hat{\check{\gamma}}_{22}\,,\; \check{\gamma}_{12}\hat{\check{\gamma}}_{12}\,,\; \check{\gamma}_{12}\hat{\check{\gamma}}_{22}\begin{cases} \sim O\left(\frac{\Delta^2 d}{L^3}\right) & \text{associated with } U_1' \text{ and } \varphi' \\ \sim O\left(\frac{\Delta^2 d^2}{L^4}\right) & \text{associated with } U_2'' \text{ and } U_3'' \end{cases} \tag{4.58}$$

The interaction terms due to the bending curvature $\check{\rho}_{12}$ are

$$h\check{\rho}_{12}\hat{\check{\gamma}}_{12}\,,\; h\check{\rho}_{12}\hat{\check{\gamma}}_{22} \sim O\left(\frac{\Delta^2 h}{L^3}\right) \text{ associated with } U_1' \text{ and } \varphi' \tag{4.59}$$

$$h^2\check{\rho}_{12}\hat{\rho}_{12}\,,\; h^2\check{\rho}_{12}\hat{\rho}_{22} \sim O\left[\frac{\Delta^2 d}{L^3}\left(\frac{h^2}{d^2}\right)\right] \text{ associated with } U_1' \text{ and } \varphi' \tag{4.60}$$

These terms are of higher order in comparison with the membrane contribution associated with U_1' and φ' in Eq. (4.58), and may be neglected. The remaining interaction terms associated with $\hat{\rho}_{12}$ and $\hat{\rho}_{22}$, namely

$$h\check{\gamma}_{11}\hat{\rho}_{12}\,,\; h\check{\gamma}_{11}\hat{\rho}_{22}\,,\; h\check{\gamma}_{12}\hat{\rho}_{12}\,,\; h\check{\gamma}_{12}\hat{\rho}_{22}\begin{cases} \sim O\left(\frac{\Delta^2 h}{L^3}\right) & \text{associated with } U_1' \text{ and } \varphi' \\ \sim O\left(\frac{\Delta^2 hd}{L^4}\right) & \text{associated with } U_2'' \text{ and } U_3'' \end{cases} \tag{4.61}$$

are of higher order when compared to the corresponding membrane ones, listed in (4.58). Therefore in order to determine the functions $\tilde{w}_i$ one has to minimize the shell energy expressed by

$$I = \int_0^L \oint \Phi(\check{\gamma}_{11}, 2\check{\gamma}_{12} + 2\hat{\check{\gamma}}_{12}, \hat{\check{\gamma}}_{22}, 0, 0, 0)\, ds dx \tag{4.62}$$

The contribution of the new corrections in the work done by external forces is negligible compared to the first-order approximation. Consequently its contribution is neglected in Eq. (4.62). It is worth noting that the bending contribution does not appear in Eq. (4.62). That is, to the second order approximation the shell energy corresponds to a membrane state.

The first variation of the energy functional is

$$\delta I = \int_0^L \oint \left\{ \frac{\partial \Phi}{\partial (2\gamma_{12})} \delta \left(\frac{\partial \tilde{w}_1}{\partial s} \right) + \frac{\partial \Phi}{\partial \gamma_{22}} \delta \left(\frac{\partial \tilde{w}_2}{\partial s} + \frac{\tilde{w}}{R} \right) \right\} ds dx \tag{4.63}$$

Recall that $\frac{\partial \Phi}{\partial (2\gamma_{12})} = N_{12}$ and $\frac{\partial \Phi}{\partial \gamma_{22}} = N_{22}$, Eq. (4.63) takes the form

$$\delta I = \int_0^L \oint \left\{ N_{12} \frac{\partial (\delta \tilde{w}_1)}{\partial s} + N_{22} \left(\frac{\partial (\delta \tilde{w}_2)}{\partial s} + \frac{1}{R} \delta \tilde{w} \right) \right\} ds dx$$

Set the first variation of the energy to zero, to obtain Eqs. (4.39) and (4.40). By setting N_{22} to zero, the energy density is expressed in terms of γ_{11} and γ_{12} only as given by Eq. (4.41). The function $\tilde{w}_1$ can be determined from Eq. (4.39) and (4.41) and by enforcing the condition on $\tilde{w}_1$ to be single valued as previously outlined in section 4.4.2. Substitute from Eqs. (4.53) and (4.54) into (4.45) to get

$$\frac{1}{2} \overbrace{B}^{(Eh)} \left[\overbrace{U_1'(x)}^{\left(\frac{\Delta}{L}\right)} - \overbrace{y(s)U_2''}^{\left(\frac{\Delta d}{L^2}\right)} - \overbrace{z(s)U_3''}^{\left(\frac{\Delta d}{L^2}\right)} + \overbrace{G(s)\varphi''(x)}^{\left(\frac{\Delta d}{L^2}\right)} + \overbrace{g_1(s)U_1''(x)}^{\left(\frac{\Delta d}{L^2}\right)} + \overbrace{\frac{\partial \tilde{w}_1}{\partial x}}^{\left(\frac{\Delta d^2}{L^3}\right)} \right]$$

$$+ \frac{1}{4} \overbrace{C}^{(Eh)} \left[\overbrace{\frac{2A_\epsilon}{l\bar{c}} c\varphi'(x)}^{\left(\frac{\Delta}{L}\right)} + \overbrace{\frac{dg_1}{ds} U_1'(x)}^{\left(\frac{\Delta}{L}\right)} + \overbrace{\frac{\partial \tilde{w}_2}{\partial x}}^{\left(\frac{\Delta d^2}{L^3}\right)} + \overbrace{\frac{\partial \tilde{w}_1}{\partial s}}^{\left(\frac{\Delta d}{L^2}\right)} \right] = \text{constant} \tag{4.64}$$

Comparing the order of magnitude of each kinematical variable, Eq. (4.64) reduces to

$$\frac{1}{2} B \left[U_1'(x) - y(s)U_2'' - z(s)U_3'' \right] + \frac{1}{4} C \left[\frac{2A_\epsilon}{l\bar{c}} c\varphi'(x) + \frac{dg_1}{ds} U_1'(x) + \frac{\partial \tilde{w}_1}{\partial s} \right] = \text{constant} \tag{4.65}$$

Using the single value condition of function $\tilde{w}_1$, the following simple analytical solution of Eq. (4.65) is obtained

$$\tilde{w}_1 = g_2 U_2''(x) + g_3(s) U_3''(x) \tag{4.66}$$

where

$$g_2(s) = -\int_0^s \left[b(\tau)y(\tau) - \frac{\overline{by}}{\overline{c}}c(\tau)\right]d\tau \sim O\left(d^2\right)$$

$$g_3(s) = -\int_0^s \left[b(\tau)z(\tau) - \frac{\overline{bz}}{\overline{c}}c(\tau)\right]d\tau \sim O\left(d^2\right) \tag{4.67}$$

It is seen from expression (4.50) and (4.67) that $G(s)$, $g_1(s)$, $g_2(s)$ and $g_3(s)$ are single-valued functions, with

$$G(0) = G(l) = g_1(0) = g_1(l) = g_2(0) = g_2(l) = g_3(0) = g_3(l) = 0$$

Using Eqs. (4.66) and (4.67), $\tilde{w}_1$ is found to be of order $\left(\frac{\Delta d^2}{L^2}\right)$ and the assumption in Eq. (4.55) is justified.

4.4.4 Convergence of Displacement Field

The displacement field corresponding to the second correction is obtained by substituting Eq. (4.66) into Eq. (4.52) and dropping $\tilde{w}_2$ and $\tilde{w}$ since their contribution to the shell energy is negligible compared to $\tilde{w}_1$. The result is

$$\begin{aligned} v_1 &= \underline{U_1(x)} - \underline{y(s)U_2'(x)} - \underline{z(s)U_3'(x)} + \underline{G(s)\varphi'(x)} \\ &\quad + g_1(s)U_1'(x) + g_2(s)U_2''(x) + g_3(s)U_3''(x) \\ \underline{v_2} &= U_2(x)\frac{dy}{ds} + U_3(x)\frac{dz}{ds} + \varphi(x)r_n \\ \underline{v} &= U_2(x)\frac{dz}{ds} - U_3(x)\frac{dy}{ds} - \varphi(x)r_t \end{aligned} \tag{4.68}$$

A third cycle is carried out, however no additional terms of the same order in the energy functional result as shown in the Appendix, and the final displacement field converges to the expression given in Eq. (4.68).

The underlined terms in Eq. (4.68) correspond to the classical theory of extension, bending and torsion of beams. The additional terms $g_1(s)U_1'$, $g_2(s)U_2''$ and $g_3(s)U_3''$ in Eq. (4.68) represent warping due to axial strain and bending . These new terms

emerge naturally in addition to the classical torsional related warping $G(s)\varphi'$. They are strongly influenced by the material anisotropy, and vanish for materials that are either orthotropic or whose properties are antisymmetric relative to the shell middle surface. For these layups the coupling parameter $b(s)$ defined in Eqs. (4.50) and (4.42) vanishes. The significance of the axial and bending-related warping terms and their effect on the accuracy, is shown in the applications of Chapter V. Moreover, the expression for torsional related warping $G(s)$ differs from the work of Refs. [30] and [42]-[46]. A comparison of these expressions is presented in section 4.6.

4.4.5 Strain Field

We now substitute the displacement field of Eq. (4.68) into the in-plane strain components of Eq. (4.7), while using Eq. (4.50), to obtain

$$\begin{aligned}
\gamma_{11} &= \overbrace{U_1'(x)}^{(\frac{\Delta}{L})} - \overbrace{yU_2''(x)}^{(\frac{\Delta d}{L^2})} - \overbrace{zU_3''(x)}^{(\frac{\Delta d}{L^2})} + \overbrace{G(s)\varphi''(x)}^{(\frac{\Delta d}{L^2})} \\
&\quad + \overbrace{g_1(s)U_1''(x)}^{(\frac{\Delta d}{L^2})} + \overbrace{g_2U_2'''(x)}^{(\frac{\Delta d^2}{L^3})} + \overbrace{g_3U_3'''(x)}^{(\frac{\Delta d^2}{L^3})} \\
2\gamma_{12} &= \overbrace{\frac{2A_e}{l\bar{c}}c\varphi'(x)}^{(\frac{\Delta}{L})} + \overbrace{\frac{dg_1}{ds}U_1'(x)}^{(\frac{\Delta}{L})} + \overbrace{\frac{dg_2}{ds}U_2''(x)}^{(\frac{\Delta d}{L^2})} + \overbrace{\frac{dg_3}{ds}U_3''(x)}^{(\frac{\Delta d}{L^2})} \\
\gamma_{22} &= 0
\end{aligned} \tag{4.69}$$

The terms g_1U_1'', g_2U_2''', and g_3U_3''' can be neglected in comparison with U_1', yU_2'', and zU_3'', respectively. Therefore, the in-plane strain components become

$$\begin{aligned}
\gamma_{11} &= U_1'(x) - y(s)U_2''(x) - z(s)U_3''(x) + G\varphi'' \\
2\gamma_{12} &= \frac{2A_e}{l\bar{c}}c\varphi' + \frac{dg_1}{ds}U_1' + \frac{dg_2}{ds}U_2'' + \frac{dg_3}{ds}U_3'' \\
\gamma_{22} &= 0
\end{aligned} \tag{4.70}$$

Using Eq. (4.70), the shell energy density, Eq. (4.41), can be written as

$$
\begin{aligned}
2\Phi_1 \;=\; & \overbrace{A}^{(Eh)}\Bigg[\overbrace{(U_1')^2}^{\left(\frac{\Delta^2}{L^2}\right)} + (yU_2'')^2 + (zU_3'')^2 + \overbrace{\underline{(G\varphi'')^2}}^{\left(\frac{\Delta^2 d^2}{L^4}\right)} - 2yU_1'U_2'' - 2zU_1'U_3'' \\
& + \overbrace{\underline{2GU_1'\varphi''}}^{\left(\frac{\Delta^2 d}{L^3}\right)} + 2yzU_2''U_3'' - \overbrace{\underline{2yGU_2''\varphi''}}^{\left(\frac{\Delta^2 d^2}{L^4}\right)} - \overbrace{\underline{2zGU_3''\varphi''}}^{\left(\frac{\Delta^2 d^2}{L^4}\right)}\Bigg] \\
& + \overbrace{B}^{(Eh)}\Bigg[\frac{dg_1}{ds}(U_1')^2 - y\frac{dg_2}{ds}(U_2'')^2 - z\frac{dg_3}{ds}(U_3'')^2 + \overbrace{\underline{G\frac{2A_\epsilon}{l\bar{c}}c\varphi'\varphi''}}^{\left(\frac{\Delta^2 d}{L^3}\right)} \\
& + \frac{2A_\epsilon}{l\bar{c}}cU_1'\varphi' + \frac{dg_2}{ds}U_1'U_2'' + \frac{dg_3}{ds}U_1'U_3'' - \frac{2A_\epsilon}{l\bar{c}}cyU_2''\varphi' \\
& - y\frac{dg_1}{ds}U_2''U_1' - y\frac{dg_3}{ds}U_2''U_3'' - \frac{2A_\epsilon}{l\bar{c}}czU_3''\varphi' - z\frac{dg_1}{ds}U_3''U_1' \\
& - z\frac{dg_2}{ds}U_3''U_2'' + \overbrace{\underline{G\frac{dg_1}{ds}\varphi''U_1'}}^{\left(\frac{\Delta^2 d}{L^3}\right)} + \overbrace{\underline{G\frac{dg_2}{ds}\varphi''U_2''}}^{\left(\frac{\Delta^2 d^2}{L^4}\right)} + \overbrace{\underline{G\frac{dg_3}{ds}\varphi''U_3''}}^{\left(\frac{\Delta^2 d^2}{L^4}\right)}\Bigg] \\
& + \frac{1}{4}\overbrace{C}^{(Eh)}\Bigg[\overbrace{\left(\frac{2A_\epsilon}{l\bar{c}}c\varphi'\right)^2}^{\left(\frac{\Delta^2}{L^2}\right)} + \left(\frac{dg_1}{ds}U_1'\right)^2 + \left(\frac{dg_2}{ds}U_2''\right)^2 + \left(\frac{dg_3}{ds}U_3''\right)^2 \\
& + \overbrace{\frac{4A_\epsilon}{l\bar{c}}c\frac{dg_1}{ds}U_1'\varphi'}^{\left(\frac{\Delta^2}{L^2}\right)} + \overbrace{\frac{4A_\epsilon}{l\bar{c}}c\frac{dg_2}{ds}U_2''\varphi'}^{\left(\frac{\Delta^2 d}{L^3}\right)} + \overbrace{\frac{4A_\epsilon}{l\bar{c}}c\frac{dg_3}{ds}U_3''\varphi'}^{\left(\frac{\Delta^2 d}{L^3}\right)} \\
& + 2\frac{dg_1}{ds}\frac{dg_2}{ds}U_1'U_2'' + 2\frac{dg_1}{ds}\frac{dg_3}{ds}U_1'U_3'' + 2\frac{dg_2}{ds}\frac{dg_3}{ds}U_2''U_3''\Bigg]
\end{aligned}
\tag{4.71}
$$

where the underlined terms are associated with the $G\varphi''$ contribution in Eq. (4.70). These terms are of higher order and may be neglected in comparison with the remain-

ing overbraced leading terms, as shown in Eq. (4.71). Therefore, one may drop $G\varphi''$ from Eq. (4.70), and the final expressions for the in-plane strain components, using Eqs. (4.50) and (4.67), become

$$\gamma_{11} = U_1'(x) - y(s)U_2''(x) - z(s)U_3''(x)$$

$$\begin{aligned} 2\gamma_{12} &= \frac{2A_\epsilon}{l\overline{c}}c(s)\varphi' + \left[b(s) - \frac{\overline{b}}{\overline{c}}c(s)\right]U_1' \\ &\quad - \left[b(s)y(s) - \frac{\overline{by}}{\overline{c}}c(s)\right]U_2'' \\ &\quad - \left[b(s)z(s) - \frac{\overline{bz}}{\overline{c}}c(s)\right]U_3'' \end{aligned} \tag{4.72}$$

$$\gamma_{22} = 0$$

It is worth noting that the vanishing of hoop stress resultant in Eq. (4.40) and hoop strain in Eq. (4.72) should be interpreted as negligible contribution relative to other parameters. The longitudinal strain γ_{11} is a linear function of y and z. This result was adopted as an assumption in the work of Ref. [29].

In the present formulation, parameters A, B and C where assumed to be of the same order. However, the results are valid for configurations which satisfy the following inequalities

$$\frac{A}{C}\left(\frac{d}{L}\right) << 1 \qquad \frac{B}{C}\left(\frac{d}{L}\right) << 1$$

4.4.6 Constitutive Relationships

Dropping the underlined terms in Eq. (4.71) and integrating over the shell middle surface to get the energy of $1D$ beam theory

$$I = \int_0^L \Phi_2 dx - \int P_i u_i dx ds \tag{4.73}$$

where

$$\begin{aligned}\Phi_2 &= \frac{1}{2}\left[C_{11}(U_1')^2 + C_{22}(\varphi')^2 + C_{33}(U_3'')^2 + C_{44}(U_2'')^2\right] \\ &+C_{12}U_1'\varphi' + C_{13}U_1'U_3'' + C_{14}U_1'U_2'' \\ &+C_{23}\varphi'U_3'' + C_{24}\varphi'U_2'' + C_{34}U_2''U_3'' \end{aligned} \tag{4.74}$$

Explicit expressions for the stiffness coefficients C_{ij} $(i, j = 1, 4)$ are given in Eq. (4.78).

The constitutive relationships can be written in terms of stress resultants and kinematic variables by differentiating Eq. (4.74) with respect to the associated kinematic variable or by relating the traction T, torsional moment M_x, and bending moments M_y and M_z to the shear flow and axial stress as follows

$$\begin{aligned} T &= \frac{\partial \Phi_2}{\partial U_1'} = \oint \int \sigma_{11} d\xi ds = \oint N_{11} ds \\ M_x &= \frac{\partial \Phi_2}{\partial \varphi'} = \oint \int \sigma_{12} r_n(s) d\xi ds = \oint N_{12} r_n(s) ds \\ M_y &= \frac{\partial \Phi_2}{\partial U_3''} = -\oint \int \sigma_{11} z d\xi ds = -\oint N_{11} z(s) ds \\ M_z &= \frac{\partial \Phi_2}{\partial U_2''} = -\oint \int \sigma_{11} y d\xi ds = -\oint N_{11} y(s) ds \end{aligned} \tag{4.75}$$

The shear flow N_{12} is derived from the energy density in Eq. (4.45) and the axial stress resultant N_{11} is given by

$$N_{11} = \frac{\partial \Phi_1}{\partial \gamma_{11}} = A(s)\gamma_{11} + B(s)\gamma_{12} \tag{4.76}$$

and the associated axial and shear stresses are uniform through the wall thickness.

Substitute Eq. (4.72) into Eqs. (4.45) and (4.76) and use Eq. (4.75) to get

$$\begin{Bmatrix} T \\ M_x \\ M_y \\ M_z \end{Bmatrix} = \begin{bmatrix} C_{11} & C_{12} & C_{13} & C_{14} \\ C_{12} & C_{22} & C_{23} & C_{24} \\ C_{13} & C_{23} & C_{33} & C_{34} \\ C_{14} & C_{24} & C_{34} & C_{44} \end{bmatrix} \begin{Bmatrix} U_1' \\ \varphi' \\ U_3'' \\ U_2'' \end{Bmatrix} \tag{4.77}$$

where expressions for the stiffness coefficients C_{ij} $(i, j = 1, 4)$ in terms of the cross section geometry and materials properties are as follows

$$C_{11} = \oint (A - \overbrace{\frac{B^2}{C}}^{\text{due to } g_1 U_1'})ds + \frac{[\oint (B/C)ds]^2}{\oint (1/C)ds}$$

$$C_{12} = \frac{\oint (B/C)ds}{\oint (1/C)ds} A_e$$

$$C_{13} = -\oint (A - \overbrace{\frac{B^2}{C}}^{\text{due to } g_1 U_1' \text{ and } g_3 U_3''})zds - \frac{\oint (B/C)ds \ \oint (B/C)zds}{\oint (1/C)ds}$$

$$C_{14} = -\oint (A - \overbrace{\frac{B^2}{C}}^{\text{due to } g_1 U_1' \text{ and } g_2 U_2''})yds - \frac{\oint (B/C)ds \ \oint (B/C)yds}{\oint (1/C)ds}$$

$$C_{22} = \frac{1}{\oint (1/C)ds} A_e^2 \qquad (4.78)$$

$$C_{23} = -\frac{\oint (B/C)zds}{\oint (1/C)ds} A_e$$

$$C_{24} = -\frac{\oint (B/C)yds}{\oint (1/C)ds} A_e$$

$$C_{33} = \oint (A - \overbrace{\frac{B^2}{C}}^{\text{due to } g_3 U_3''})z^2 ds + \frac{[\oint (B/C)zds]^2}{\oint (1/C)ds}$$

$$C_{34} = \oint (A - \overbrace{\frac{B^2}{C}}^{\text{due to } g_2 U_2'' \text{ and } g_3 U_3''})yzds + \frac{\oint (B/C)yds \ \oint (B/C)zds}{\oint (1/C)ds}$$

$$C_{44} = \oint (A - \overbrace{\frac{B^2}{C}}^{\text{due to } g_2 U_2''})y^2 ds + \frac{[\oint (B/C)yds]^2}{\oint (1/C)ds}$$

The out-of-plane warping contribution to the stiffnesses due to the axial strain (i.e., due to $g_1 U_1'$), bending about y axis (i.e., due to $g_3 U_3''$), and bending about z axis (i.e., due to $g_2 U_2''$) is shown by the overbraces in Eq. (4.78).

The coefficients C_{ij} $(i, j = 1, 4)$ can be expressed in terms of the in-plane axial stiffness coefficients A_{ij} of Classical Lamination Theory (CLT) if one neglects the through-the-thickness contribution to the stiffnesses in Eq. (4.78). The result is

$$C_{11} = \oint (K_{11} - \frac{K_{12}^2}{K_{22}})ds + \frac{[\oint (K_{12}/K_{22})ds]^2}{\oint (1/K_{22})ds}$$

$$C_{12} = 2A_e \frac{\oint (K_{12}/K_{22})ds}{\oint (1/K_{22})ds}$$

$$C_{13} = -\oint (K_{11} - \frac{K_{12}^2}{K_{22}})zds - \frac{\oint (K_{12}/K_{22})ds \ \oint (K_{12}/K_{22})zds}{\oint 1/K_{22}ds}$$

$$C_{14} = -\oint (K_{11} - \frac{K_{12}^2}{K_{22}})yds - \frac{\oint (K_{12}/K_{22})ds \ \oint (K_{12}/K_{22})yds}{\oint 1/K_{22}ds}$$

$$C_{22} = 4A_e^2 \frac{1}{\oint (1/K_{22})ds}$$

$$C_{23} = -2A_e \frac{\oint (K_{12}/K_{22})zds}{\oint (1/K_{22})ds}$$

$$C_{24} = -2A_e \frac{\oint (K_{12}/K_{22})yds}{\oint (1/K_{22})ds}$$

$$C_{33} = \oint (K_{11} - \frac{K_{12}^2}{K_{22}})z^2ds + \frac{[\oint (K_{12}/K_{22})zds]^2}{\oint (1/K_{22})ds}$$

$$C_{34} = \oint (K_{11} - \frac{K_{12}^2}{K_{22}})yzds + \frac{\oint (K_{12}/K_{22})yds \ \oint (K_{12}/K_{22})zds}{\oint 1/K_{22}ds}$$

$$C_{44} = \oint (K_{11} - \frac{K_{12}^2}{K_{22}})y^2ds + \frac{[\oint (K_{12}/K_{22})yds]^2}{\oint (1/K_{22})ds}$$

where, the stiffnesses K_{ij} are

$$K_{11} = A_{11} - \frac{(A_{12})^2}{A_{22}}$$

$$K_{12} = A_{16} - \frac{A_{12}A_{26}}{A_{22}} \qquad (4.79)$$

$$K_{22} = A_{66} - \frac{(A_{26})^2}{A_{22}}$$

4.4.7 Equilibrium Equations

The equilibrium equations are derived using the principle of virtual work. The variation of the internal strain energy is

$$\delta U = \int_0^L \oint (N_{xx}\delta\gamma_{xx} + 2N_{xs}\delta\gamma_{xs})\, ds dx$$

Using the strain displacement relations, one-dimensional stretching, twisting, and bending generalized internal forces are defined as

$$T = \oint N_{xx} ds$$

$$M_x = 2A_e N_{xs}$$

$$M_y = -\oint N_{xx} z ds$$

$$M_z = -\oint N_{xx} y ds$$

Consider a beam subjected to external forces and moment resultants $\overline{T}$, $\overline{M}_x$, $\overline{M}_y$, and $\overline{M}_z$ at both ends. Moreover, surface tractions P_x, P_y, and P_z are applied along the x, y, and z directions, respectively. The variation of the virtual work of the external forces can be written as

$$\begin{aligned}\delta W_e &= \overline{T}\delta U_1|_0^L + \overline{M}_x\delta\varphi|_0^L - \overline{M}_y\delta U_3'|_0^L - \overline{M}_z\delta U_2'|_0^L \\ &\quad + \int_0^L \left[\left(\oint P_x ds\right)\delta U_1 - \left(\oint P_x y ds\right)\delta U_2' - \left(\oint P_x z ds\right)\delta U_3' + \left(\oint P_y ds\right)\delta U_2 \right. \\ &\quad \left. - \left(\oint P_y z ds\right)\delta\varphi - \left(\oint P_z ds\right)\delta U_3' - \left(\oint P_z y ds\right)\delta\varphi\right] dx\end{aligned}$$

Using the principle of virtual work

$$\delta U = \delta W_e$$

one obtains a system of linear equilibrium equations as follows

$$T' + \oint P_x ds = 0$$

$$M_x' + \oint (P_z y - P_y z) ds = 0$$

$$M_y'' + (\oint P_x z ds)' + \oint P_z ds = 0 \tag{4.80}$$

$$M_z'' + (\oint P_x y ds)' + \oint P_y ds = 0$$

One of the member of each of the following four pairs must be prescribed at the beam ends :

$$T \text{ or } U_1,\ M_x \text{ or } \varphi,\ M_y \text{ or } U_3', \text{and } M_z \text{ or } U_2' \tag{4.81}$$

4.5 Summary of governing equations

The development presented in this work encompasses five equations. The first, is the displacement field given in Eq. (4.68). Its functional form was determined based on an asymptotical expansion of shell energy. The associated strain field is given in Eq. (4.72) and the stress resultants in Eq. (4.45), (4.75) and (4.76). The fourth, are the constitutive relationships in Eq. (4.77) with the stiffness coefficients expressed as integral of material properties and cross sectional geometry in Eq. (4.78). Finally the equilibrium equations and boundary conditions are given in Eqs. (4.80) and (4.81), respectively.

In the present development the determination of the displacement field is essential in obtaining accurate expressions for the beam stiffnesses. A comparison of the derived displacement field with results obtained by previous investigators is presented in the following section.

4.6 Analytical comparison with previous results

In anisotropic materials the importance of physical effects such as transverse shear strains is influenced by the relative magnitude of elastic moduli. For example in

laminated composites the extensional modulus along the fibers direction is usually large relative to the shear moduli and consequently transverse shear effects can be significant. Several theories have addressed this issue by including transverse shear in the assumed displacement field [30], and [42]-[46]. The displacement function Eq. (4.68) derived from the asymptotical analysis does not include transverse shear strain terms explicitly. This is a consequence of the vanishing of the through-the-thickness stress component σ^{i3} in Eq. (4.5) or (4.9) where the transverse shear strains are expressed in terms of other strain components. Their effect however is implicitly included in the stretching-related warping term $g_1(s)$ and the bending-related warping terms $g_2(s)$ and $g_3(s)$ as illustrated by the applications of Chapter V.

Rehfield's theory [30] recognizes the significance of transverse shear strain in thin-walled composite beams. Its displacement field is given by

$$u_1 = U_1(x) - y(s)\left[U_2'(x) - 2\gamma_{xy}(x)\right] - z(s)\left[U_3'(x) - 2\gamma_{xz}(x)\right] + g(s,x)$$

$$u_2 = U_2(x) - z(s)\varphi(x) \tag{4.82}$$

$$u_3 = U_3(x) + y(s)\varphi(x)$$

where γ_{xy} and γ_{xz} are the transverse shear strains. The warping function $g(s,x)$ is given as

$$g(s,x) = \tilde{G}(s)\varphi'(x) \tag{4.83}$$

with

$$\tilde{G}(s) = 2A_e\frac{s}{l} - \int_0^s r_n(\tau)d\tau \tag{4.84}$$

A comparison of the displacement fields in Eq. (4.68) and (4.82) shows that the warping function in Rehfield's formulation includes the torsional-related contribution and does not include explicit terms that express the bending-related warping. The torsional-related warping function $G(s)$ in Eq. (4.50) is different from the function in

Eq. (4.84). The two expressions coincide when c = constant that is, when the wall stiffness and thickness are uniform along the cross section circumference.

The torsional related warping function in Eq. (4.84) was modified by Atilgan [44], and Rehfield and Atilgan [43] as

$$\hat{G}(s) = \int_0^s \left[\frac{2A_\epsilon}{l\,\overline{c_1}} c_1 - \tau_n(\tau)\right] d\tau \tag{4.85}$$

where

$$c_1 = \frac{1}{A'_{66} - \frac{(A'_{16})^2}{A'_{11}}} \tag{4.86}$$

and

$$\begin{bmatrix} A'_{11} & A'_{16} \\ A'_{16} & A'_{66} \end{bmatrix} = \begin{bmatrix} A_{11} - \frac{(A_{12})^2}{A_{22}} & A_{16} - \frac{A_{12}A_{26}}{A_{22}} \\ A_{16} - \frac{A_{12}A_{26}}{A_{22}} & A_{66} - \frac{(A_{26})^2}{A_{22}} \end{bmatrix} \tag{4.87}$$

The A_{ij} in Eq. (4.87) are the in-plane axial stiffnesses of CLT, Refs. [19] and [50], they are related to the modulus tensor by

$$A_{11} =< E^{1111} > \quad , \quad A_{12} =< E^{1122} > \quad , \quad A_{22} =< E^{2222} >$$

$$A_{16} =< E^{1112} > \quad , \quad A_{26} =< E^{1222} > \quad , \quad A_{66} =< E^{1212} >$$

A comparison of the modified torsional warping function in Eq. (4.85) and $G(s)$ in Eq. (4.50) shows that they coincide for laminates with no extension-shear coupling ($< D^{1112} >=< D^{1222} >= 0$, in Eq. (4.10)). For the case where the through-the-thickness contribution is neglected in Eq. (4.10), this reduces to $A_{16} = A_{26} = 0$.

The warping function obtained in Refs. [42] and [46] for composite box beams is identical to the expression of Refs. [43] and [44] in Eqs. (4.83) and (4.85).

An assessment of all the previous warping expressions can be made by checking whether they reduce to the exact expression for isotropic materials (see, for example, Ref. [59])

$$\hat{\bar{G}}(s) = \int_0^s \left[\frac{2A_\epsilon}{l\,\overline{c_2}} c_2 - \tau_n(\tau)\right] d\tau \tag{4.88}$$

with

$$c_2 = \frac{1}{\mu h(s)}$$

where μ is the shear modulus.

For isotropic materials the in-plane coupling b is zero and consequently g_1, g_2 and g_3 in Eqs. (4.50) and (4.67) vanish. That is the warping is torsion-related and reduces to $G(s)\varphi'$. Moreover, the shear parameter c is equal to $\frac{1}{4\mu h(s)}$ and the expressions for $G(s)$ and $\tilde{\bar{G}}(s)$ in Eqs. (4.50) and (4.88) coincide.

Rehfield's warping function in Eq. (4.84) coincides with Eq. (4.88) when the material is isotropic and the wall thickness is constant. Also the works of Refs. [43], [44] and [46] reduce to Eq. (4.88) for isotropic materials.

4.7 Closing Remarks

The major advantage of the approach adopted in this work is the fact that the displacement function emerges as a result of the asymptotical analysis of the shell energy. The influence of the material's anisotropy is accounted for in a consistent manner and the deformation modes are determined on the basis of their contribution to the associated energy. Two new contributions to the warping emerge due to stretching and bending. They are of the same order of the classical torsional-related warping. Their significance is illustrated in the applications provided in the next chapter.

CHAPTER V

APPLICATIONS OF ANISOTROPIC THIN-WALLED BEAM THEORY

An evaluation of the variationally consistent theory developed in chapter IV is provided. The theory is applied to beams with arbitrary closed cross-sections made of laminated composite materials with variable thickness and stiffness subjected to axial load, torsion and bending. A comparison of flexibility coefficients and deformation with finite element predictions, closed form solutions and experimental data is performed to validate predictions and isolate the influence of different contributions to the section warping. In addition to the torsional related warping, two new contributions namely, axial strain and bending related out-of-plane warping were identified in the developed theory. Extension and bending related out-of-plane warping are shown to have a significant effect on the accuracy of predictions. Comparison of predictions provides also a check of the asymptotical analysis result regarding the contribution of shear deformation. Although the resulting displacement field does not include an explicit shear deformation term similar to Timoshenko's theory, shear deformation contribution is shown to be implicitly accounted for through the out-of-plane warping due to extension and bending.

Two special layups: The circumferentially uniform stiffness (CUS) and circumferentially Asymmetric stiffness (CAS) have been considered in Refs. [41]-[46] and [51]. They are associated with different non-classical behaviors. These behaviors are

shown to be influenced by the out-of-plane warping due to extension and bending in the next section.

5.1 Effect of Out-of-Plane Warping due to Extension and Bending

5.1.1 CUS Configuration

This configuration produces both extension-twist and bending-transverse shear couplings. The axial, coupling and in-plane stiffnesses A, B, and C given in Eq. (4.42) are constant throughout the cross section and hence the name circumferentially uniform stiffness (CUS) adopted in Ref. [43], [44], [45] and [51]. Such a configuration is manufactured by wrapping the composite lay-up using a winding technique. For a box-beam, the ply lay-ups on opposite sides are of reversed orientation, and hence the name antisymmetric configuration adopted in Refs. [41], [42], and [46].

Since A, B, and C are constants, the stiffness matrix in Eq. (4.78), for a centroidal coordinate system, reduces to

$$[C_{ij}] = \begin{bmatrix} C_{11} & C_{12} & 0 & 0 \\ C_{12} & C_{22} & 0 & 0 \\ 0 & 0 & C_{33} & 0 \\ 0 & 0 & 0 & C_{44} \end{bmatrix} \tag{5.1}$$

The nonzero stiffness coefficients are given by

$$\begin{aligned} C_{11} &= Al \\ C_{12} &= BA_e \\ C_{22} &= \frac{C}{l}A_e^2 \\ C_{33} &= A\oint z^2 ds - \underline{\frac{B^2}{C}\oint z^2 ds} \\ C_{44} &= A\oint y^2 ds - \underline{\frac{B^2}{C}\oint y^2 ds} \end{aligned} \tag{5.2}$$

where l denotes the length of the closed contour Γ. For such a case the out-of-plane warping due to axial strain vanishes and g_1 does not affect the response. This is shown by considering A, B, and C as constants in Eq. (4.78). The influence of the out-of-plane warping due to bending in the x-z and x-y planes are expressed by the underlined terms in the expressions of C_{33} and C_{44}, respectively. These terms are significant in predicting the deflection of antisymmetric configurations.

5.1.2 CAS Configuration

This configuration produces both bending-twist and extension-transverse shear couplings. The stiffness A is constant throughout the cross section. For a box beam, the coupling stiffness, B, vanishes for the vertical members, while its values in the top and bottom members are of opposite signs

$$B_{top} = -B_{bottom}$$

$$B_{vertical\ members} = 0 \tag{5.3}$$

and hence the name circumferentially asymmetric stiffness (CAS) adopted in Ref. [43], [44], [45] and [51]. For a box-beam, the ply lay-ups on opposite sides are mirror images, and hence the name symmetric configuration adopted in Ref. [41],[42], and [46]. The stiffness C along the horizontal and vertical members are equal and expressed by

$$C_{top} = C_{bottom}$$

$$C_{vertical\ left} = C_{vertical\ right} \tag{5.4}$$

The stiffness matrix, for a centroidal system of axes, reduces to

$$[C_{ij}] = \begin{bmatrix} C_{11} & 0 & 0 & 0 \\ 0 & C_{22} & C_{23} & 0 \\ 0 & C_{23} & C_{33} & 0 \\ 0 & 0 & 0 & C_{44} \end{bmatrix} \tag{5.5}$$

The nonzero stiffness coefficients are expressed by

$$
\begin{aligned}
C_{11} &= Al - \underline{2\frac{B_t^2}{C_t}d} \\
C_{22} &= \frac{C_t}{2\left[d + a\left(\frac{C_t}{C_v}\right)\right]}A_\epsilon^2 \\
C_{23} &= \frac{B_t}{2\left[d + a\left(\frac{C_t}{C_v}\right)\right]}A_\epsilon^2 \\
C_{33} &= A\oint z^2 ds - \underline{\frac{B_t^2}{2C_t}\left\{a - \frac{A_\epsilon}{\left[d + a\left(\frac{C_t}{C_v}\right)\right]}\right\}A_\epsilon} \\
C_{44} &= A\oint y^2 ds - \underline{\frac{B_t^2 d^3}{6C_t}}
\end{aligned}
\tag{5.6}
$$

Subscripts t and v denote top and vertical members, respectively. The box width and height are represented by d and a, respectively. Equations (5.6) are derived by substituting Eqs. (5.3) and (5.4) into Eq. (4.78) and considering A to be constant. The underlined term in the expression of the axial stiffness C_{11} represents the extension contribution to the out-of-plane warping. The bending contributions to the out-of-plane warping are represented by the underlined terms in the expressions of C_{33} and C_{44}. For the CAS configuration, bending about the y-axis is coupled with torsion while extension and bending about the z-axis are decoupled.

In order to assess the accuracy of the predictions and isolate the influence of stretching and bending-related warping, the present theory is applied to the box beam given in Ref. [51]. The cross sectional configuration is shown in Fig. 5.1 and the material properties in Table 5.1.

5.2 Comparison of Flexibility Coefficients

A comparison of the flexibility coefficients S_{ij} with the predictions from two models is provided in Table 5.2. The flexibility coefficients S_{ij} are obtained by inverting

Table 5.1: Properties of T300/5208 Graphite/Epoxy

$E_{11} = 21.3$ Msi
$E_{22} = E_{33} = 1.6$ Msi
$G_{12} = G_{13} = 0.9$ Msi
$G_{23} = 0.7$ Msi
$\nu_{12} = \nu_{13} = 0.28$
$\nu_{23} = 0.5$

the 4×4 matrix in Eq. (4.77). NABSA (Nonhomogeneous Anisotropic Beam Section Analysis) is a finite element model based on an extension of the work presented in Ref. [32]. In this model all possible types of warping are accounted for. The TAIL model is based on Ref. [30], but neglecting the restrained torsional warping. The predictions of the NABSA and TAIL models are provided in Ref. [51]. The percentage differences appearing in Table 5.2 are relative to the NABSA predictions. The present theory is in good agreement with NABSA. Its predictions show a difference ranging from +0.7 to +3.6 percent while those based on Ref. [30] range from +3.6 to −18.4 percent.

Since the box beam has a CUS configuration, the out-of-plane warping due to bending has a significant effect on the prediction of the bending flexibilities $(\frac{1}{C_{33}})$ and $(\frac{1}{C_{44}})$ as shown in Eq. (5.2). Neglecting g_3 and g_2 in the expressions of C_{33} and C_{44} leads to values of 0.11424×10^{-4} $\text{lb}^{-1}\text{in}^{-2}$ and 0.38410×10^{-4} $\text{lb}^{-1}\text{in}^{-2}$ for S_{33} and S_{44}, respectively. Comparison of these values with the underlined results in Table 5.2 shows a 65 percent increase in the bending flexibilities due to out-of-plane bending

Table 5.2: Comparison of Flexibility Coefficients of NABSA, TAIL and Present (lb, in units)

Flexibility	NABSA	PRESENT	% Diff.	TAIL	% Diff.
$S_{11} \times 10^5$	0.143883	0.14491	+0.7	0.14491	+0.7
$S_{22} \times 10^4$	0.312145	0.32364	+3.6	0.32364	+3.6
$S_{12} \times 10^5$	−0.417841	−0.43010	+2.9	−0.43010	+2.9
$S_{33} \times 10^4$	0.183684	0.1886	+2.6	0.17294	−5.8
$S_{44} \times 10^5$	0.614311	0.63429	+3.2	0.50157	−18.4

related warping.

5.3 Comparison of Deformation

The present theory is applied to the prediction of the tip deformation in a cantilevered beam made of Graphite/Epoxy and subjected to different types of loading. The beam has a CUS square cross section with $[+12]_4$ lay-up. The geometry and mechanical properties are given in Table 5.3. Comparison of results with the MSC/NASTRAN finite element analysis of Ref. [38] is provided in Table 5.4. The applied axial and transverse forces are equal to 100 lb, while the applied torsional moment is 100 lb·in.

The MSC/NASTRAN analysis is based on a $2D$ plate model accounting for both shear deformation and warping. The predictions of the present theory range from +1.7 to −0.7 percent difference relative to the finite element results.

The deflection due to transverse load neglecting out-of-plane bending related warping is equal to 1.341 inch compared to 1.853 inch (38% difference) in Table 5.4. For a CUS configuration, the extension-torsional response is decoupled from bending as shown in Eq. (5.2). Since C is constant and g_1 does not affect the stiffness coefficients,

Table 5.3: Geometry and Mechanical Properties of Thin-Walled Beam with $[+12]_4$ CUS square cross-section

Length = 24.0 in.	$E_{11} = E_{22} = E_{33} = 11.65$ Msi
Width = depth = 1.17 in.	$G_{12} = G_{13} = 0.82,\ G_{23} = 0.7$ Msi
Ply thickness = 0.0075 in.	$\nu_{12} = \nu_{13} = 0.05,\ \nu_{23} = 0.3$

as outlined in section 5.1.1, the flexibility coefficients controlling extension and twist response, S_{11}, S_{12} and S_{22} coincide with those of Refs. [43] and [44]. As a consequence, the axial displacement and twist angle predictions coincide. However, the lateral deflection under transverse load differs. The tip lateral deflection predicted using the theory of Ref. [30], which includes shear deformation, and Refs. [43] and [44], which include a shear deformation correction to Ref. [30], is 1.724 inch resulting in -7.6 percentage difference compared to the NASTRAN result. This is due to the effect of bending-related out-of-plane warping on the bending flexibilities $\frac{1}{C_{33}}$ and $\frac{1}{C_{44}}$, ($C_{33} = C_{44}$ for this case), as shown by the underlined terms in Eq. (5.2).

Figures 5.2 and 5.3 show the bending slope variation along the beam span for antisymmetric and symmetric cantilevers under a 1 lb transverse tip load, respectively. The beam geometry and its material properties are given in Table 5.5. The experimental results are reported in Refs. [41], [42], and [46]. The influence of the out-of-plane warping due to bending is isolated in these figures. The bending related out-of-plane warping, g_2U_2'' and g_3U_3'' terms in Eq. (4.68), results in a 91 and 20 % increase in the bending slope for the antisymmetric and symmetric configurations,

Table 5.4: MSC/NASTRAN and Present Solutions for a CUS Cantilevered Beam with $[+12]_4$ Layups Subjected to Various Tip Load Cases

Tip Load	Tip Deformation			% Diff.
		NASTRAN	Present	
Axial Force	Axial Disp. :	0.002189 in.	0.002202 in.	+0.6 %
Axial Force	Twist :	0.3178 deg.	0.32325 deg.	+1.7 %
Torsional Moment	Twist :	2.959 deg.	2.998 deg.	+1.32 %
Transverse Force	Deflection :	1.866 in.	1.853 in.	−0.7 %

respectively. The analytical predictions reported in Refs. [41], [42], and [46] together with results obtained on the basis of the analyses in Ref. [30], [43], [44] and the present theory are combined in Figs. 5.4 and 5.5. Results show that the present theory is in good agreement with the test data and the closest when compared to the other analytical approaches which include shear deformation, Refs. [30], [42], and [46], and shear deformation corrections, Refs. [43] and [44].

The bending slope in Figs. 5.2-5.5 is defined in terms of the cross section rotation for theories including shear deformation. For the geometry and material properties considered, this effect is negligible as shown in Figs. 5.4 and 5.5 where the spanwise slope at the fixed end from theories with shear deformation, is indistinguishable from zero. The nonzero value shown by the test data may be due to the experimental set up used to achieve clamped end conditions.

The spanwise twist distribution of symmetric cantilevered beam with $[30]_6$ and $[45]_6$ lay-ups is plotted in Figs. 5.6 and 5.7, respectively. The beams are subjected to a transverse tip load of 1 lb. Their dimensions and material properties are given in Table 5.5. Results show that the present theory and those of Refs. [43] and [44] are

Table 5.5: Cantilever Geometry and Properties

Width = 0.953 in.	E_{11} = 20.59 Msi, $E_{22} = E_{33}$ = 1.42 Msi
Depth = 0.53 in.	$G_{12} = G_{13}$ = 0.87 Msi, G_{23} = 0.7 Msi
Ply thickness = 0.005 in.	$\nu_{12} = \nu_{13}$ = 0.42, ν_{23} = 0.5

the closest to the test data. A similar behavior is found for the bending slope and the twist angle at the mid-span of the symmetric cantilevered beams appearing in Figs. 5.8 and 5.9. The beams are subjected to a tip torque of 1 lb-in.

5.4 Shear Deformation Contribution

The significance of the out-of-plane warping due to bending is illustrated in Fig. 5.2. A similar behavior is obtained in Ref. [65] when the shear deformation contribution is neglected. This indicates that the out-of-plane warping due to bending includes implicitly the shear deformation contribution. In order to assess this similarity, the present theory and the numerical work of Ref. [65] are applied to the prediction of the deflection in a cantilevered beam made of graphite/epoxy and subjected to a transverse tip load of 1 lb. The beam has a CUS cross-section with $[+15]_6$ lay-up. The geometry and mechanical property, provided in Ref. [65], are given for convenience in Table 5.6. Figure 5.10 shows a similar behavior suggesting that in the present theory, shear deformation is implicitly accounted through bending-related warping. The prediction of Ref. [65] are referred to Classical when shear deformation is neglected. Further evidence could be provided by estimating the equivalent shear deformation strain. This can be expressed by the slope of the plane that approximates

Table 5.6: Cantilever Geometry and Properties

Width = 0.923 in.	E_{11} = 20.6 Msi, $E_{22} = E_{33}$ = 1.42 Msi
Depth = 0.50 in.	$G_{12} = G_{13}$ = 0.87 Msi, G_{23} = 0.696 Msi
Ply thickness = 0.005 in.	$\nu_{12} = \nu_{13} = 0.3$, $\nu_{23} = 0.34$

the cross-section warping and is given [66] by

$$2\gamma_{xy} = -\frac{\int y\, v_1\, dA}{I_{zz}} \tag{5.7}$$

where A and I_{zz} represent the cross-sectional area and moment of inertia about the z-axis, respectively.

For a CUS box cross-section subjected to a vertical tip transverse load p_z, the shear strain distribution across the cantilever length is obtained by substituting the axial displacement v_1 from Eq. (4.68) into Eq. (5.7). The result is the following analytical expression

$$2\gamma_{xy} = \frac{(L - x_1)\, had}{4I_{zz}} \left(\frac{a^2}{3} + ad + \frac{d^2}{3}\right) S_{33} p_z \tag{5.8}$$

where

S_{33} = Bending flexibility

L = Length of cantilever

x_1 = Cross-section position measured from the fixed end

h = Laminate thickness

a = Box height

d = Box width

A comparison of the shear strain γ_{xy} over the length of the cantilever with the prediction of Ref. [65] is shown in Fig. 5.11. The shear strain at the fixed end is 4.5924×10^{-4} based on Eq. (5.8) which is within 2 percent of 4.6857×10^{-4} calculated on the basis of Ref. [65].

5.5 Conclusion

The anisotropic thin-walled closed section has been validated by comparison of response predictions with finite element solutions, other closed form analyses and test data. The influence of the two new nonclassical contributions namely, extensional and bending related out-of-plane warping on the accuracy of the response predictions is shown to be significant. Moreover, the contribution of shear deformation is shown to be implicitly accounted for through the bending related out-of-plane warping, and in-plane warping effect is found to be negligible.

5.6 Closing Remarks

For anisotropic beams, the major reason for the discrepancy in the predictions of the analytical models of Refs. [30] and [41]-[46] and the present theory is due to the apriori assumed displacement fields which neglect the extension and bending-related out-of-plane warping. The influence of the material's anisotropy on the displacement is too complex to cast in a kinematic assumption similar to classical theory of extension-bending and torsion.

A consistent approach to account for the various behavioral modes associated with anisotropic beams was adopted in this work. It is based on an asymptotical analysis of the energy. The influence of the material's anisotropy on the displacement and stiffness coefficients was isolated, and by comparison an assessment of previous

analyses was performed. In particular, this approach accounts implicitly the shear deformation contribution shown to be significant in previous models. The difference being the consistent order of magnitude that this contribution is accounted for and its significance relative to other contributions.

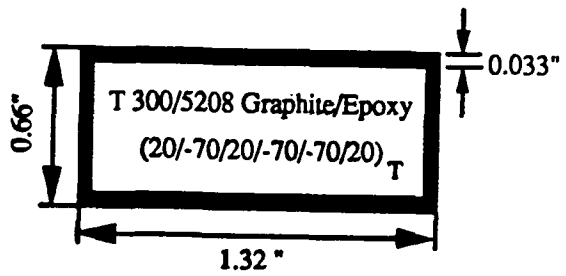

Figure 5.1: Beam Cross Section

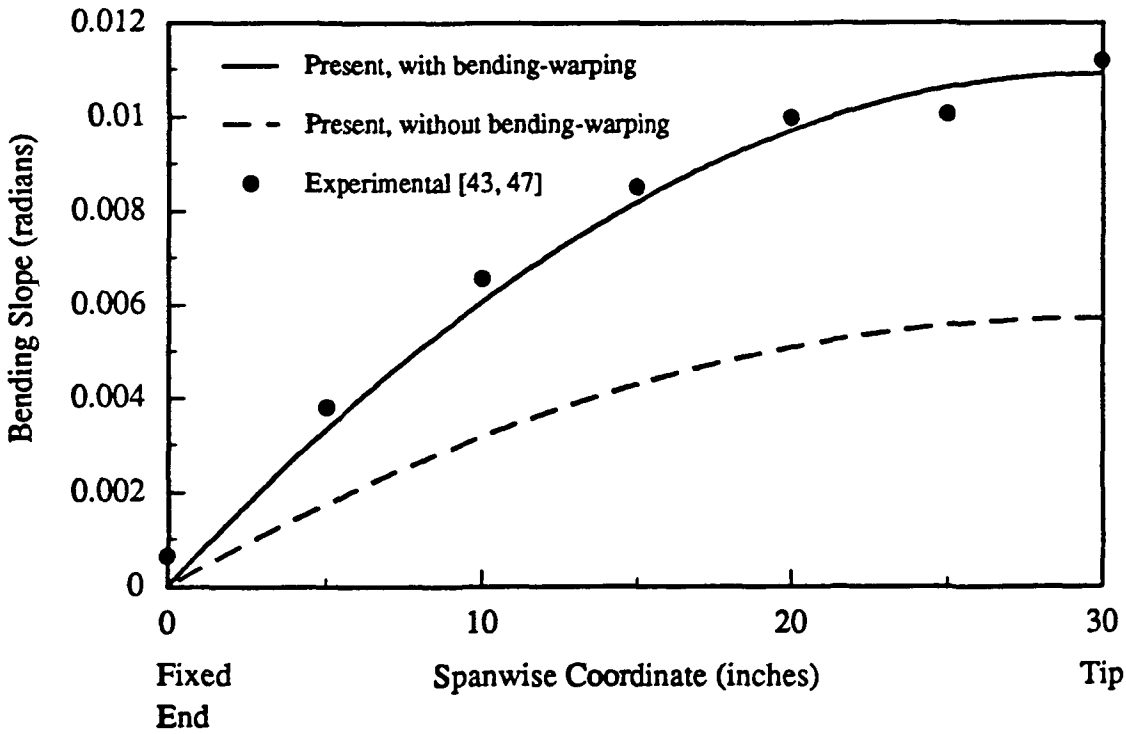

Figure 5.2: Significance of out-of-plane bending related warping on the bending slope of an antisymmetric $[15]_6$ cantilever under 1 lb transverse tip Load

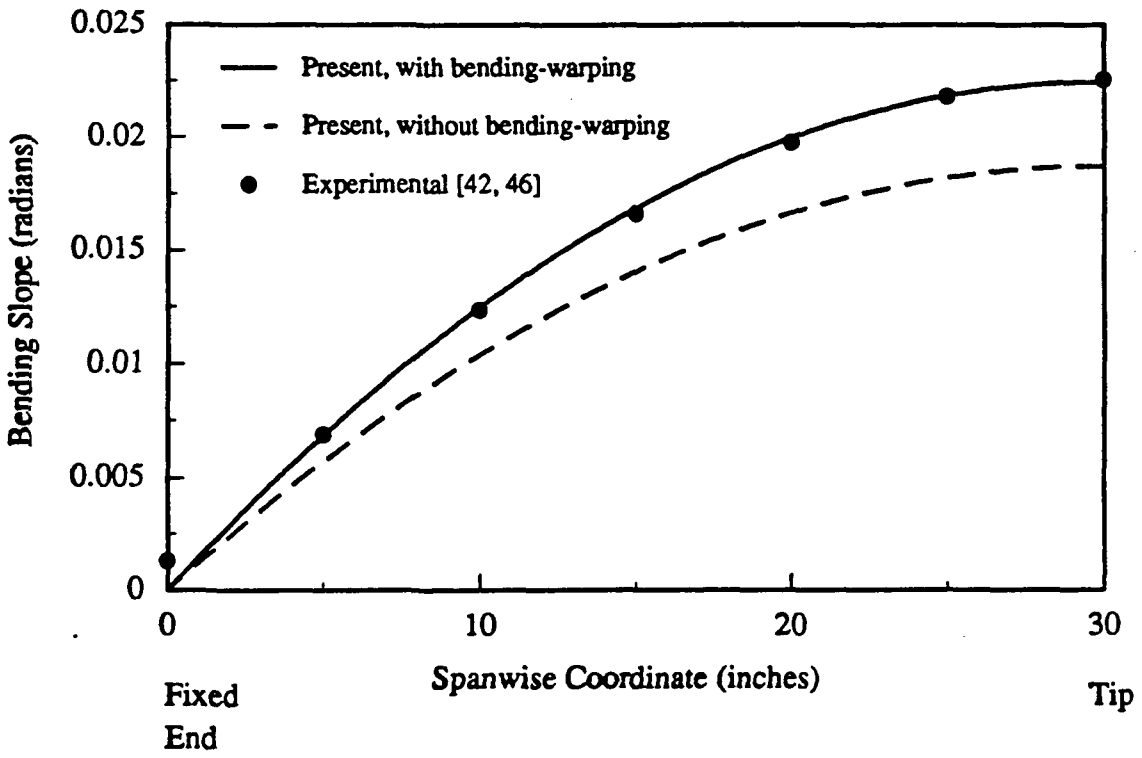

Figure 5.3: Significance of out-of-plane bending related warping on the bending slope of a symmetric $[30]_6$ cantilever under 1 lb transverse tip Load

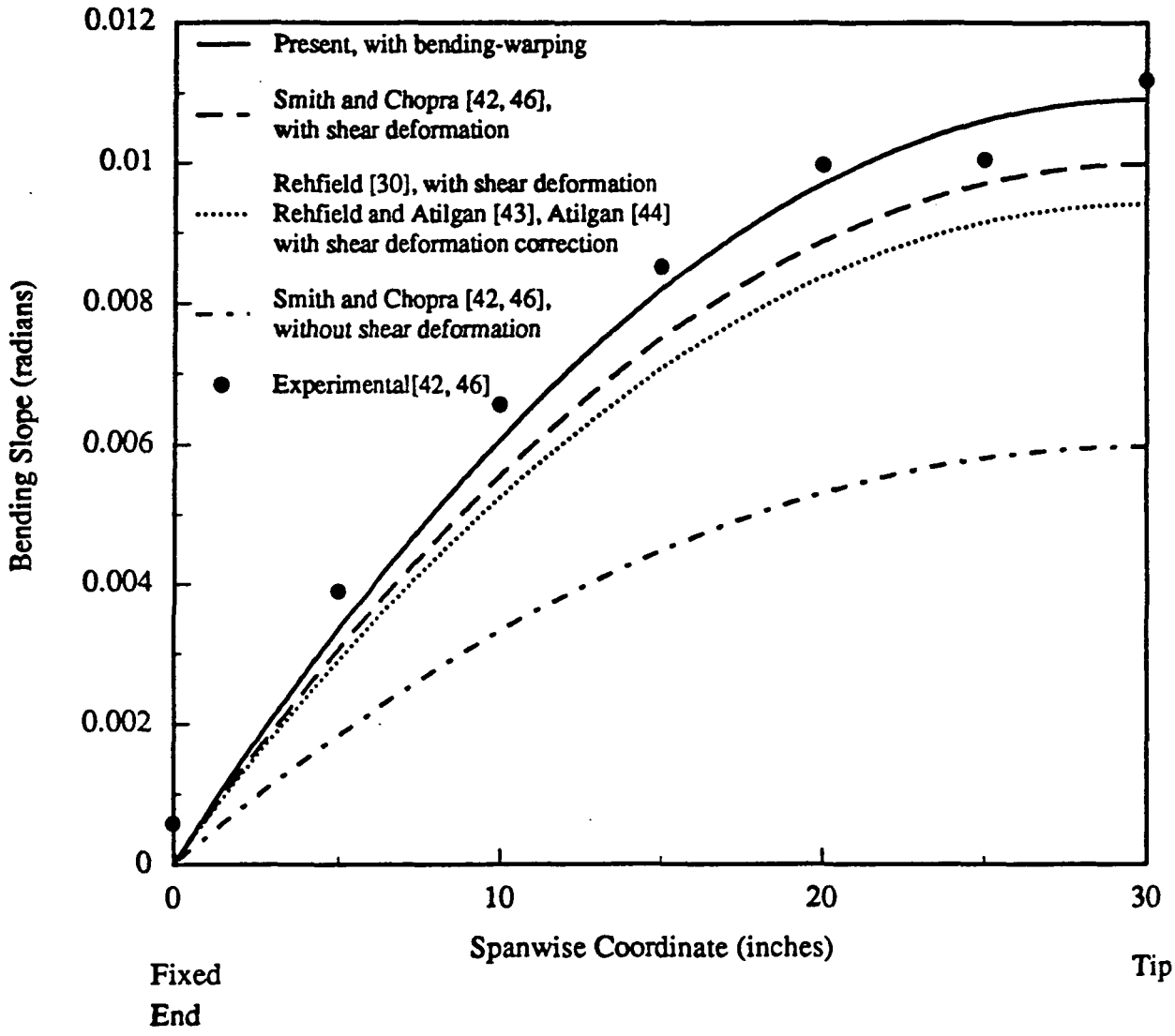

Figure 5.4: Bending Slope of an Anti-Symmetric $[15]_6$ Cantilever Under 1 lb Transverse Tip Load

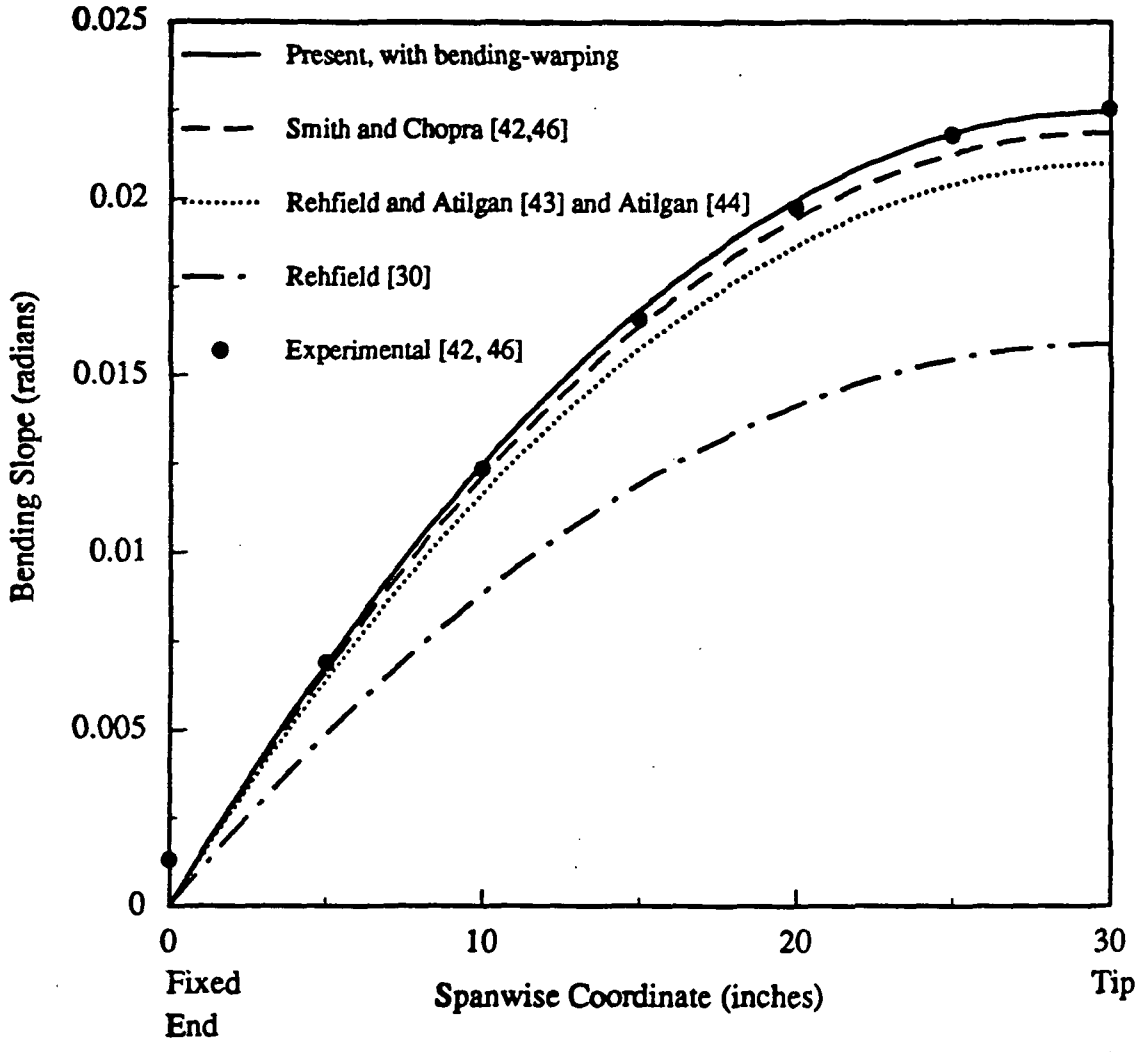

Figure 5.5: Bending Slope of a Symmetric $[30]_6$ Cantilever Under 1 lb Transverse Tip Load

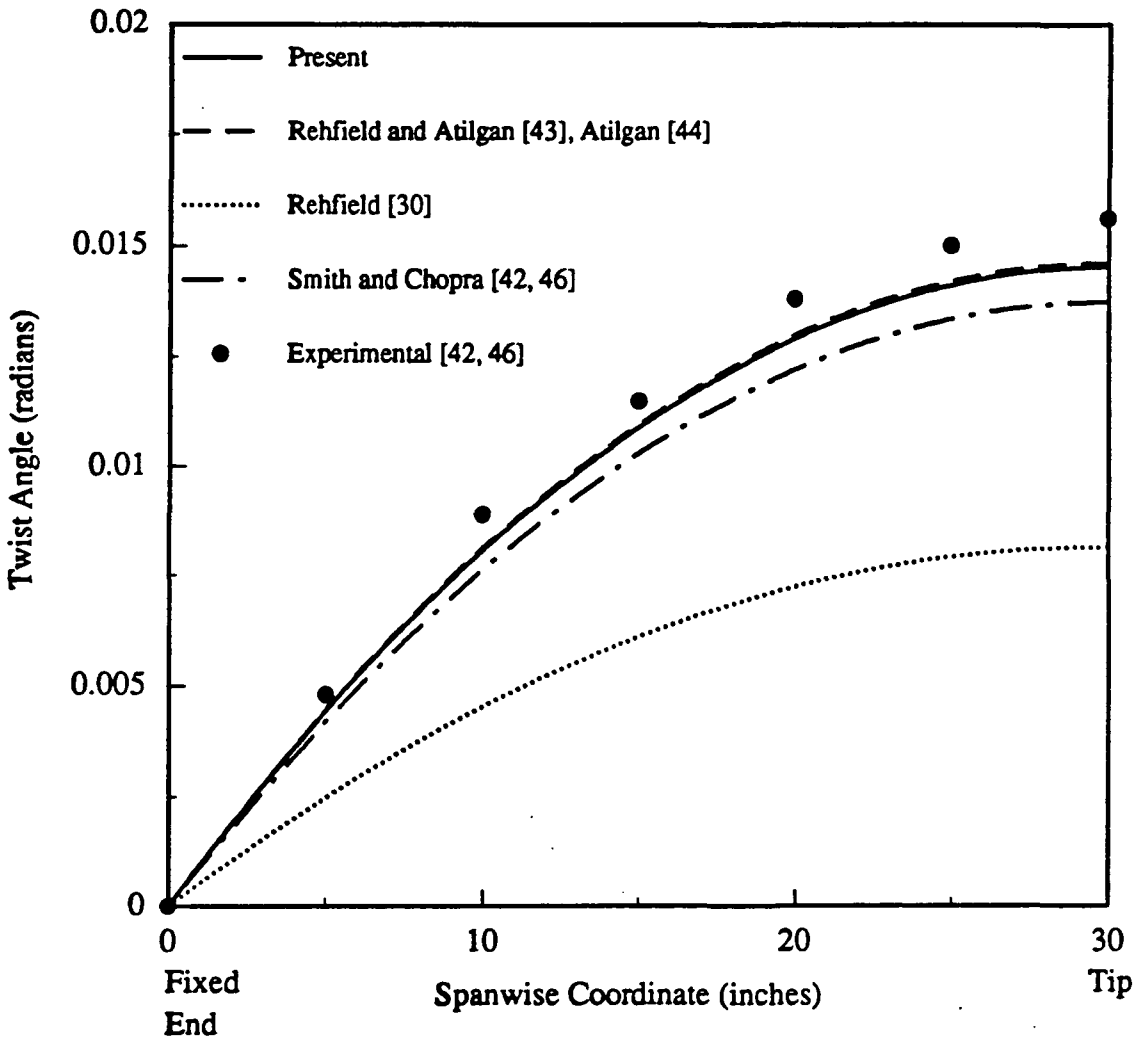

Figure 5.6: Twist of a Symmetric $[30]_6$ Cantilever Under 1 lb Transverse Tip Load

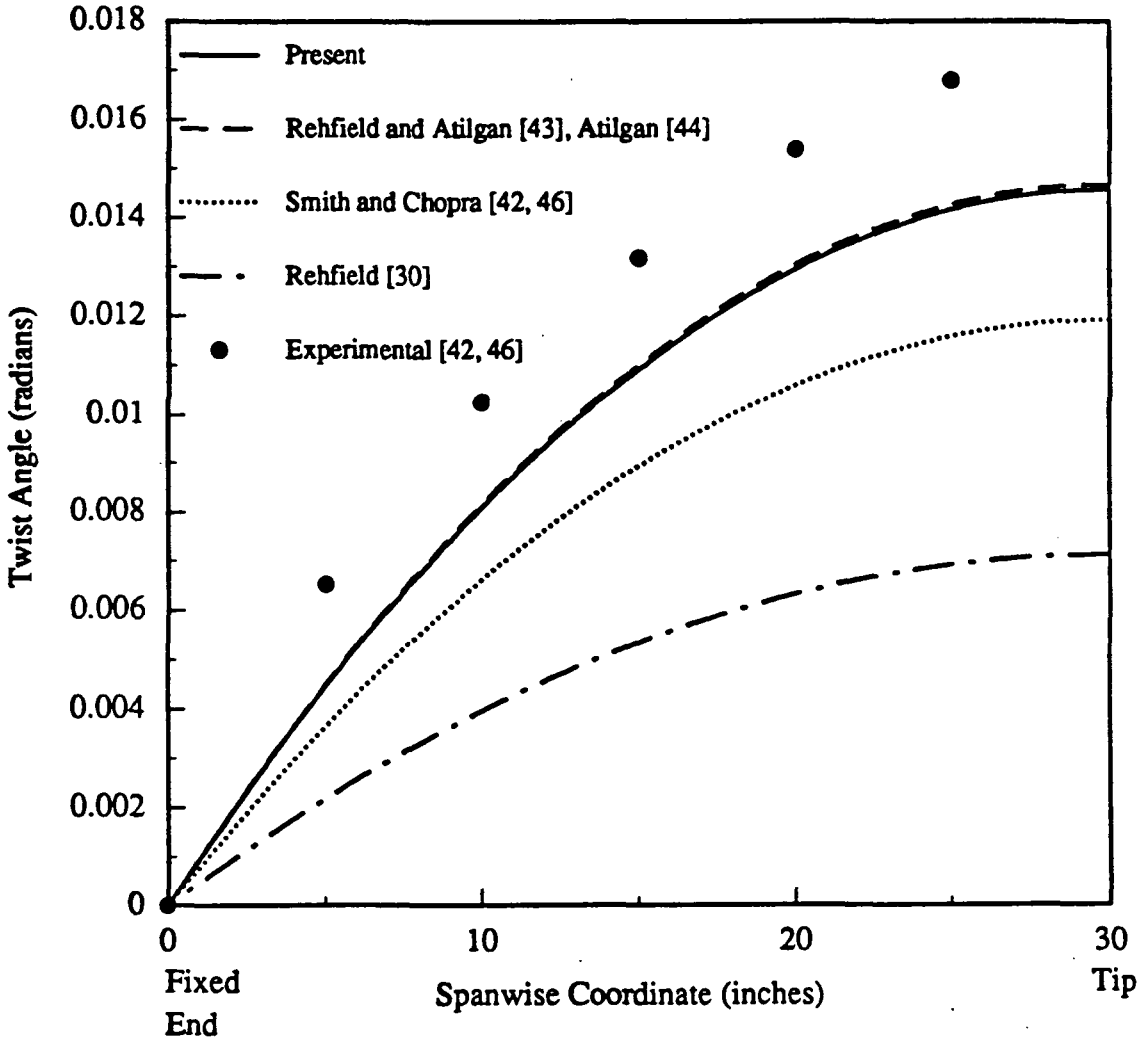

Figure 5.7: Twist of a Symmetric $[45]_6$ Cantilever Under 1 lb Transverse Tip Load

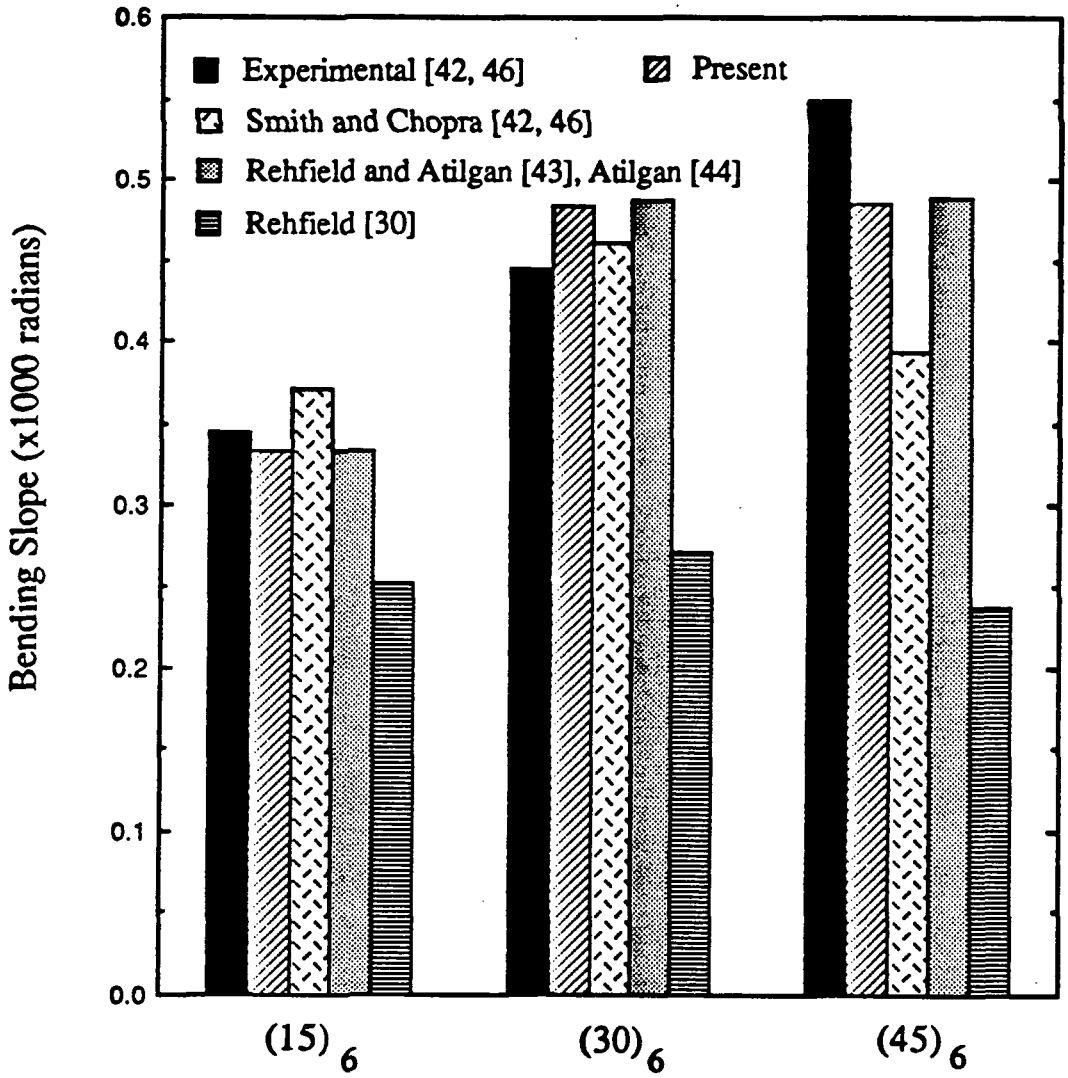

Figure 5.8: Bending Slope at Mid-Span Under Unit Tip Torque of Symmetric Lay-up Cantilever Beams

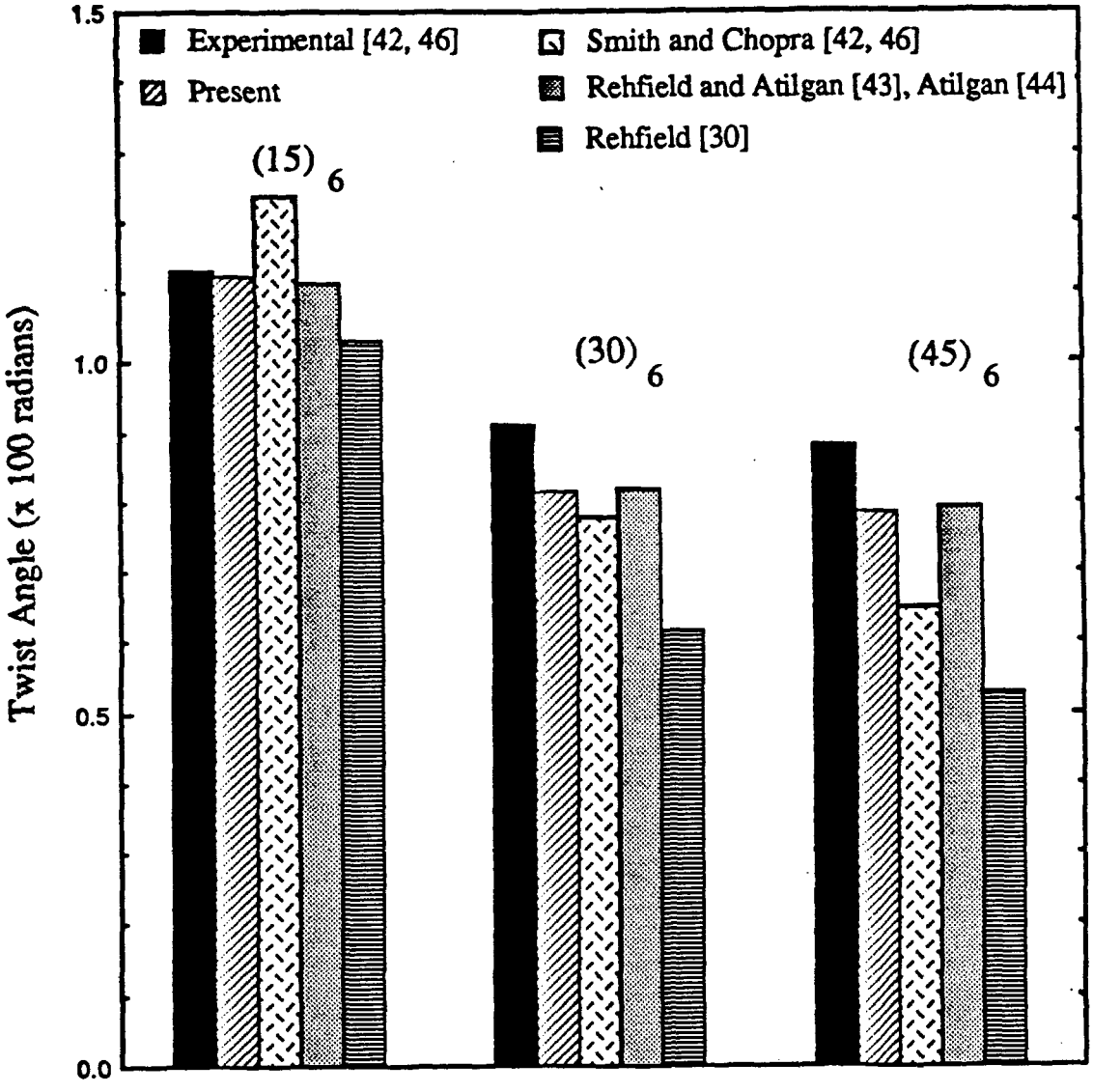

Figure 5.9: Twist at Mid-Span Under Unit Tip Torque of Symmetric Lay-up Cantilever Beams

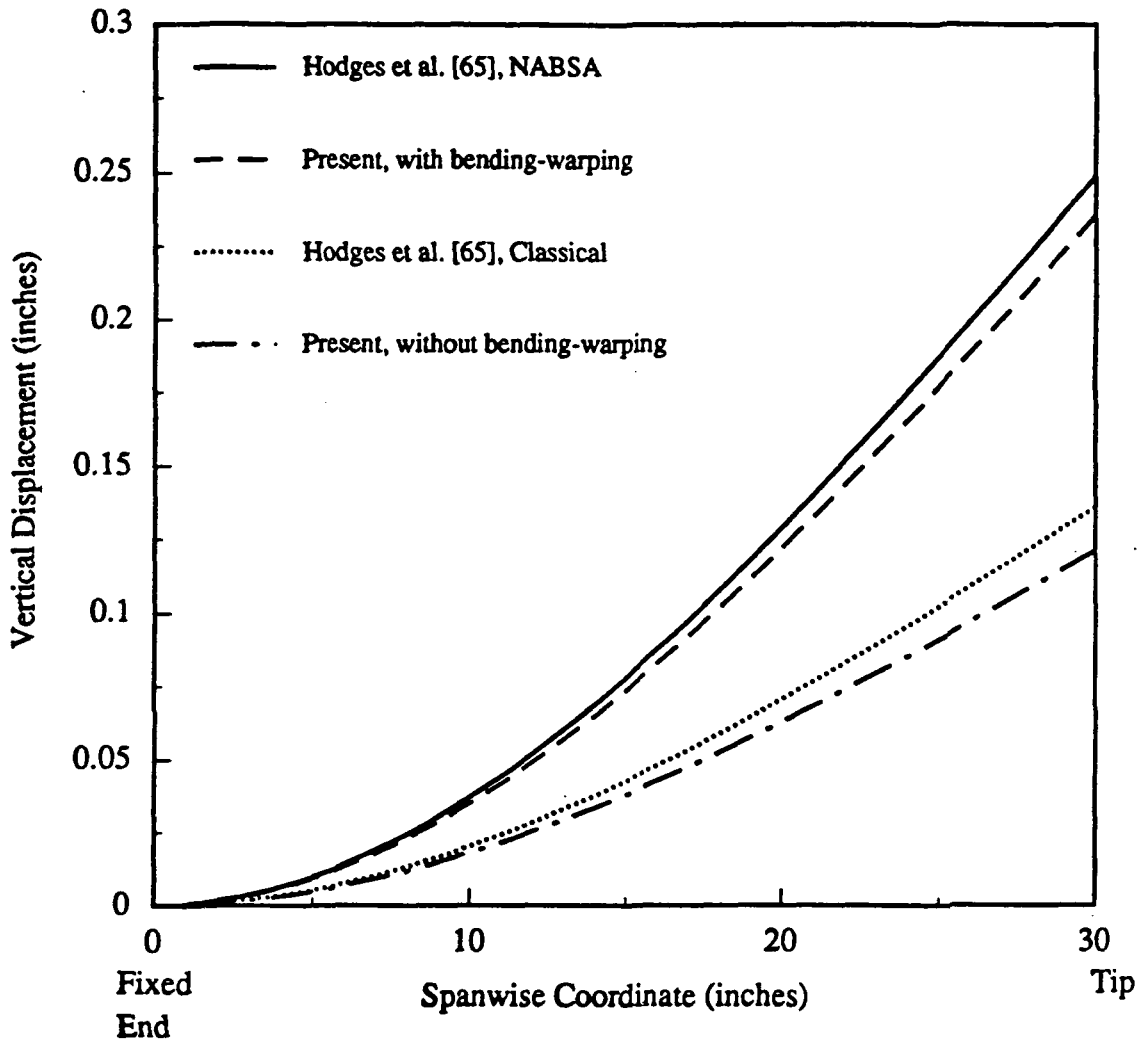

Figure 5.10: Deflection of an Antisymmetric $[15]_6$ Cantilever under 1 lb transverse tip load

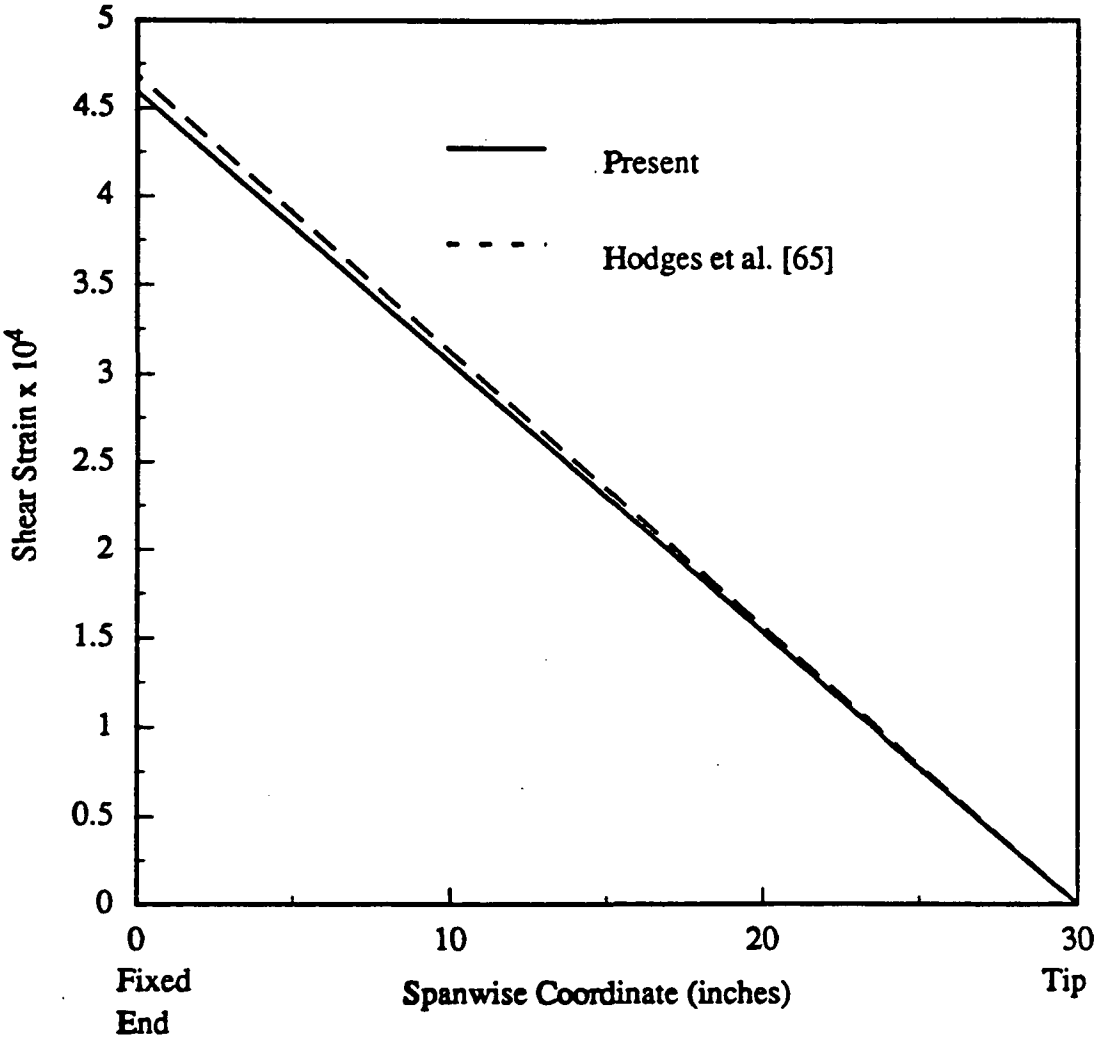

Figure 5.11: Shear Deformation γ_{xy} of an Antisymmetric $[15]_6$ Cantilever under 1 lb transverse tip load

CHAPTER VI

CONCLUSIONS AND RECOMMENDATIONS

This research addresses two key issues for the continuing implementation of composites in advanced structures namely, the understanding of the role of the material's anisotropy on its stiffness behavior and its damage modes. An analytical model based upon a shear deformation theory and a sublaminate approach was developed in order to investigate mid-plane and matrix crack-tip delaminations. This model was combined with an earlier analysis for mixed-mode free-edge delamination to form an integrated code for the prediction of damage onset in laminated composites. The code predictions were validated by comparing its results with test data. Of significance is the ability it provides for the prediction of damage progression sequence and corresponding critical strains. Moreover, the effect of hygrothermal stresses on the strain energy release rate and interlaminar stresses was isolated. The increase in strain energy release rate and interlaminar stresses associated with curing stresses can precipitate failure and should be considered for an accurate prediction of failure.

The findings of this research work point to new research inquiries. The first is characterization and prediction of damage onset and growth under cyclic loading including the effect of hygrothermal stresses. The investigation can lead to the determination of composite components' life and inspection intervals. The second is the study of the effect of damage modes and their interactions on the vibration characteristics and damping of laminated composites. The result of this investigation will assess the effect of damage modes on the natural frequencies and mode shapes and

can lead to the development of Non-Destructive Evaluation methods.

The asymptotical analysis used to develop the thin-walled anisotropic beam theory provides a rigorous basis for the prediction of the beam stiffnesses and associated displacement field. Closed-form expressions for the stiffnesses have been developed and new contributions to the warping have been found. This analysis can be extended to beams with multi-cell type cross sections and pretwisted configurations. Moreover, the previous results on the effects of hygrothermal stresses point to the significance of including their contribution in the thin-walled closed section beam analysis. The consideration of dynamic and aerodynamic loadings using asymptotical analysis will provide a rigorous basis for the investigation of the dynamic and aeroelastic response of composite structures. Finally, the presence of embedded delamination on the response of composite beams is a first step toward studying the effect of damage modes on their stiffness and strength. In this respect, the analysis of composite beams with open cross section can be regarded as the final stage of damage in a closed section beam.

When accomplished, these recommended research tasks will provide an understanding of the effects of damage on the performance of advanced structures made out of composite and will lead to the development of reliable design tools to ensure their damage tolerance.

Appendix A

Convergence of Displacement Field

In this appendix detailed calculation of the third and final cycle is provided. Results show that no additional correction terms of the same order in the energy functional emerge and the displacement field given in Eq. (4.68) is the converged one.

1.1 Third-Order Approximation

A third cycle is carried out by rewriting the displacement field in Eq. (4.68) in the form

$$\begin{aligned} v_1 &= U_1(x) - y(s)U_2'(x) - z(s)U_3'(x) + G(s)\varphi'(x) \\ &\quad + g_1(s)U_1'(x) + g_2(s)U_2''(x) + g_3(s)U_3''(x) + \tilde{\bar{w}}_1(s,x) \\ v_2 &= U_2(x)\frac{dy}{ds} + U_3(x)\frac{dz}{ds} + \varphi(x)r_n + \tilde{\bar{w}}_2(s,x) \\ v &= U_2(x)\frac{dz}{ds} - U_3(x)\frac{dy}{ds} - \varphi(x)r_t + \tilde{\bar{w}}(s,x) \end{aligned} \qquad (A-1)$$

where $\tilde{\bar{w}}_1, \tilde{\bar{w}}_2$ and $\tilde{\bar{w}}$ are correction functions to be determined based on their contributions to the energy functional.

Substitute Eq. (A-1) into (4.7) to obtain the strains and curvatures in terms of the displacement corrections

$$\gamma_{11} = \breve{\bar{\gamma}}_{11} + \frac{\partial \tilde{\bar{w}}_1}{\partial x}$$

$$2\gamma_{12} = 2\breve{\bar{\gamma}}_{12} + \frac{\partial \tilde{\bar{w}}_2}{\partial x} + 2\hat{\tilde{\gamma}}_{12} \quad , \quad 2\hat{\tilde{\gamma}}_{12} = \frac{\partial \tilde{\bar{w}}_1}{\partial s}$$

$$\gamma_{22} = \breve{\bar{\gamma}}_{22} + \hat{\tilde{\gamma}}_{22} \quad , \quad \hat{\tilde{\gamma}}_{22} = \frac{\partial \tilde{\bar{w}}_2}{\partial s} + \frac{\tilde{\bar{w}}}{R}$$

$$\rho_{11} = \breve{\rho}_{11} + \frac{\partial^2 \tilde{\bar{w}}}{\partial x^2} \qquad (A-2)$$

$$\rho_{12} = \breve{\rho}_{12} + \frac{\partial^2 \tilde{\bar{w}}}{\partial s \partial x} - \frac{3}{4R}\frac{\partial \tilde{\bar{w}}_2}{\partial x} + \hat{\bar{\rho}}_{12} \quad , \quad \hat{\bar{\rho}}_{12} = \frac{1}{4R}\frac{\partial \tilde{\bar{w}}_1}{\partial s}$$

$$\rho_{22} = \breve{\rho}_{22} + \hat{\bar{\rho}}_{22} \quad , \quad \hat{\bar{\rho}}_{22} = \frac{\partial^2 \tilde{\bar{w}}}{\partial s^2} - \frac{\partial}{\partial s}\left(\frac{\tilde{\bar{w}}_2}{R}\right)$$

where $\breve{\gamma}_{\alpha\beta}$ and $\breve{\rho}_{\alpha\beta}$ are the strains and curvatures corresponding to the second-order approximation. These are expressed as

$$\breve{\gamma}_{11} = \overbrace{U_1'(x)}^{\left(\frac{\Delta}{L}\right)} - \overbrace{yU_2''(x)}^{\left(\frac{\Delta d}{L^2}\right)} - \overbrace{zU_3''(x)}^{\left(\frac{\Delta d}{L^2}\right)} + \overbrace{G(s)\varphi''(x)}^{\left(\frac{\Delta d}{L^2}\right)}$$
$$+ \overbrace{g_1(s)U_1''(x)}^{\left(\frac{\Delta d}{L^2}\right)} + \overbrace{g_2U_2'''(x)}^{\left(\frac{\Delta d^2}{L^3}\right)} + \overbrace{g_3U_3'''(x)}^{\left(\frac{\Delta d^2}{L^3}\right)}$$

$$2\breve{\gamma}_{12} = \overbrace{\frac{2A_\epsilon}{l\bar{c}}c\varphi'(x)}^{\left(\frac{\Delta}{L}\right)} + \overbrace{\frac{dg_1}{ds}U_1'(x)}^{\left(\frac{\Delta}{L}\right)} + \overbrace{\frac{dg_2}{ds}U_2''(x)}^{\left(\frac{\Delta d}{L^2}\right)} + \overbrace{\frac{dg_3}{ds}U_3''(x)}^{\left(\frac{\Delta d}{L^2}\right)}$$

$$\breve{\gamma}_{22} = 0$$

$$\breve{\rho}_{11} = U_2''(x)\frac{dz}{ds} - U_3''(x)\frac{dy}{ds} - \varphi''(x)r_t \sim O\left(\frac{\Delta}{L^2}\right) \qquad (A-3)$$

$$\breve{\rho}_{12} = \frac{1}{4R}\frac{dg_1}{ds}U_1'(x) + \left(\frac{1}{4R}\frac{2A_\epsilon}{l\bar{c}}c - 1\right)\varphi'(x) \sim O\left(\frac{\Delta}{dL}\right)$$

$$\breve{\rho}_{22} = 0$$

An order of magnitude comparison for each strain and curvature measure shows that some terms of higher order in $\breve{\gamma}_{11}$ can be cancelled and its expression simplifies to

$$\breve{\gamma}_{11} = \overbrace{U_1'(x)}^{\left(\frac{\Delta}{L}\right)} - \overbrace{yU_2''(x)}^{\left(\frac{\Delta d}{L^2}\right)} - \overbrace{zU_3''(x)}^{\left(\frac{\Delta d}{L^2}\right)} + \overbrace{G(s)\varphi''(x)}^{\left(\frac{\Delta d}{L^2}\right)}$$

Among the new terms introduced by the function $\tilde{\bar{w}}_i$ the leading ones are denoted by superscript $\hat{}$ in Eq. (A-2). The order of $\tilde{\bar{w}}_i$ is assumed to be

$$\tilde{\bar{w}}_i \sim O\left(\frac{\Delta d^3}{L^3}\right) \qquad (A-4)$$

Consequently, the order of magnitude of the leading terms in Eq. (A-2), is as follows

$$\hat{\tilde{\gamma}}_{12} \sim \hat{\tilde{\gamma}}_{22} \sim O\left(\frac{\Delta d^2}{L^3}\right)$$

$$\hat{\tilde{\rho}}_{12} \sim \hat{\tilde{\rho}}_{22} \sim O\left(\frac{\Delta d}{L^3}\right) \qquad (A-5)$$

The energy functional can be represented by $\Phi(\gamma_{11}, 2\gamma_{12}, \gamma_{22}, \rho_{11}, \rho_{12}, \rho_{22})$. By keeping the strains and curvature associated with the second-order approximation and the leading terms contribution over the other terms (i.e., by dropping the terms $\frac{\partial \hat{\tilde{w}}_1}{\partial x}$, $\frac{\partial \hat{\tilde{w}}_2}{\partial x}$, $\frac{\partial^2 \hat{\tilde{w}}}{\partial x^2}$, and $\frac{\partial^2 \hat{\tilde{w}}}{\partial s \partial x} - \frac{1}{4R}\frac{\partial \hat{\tilde{w}}_2}{\partial x}$ in Eq. (A-2)) the energy function can be written as

$$\Phi(\breve{\tilde{\gamma}}_{11}, 2\breve{\tilde{\gamma}}_{12} + 2\hat{\tilde{\gamma}}_{12}, 0 + \hat{\tilde{\gamma}}_{22}, \breve{\tilde{\rho}}_{11}, \breve{\tilde{\rho}}_{12} + \hat{\tilde{\rho}}_{12}, 0 + \hat{\tilde{\rho}}_{22}) \qquad (A-6)$$

In the following, the order of magnitude of the energy due to bending, i.e. due to $\breve{\tilde{\rho}}_{11}$, $\breve{\tilde{\rho}}_{12}$, $\hat{\tilde{\rho}}_{12}$, and $\hat{\tilde{\rho}}_{22}$, is assessed.

The interaction terms associated with $\breve{\tilde{\rho}}_{11}$, namely

$$h\breve{\tilde{\rho}}_{11}\hat{\tilde{\gamma}}_{12}\,,\; h\breve{\tilde{\rho}}_{11}\hat{\tilde{\gamma}}_{22}\,,\; h^2\breve{\tilde{\rho}}_{11}\hat{\tilde{\rho}}_{12}\,,\; h^2\breve{\tilde{\rho}}_{11}\hat{\tilde{\rho}}_{22}$$

are of order $\left(\frac{\Delta^2 h d^2}{L^5}\right)$ or smaller. They are neglected in comparison with the following membrane contribution to the energy

$$\breve{\tilde{\gamma}}_{11}\hat{\tilde{\gamma}}_{12}\,,\; \breve{\tilde{\gamma}}_{11}\hat{\tilde{\gamma}}_{22}\,,\; \breve{\tilde{\gamma}}_{12}\hat{\tilde{\gamma}}_{12}\,,\; \breve{\tilde{\gamma}}_{12}\hat{\tilde{\gamma}}_{22} \begin{cases} \sim O\left(\frac{\Delta^2 d^2}{L^4}\right) & \text{associated with } U_1' \text{ and } \varphi' \\ \sim O\left(\frac{\Delta^2 d^3}{L^5}\right) & \text{associated with } U_2'' \text{ and } U_3'' \end{cases} \qquad (A-7)$$

The interaction terms due to the bending curvature $\breve{\tilde{\rho}}_{12}$ are

$$h\breve{\tilde{\rho}}_{12}\hat{\tilde{\gamma}}_{12}\,,\; h\breve{\tilde{\rho}}_{12}\hat{\tilde{\gamma}}_{22} \sim O\left(\frac{\Delta^2 h d}{L^4}\right) \text{ associated with } U_1' \text{ and } \varphi'$$

$$h^2\breve{\tilde{\rho}}_{12}\hat{\tilde{\rho}}_{12}\,,\; h^2\breve{\tilde{\rho}}_{12}\hat{\tilde{\rho}}_{22} \sim O\left(\frac{\Delta^2 h^2}{L^4}\right) \text{ associated with } U_1' \text{ and } \varphi'$$

These terms are of higher order of magnitude in comparison with the corresponding membrane contribution in Eq. (A-7), and may be neglected. The remaining interaction terms associated with $\hat{\tilde{\rho}}_{12}$ and $\hat{\tilde{\rho}}_{22}$, namely

$$h\breve{\tilde{\gamma}}_{11}\hat{\tilde{\rho}}_{12}\,,\; h\breve{\tilde{\gamma}}_{12}\hat{\tilde{\rho}}_{12}\,,\; h\breve{\tilde{\gamma}}_{11}\hat{\tilde{\rho}}_{22}\,,\; h\breve{\tilde{\gamma}}_{12}\hat{\tilde{\rho}}_{22}\begin{cases}\sim O\left(\frac{\Delta^2 hd}{L^4}\right) & \text{associated with } U_1' \text{ and } \varphi' \\ \sim O\left(\frac{\Delta^2 hd^2}{L^5}\right) & \text{associated with } U_2'' \text{ and } U_3''\end{cases}$$

may also be neglected in comparison with (A-7). Therefore in order to determine the functions $\tilde{\tilde{w}}_i$ one has to minimize the shell energy expressed by

$$I = \int_0^L \oint \Phi(\breve{\tilde{\gamma}}_{11}, 2\breve{\tilde{\gamma}}_{12} + 2\hat{\tilde{\gamma}}_{12}, \hat{\tilde{\gamma}}_{22}, 0, 0, 0)\, ds dx \qquad (A-8)$$

Setting the first variation of the energy functional to zero to get Eq. (4.45). Substitute from Eq. (A-2) into Eq. (4.45) to obtain

$$\frac{1}{2}\overbrace{B}^{(Eh)}\left[\overbrace{U_1'(x)}^{\left(\frac{\Delta}{L}\right)} - \overbrace{y(s)U_2''}^{\left(\frac{\Delta d}{L^2}\right)} - \overbrace{z(s)U_3''}^{\left(\frac{\Delta d}{L^2}\right)} + \overbrace{G(s)\varphi''(x)}^{\left(\frac{\Delta d}{L^2}\right)} + \overbrace{\frac{\partial \tilde{\tilde{w}}_1}{\partial x}}^{\left(\frac{\Delta d^3}{L^4}\right)}\right]$$

$$+ \frac{1}{4}\overbrace{C}^{(Eh)}\left[\overbrace{\frac{2A_\epsilon}{l\bar{c}}c\varphi'(x)}^{\left(\frac{\Delta}{L}\right)} + \overbrace{\frac{dg_1}{ds}U_1'(x)}^{\left(\frac{\Delta}{L}\right)} + \overbrace{\frac{dg_2}{ds}U_2''(x)}^{\left(\frac{\Delta d}{L^2}\right)}\right.$$

$$\left. + \overbrace{\frac{dg_3}{ds}U_3''(x)}^{\left(\frac{\Delta d}{L^2}\right)} + \overbrace{\frac{\partial \tilde{\tilde{w}}_2}{\partial x}}^{\left(\frac{\Delta d^3}{L^4}\right)} + \overbrace{\frac{\partial \tilde{\tilde{w}}_1}{\partial s}}^{\left(\frac{\Delta d^2}{L^3}\right)}\right] = \text{constant} \qquad (A-9)$$

Equation (A-9) shows that the contribution of $\tilde{\tilde{w}}$ is of higher order in comparison with all other terms and may be cancelled from the left hand side. Therefore no additional corrections to the displacement field emerges, and the displacement field obtained in

Eq. (4.68) is the converged one. An alternative is to neglect the terms of higher order in Eq. (A-9), while keeping the leading $\tilde{w}_1$ term, to obtain

$$\frac{1}{2}B\left[U_1'(x) - y(s)U_2'' - z(s)U_3''\right]$$

$$+\frac{1}{4}C\left[\frac{2A_e}{l\bar{c}}c\varphi'(x) + \frac{dg_1}{ds}U_1'(x) + \frac{dg_2}{ds}U_2''(x) + \frac{dg_3}{ds}U_3''(x) + \frac{\partial\tilde{w}_1}{\partial s}\right] = \text{constant} \qquad (A-10)$$

Solution of Eq. (A-10) is determined using the single value condition of the axial displacement and $\tilde{w}_1$ is found to be a function of x only. Such a function has already been considered and no new terms of the same order in the energy functional are generated from the third and therefore final cycle.

Bibliography

[1] O'Brien, T.K., "Characterization of Delamination Onset and Growth in a Composite Laminate," Damage in Composite Materials, *ASTM STP 775*, K.L. Reifsnider, Ed., 1982, pp. 140-167.

[2] Wilkins, D.J., Eisemann, J.R., Camin, R.A., Margolis, W.S., and Benson, R.A., "Characterizing Delamination Growth in Graphite-Epoxy," Damage in Composite Materials, *ASTM STP 775*, K.L. Reifsnider, Ed., 1982, pp. 168-183.

[3] O'Brien, T.K., "Mixed-Mode Strain Energy Release Rate Effects on Edge Delamination of Composites," Effects of Defects in Composite Materials, *ASTM STP 836*, 1984, pp. 125-142.

[4] Wang, S.S., and Choi, I., "The Mechanics of Delamination in Fiber Reinforced Composite Materials. Part II - Delamination Behavior and Fracture Mechanics Parameters," *NASA CR-172270*, 1983.

[5] Wang, S.S., "Edge Delamination in Angle Ply Composite Laminates," *Proceedings of the 22nd AIAA/ASME/ASC/AHS Structures, Structural Dynamics and Materials Conference*, Atlanta, Ga, 6-8 April, 1981, pp. 473-484.

[6] Armanios, E.A., and Rehfield, L.W., "Sublaminate Analysis of Interlaminar Fracture in Composites: Part I - Analytical Model," *Journal of Composites Technology and Research*, Vol. 11, No. 4, 1989, pp. 135-146.

[7] Armanios, E.A., Rehfield, L.W., Raju, I.S., and O'Brien, T.K., "Sublaminate Analysis of Interlaminar Fracture in Composites: Part II - Applications," *Journal of Composites Technology and Research*, Vol. 11, No. 4, 1989, pp. 147-153.

[8] Crossman, F.W., and Wang, A.S.D., "The Dependence of Transverse Cracking and Delamination on Ply Thickness in Graphite/Epoxy Laminates," *Damage in Composite Materials*, ASTM STP 775, K.L. Reifsnider, Ed., 1982, pp. 118-139.

[9] O'Brien, T.K., "Analysis of Local Delaminations and their Influence on Composite Laminate Behavior," Delamination and Debonding of Materials, *ASTM STP 876*, W.S. Johnson, Ed., 1985, pp. 282-297.

[10] Law, G.E., "A Mixed Mode Fracture Analysis of $(\pm 25/90_n)_s$ Graphite/Epoxy Composite Laminates," it Effects of Defects in Composite Materials, ASTM STP 836, 1984, pp. 143-160.

[11] Wang, A.S.D, Kishore, N.N., and Li, C.A., "Crack Development in Graphite Epoxy Cross Ply Laminates under Uniaxial Tension," *Composites Science and Technology*, Vol. 24, No. 1, 1985, pp. 1-31.

[12] Fish, John C. , and O'Brien, T. Kevin, "Three-Dimensional Finite Element Analysis of Delamination from Matrix Cracks in Glass-Epoxy Laminates," Testing and Design, *ASTM 10th Symposium on Composite Materials*, San Francisco, CA., April 24-25, 1990.

[13] Russell, A.J., and Street, K.N., "Moisture and Temperature Effects on the Mixed Mode Delamination Fracture of Unidirectional Graphite/Epoxy," *Delamination and Debonding of Materials*, ASTM STP 876, W.S. Johnson, Ed., 1985, pp. 349-370.

[14] O'Brien, T.K., Raju, I.S., and Garber, D.P., "Residual Thermal and Moisture Influences on the Strain Energy Release Rate Analysis of Edge Delamination," *Journal of Composites Technology and Research*, Vol. 8, No. 2, 1986, pp. 37-47.

[15] Armanios, E.A., and Mahler, M.A., "Residual Thermal and Moisture Influences on the Free-Edge Delamination of Laminated Composites," *Proceedings of the 29th AIAA/ASME/AHS/ASC Structures, Structural Dynamics and Materials Conference*, Williamsburg, Va., 18-20 April, 1988, pp. 371-381. AIAA Paper 88-2259.

[16] Aoki, Takahira and Kondo, Kyohei, "Delamination Energy Release Rates under Thermal Loading in Fiber-Reinforced Composite Laminates," *Composite Structures*, Vol. 14, 1990, pp. 213-231.

[17] Kondo, K. and Aoki, T., "An Energy Release Rate Approach for Free-Edge Delamination Problem in Composite Laminates," *Composite Structures*, Vol. 2, No. 4, 1987, pp. 241-257.

[18] Whitney, J.M., "Stress Analysis of Mode I Edge Delamination Specimen for Composite Materials," *AIAA Journal*, Vol. 24, No. 7, 1986, pp. 1163-1168.

[19] Jones, R.M., it Mechanics of Composite Materials, McGraw Hill Book Co., New York, 1975.

[20] Whitney, J. M. and Knight, M., "A Modified Free-Edge Delamination Specimen," *Delamination and Debonding of Materials*, ASTM STP 876, edited by W. S. Johnson, Philadelphia, 1985, pp. 298-314.

[21] Irwin, G. R., "Fracture I," *Handbuk der Physik*, Vol. VI, Flugge, Ed., Springler-Verlag, 1958, pp. 558-590.

[22] Armanios, E.A., Rehfield, L.W., and Weinstein, F., "Understanding and Predicting Sublaminate Damage Mechanisms in Composite Structures," Composite Materials: Testing and Design (Ninth Volume), *ASTM STP 1059*, S.P. Garbo, Ed., 1990, pp. 231-249.

[23] Wang, A.S.D., Kishore, N.N., and Feng, W.W., "On Mixed Mode Fracture in Off-Axis Unidirectional Graphite-Epoxy Composites," *Progress in Science and Engineering of Composites*, T. Hayashi, K Kawata and S. Umekawa, Eds., ICCM-IV, Tokyo, 1982, pp. 599-606.

[24] V. L. Berdichevsky, "On the Energy of an Elastic Rod," *Journal of Applied Mathematics and Mechanics (PMM)*, Vol. 45, 1982, pp.518-529.

[25] Berdichevsky, V. L., "Variational-Asymptotic Method of Constructing a Theory of Shells," *Journal of Applied Mathematics and Mechanics (PMM)* Vol. 43, No. 4, 1979, pp. 664-687

[26] Hodges, D. H., "Review of Composite Rotor Blade Modeling," *AIAA Journal*, Vol.28, No. 3, 1990, pp. 561-565.

[27] Reissner E., and Tsai, W. T., "Pure Bending, Stretching, and Twisting of Anisotropic Cylindrical Shells," *Journal of Applied Mechanics*, Vol. 39, March 1972, pp. 148-154.

[28] Mansfield, E. H., and Sobey, A. J., "The Fibre Composite Helicopter Blade - Part 1: Stiffness Properties - Part 2: Prospect for Aeroelastic Tailoring," *Aeronautical Quarterly*, Vol. 30,May 1979, pp. 413-449.

[29] Libove, C., "Stresses and Rate of Twist in Single-Cell Thin-Walled Beams with

Anisotropic Walls," *AIAA Journal*, Vol. 26, No. 9, September 1988, pp. 1107-1118.

[30] Rehfield, L. W., "Design Analysis Methodology for Composite Rotor Blades," *Proceedings of the Seventh DoD/NASA Conference on Fibrous Composites in Structural Design*, AFWAL-TR-85-3094, June 1985, pp. (V(a)-1)-(V(a)-15).

[31] Borri, M., and Merlini, T., "A Large Displacement Formulation for Anisotropic Beam Analysis," *Meccanica*, Vol.21, 1986, pp. 30-37.

[32] Giavotto, V., Borri, M., Mantegazza, P., Ghiringhelli, G., Carmashi, V., Maffioli, G.C., and Mussi, F., "Anisotropic Beam Theory and Applications," *Computers and Structures*, Vol. 16, No. 1-4, 1983, pp. 403-413.

[33] Bauchau, O.A., and Hong, C.H., "Large Displacement Analysis of Naturally Curved and Twisted Composite Beams," *AIAA Journal*, Vol. 25, No.10, 1987, pp. 1469-1475.

[34] Bauchau, O.A., and Hong, C.H., "Nonlinear Composite Beam Theory," *Journal of Applied Mechanics*, Vol.55, No.1, 1988, pp. 156-163.

[35] Librescu, L. and Song, O., "Static Aeroelastic Tailoring of Composite Aircraft Wings Modeled as Thin-Walled Beam Structure," Presented at the *Fifth Japan-US Conference on Composite Materials*, June 24-27, 1990, Tokyo, Japan.

[36] Kosmatka, J.B., "Structural Dynamic Modeling of Advanced Composite Propellers by the Finite Element Method," *Ph.D. Dissertation*, University of California, Los Angeles, 1986.

[37] Lee, S.W., and Stemple, A.D., "A Finite Element Model for Composite Beams with Arbitrary Cross-Sectional Warping," *Proceedings of the 28th Structures,*

Structural Dynamics and Materials Conference, April 6-8, 1987, Monterey, California, AIAA Paper No. 87-0773, pp. 304-313.

[38] Nixon, M.W., "Analytical and Experimental Investigations of Extension-Twist-Coupled Structures," *M.Sc. Thesis*, George Washington University, May 1989.

[39] Nixon, Mark W., "Improvements to Tilt Rotor Performance Through Passive Blade Twist Control," *NASA TM 100583, USAAVSCOM TM 88-B-010*, April 1988.

[40] Nixon, M.W., "Preliminary Structural Design of Composite Main Rotor Blades for Minimum Weight," *NASA TP 2730, AVSCOM TM 87-B-6*, July 1987.

[41] Chandra, R., Stemple, A. D., and Chopra, I., "Thin-walled Composite Beams under Bending, Torsional, and Extensional Loads," *Journal of Aircraft*, Vol. 27, No. 7, July 1990, pp. 619-626.

[42] Smith, Edward C., and Chopra, Inderjit, "Formulation and Evaluation of an Analytical Model for Composite Box-Beams," Proceedings of the 31st Structures, Structural Dynamics and Materials Conference, long Beach, California, April 2-4, 1990, pp. 759-782.

[43] Rehfield, L.W., and Atilgan, A.R., "Shear Center and Elastic Axis and Their Usefulness for Composite Thin-Walled Beams," *Proceedings of the American Society For Composites,Fourth Technical Conference*, Blacksburg, Virginia, October 3-5, 1989.

[44] Atilgan, Ali Rana, "Towards A Unified Analysis Methodology For Composite Rotor Blades," *Ph. D. Dissertation*, School of Aerospace Engineering, Georgia Institute of Technology, August 1989.

[45] Rehfield, L. W., Atilgan, A. R., and Hodges, D. H., "Nonclassical Behavior of Thin-Walled Composite Beams with Closed Cross Sections." *Journal of the American Helicopter Society*, Vol. 35, (2), April 1990, pp. 42-50.

[46] Smith, Edward C., and Chopra, Inderjit, "Formulation and Evaluation of an Analytical Model for Composite Box-Beams," *Journal of the American Helicopter Society*, July 1991, pp.23-35.

[47] Hong, C. H., and Chopra, I., "Aeroelastic Stability of a Composite Blade," *Journal of the American Helicopter Society*, Vol. 30, No. 2, 1985, pp. 57-67.

[48] Stemple, A. D., and Lee, S. W., "A Finite Element Model for Composite Beams with Arbitrary Cross-Sectional Warping," *AIAA Journal*, Vol. 26, No. 12, 1988.

[49] Berdichevsky, V. L. "Variational-Asymptotic Method of Constructing the Nonlinear Shell Theory," *W. T. Koiter and G. K. Mikhailov, Eds., Theory of Shells*, North-Holland Publishing Company , 1980, pp. 137-161.

[50] Vinson, J. R., and Sierakowski, R. L., *The Behavior of Structures Composed of Composite Materials*, Martinus Nijhoff Publishers, 1987.

[51] Hodges, D. H., Atilgan A. R., Fulton M. V., and Rehfield L. W., "Dynamic Characteristics of Composite Beam Structures," *Proceedings of the AHS National Specialists' Meeting on Rotorcraft Dynamics*, Fort Worth, Texas, Nov. 13-14, 1989.

[52] Sokolnikoff, I. S., *Mathematical Theory of Elasticity*, McGraw-Hill, New York, 1956.

[53] Timoshenko, S., and Goodier, J. N., *Theory of Elasticity*, McGraw-Hill, New York, 1951.

[54] Washizu, K., *Variational Methods in Elasticity and Plasticity*, Pergamon, New York, 1968.

[55] Wempner, G., *Mechanics of Solids with Applications to Thin Bodies*, Sijthoff & Noordhoff International Publishers, 1981.

[56] Crandall, Stephen H., Dahl, Norman C., and Lardner, Thomas J., *An Introduction to the Mechanics of Solids*, McGraw-Hill Book Company, 1978.

[57] Gjelsvik, Atle, *The Theory of Thin Walled Bars*, John Wiley & Sons, 1981.

[58] Libai, A., and Simmonds, J. G., *The Nonlinear Theory of Elastic Shells : One Spatial Dimension*, Academic Press, Inc., 1988.

[59] Megson, T. H. G., *Aircraft Structures for Engineering Students*, Second Edition, Halsted Press, 1990.

[60] Koiter, W. T., "A Consistent First Approximation in the Theory of Thin Elastic Shells," *Proc. IUTAM Symp.*, Delft, 1959.

[61] Sanders, J. L., "An Improved First-Approximation Theory for Thin Shells," *NASATR-R24*, 1959.

[62] Koiter, W. T., "A Consistent First Approximation in the General Theory of Thin Elastic Shells," *Proc. IUTAM Symp on the Theory of Thin Shells*, Delft, August 1969, 12-33, North-Holland Publ. Amsterdam, 1960, Edited by W. T. Koiter.

[63] Berdichevsky, V. L., and Misiura, V., "Effect of Accuracy Loss in Classical Shell Theory," *Journal of Applied Mechanics*, to appear.

[64] Berdichevsky, V. L., and Starosel'skii, L. A., "On the Energy of Curvilinear Timoshenko-Type Rods," *Journal of Applied Mathematics and Mechanics*

(PMM), Vol. 47, No. 6, pp. 809-817, 1983.

[65] Hodges, Dewey H., Atilgan, Ali R., Cesnik, Carlos E. S., and Fulton, Mark V., "On a Simplified Strain Energy Function for Geometrically Nonlinear Behavior of Anisotropic Beams," Presented at the Seventeenth European Rotorcraft Forum, September 24-26, 1991, Berlin, Germany. To appear in *Composite Engineering*, 1992.

[66] Hodges, Dewey H., Private Communication, School of Aerospace Engineering, Georgia Institute of Technology, December 1991.

VITA

Ashraf M. Badir was born on [redacted]. He graduated in 1982 from Alexandria University with a Bachelor of Science Degree in Civil Engineering with Honor. He worked as a Research and Teaching Assistant for the Department of Structural Engineering, Alexandria University until he earned a Master of Science Degree in Civil Engineering from Alexandria University in 1985. He also worked as a part-time design engineer for two years starting 1983 in a civil engineering consulting office in Alexandria. He was appointed assistant lecturer of theory of structures in Alexandria University in September 1985. In 1986, he joined the Civil Engineering Department of University of Windsor, Ontario, Canada where he worked as a Graduate Research and Teaching Assistant. He joined the School of Aerospace Engineering at the Georgia Institute of Technology in Winter 1988 and earned a Master's of Science Degree in 1989.

APPENDIX B

PUBLICATIONS AND PRESENTATIONS

Refereed Papers:

1. Armanios, E.A. and Rehfield, L.W., "Sublaminate Analysis of Interlaminar Fracture in Composites: Part I - Analytical Model," *Journal of Composites Technology & Research*, Vol. 11, No. 4, Winter 1989, pp. 135-146.

2. Armanios, E.A. Rehfield, L.W., Raju, I.S., and O'Brien, T.K. "Sublaminate Analysis of Interlaminar Fracture in Composites: Part II--Applications," *Journal of Composites Technology & Research*, Vol. 11, No. 4, Winter 1989, pp. 147-153.

3. Armanios, E.A. and Badir, A.M., "Hygrothermal Influence on Mode I Edge Delamination in Composites," *Journal of Composite Structures*, Vol. 15, No. 4, 1990, pp. 323-342.

4. Armanios, E.A., and Parnas, L., "Delamination Analysis of Tapered Laminated Composites Under Tensile Loading," *Composite Materials: Fatigue and Fracture (Third Volume), ASTM STP 1110*, T. K. O'Brien, Ed., American Society for Testing and Materials, Philadelphia, 1991, pp. 340-358.

5. Armanios, E.A., Sriram, P., and Badir, A.M., "Fracture Analysis of Transverse Crack-Tip and Free Edge Delamination in Laminated Composites," *Composite Materials: Fatigue and Fracture (Third Volume), ASTM STP 1110*, T. K. O'Brien, Ed., American Society for Testing and Materials, Philadelphia, 1991, pp. 269-286.

6. Berdichevsky, V., Armanios, E. A. and Badir, A., "Theory of Anisotropic Thin-walled Closed-cross-section Beams," *Composites Engineering*, Vol. 2, Nos. 5-7, pp. 411-432, 1992.

Conference Proceedings:

1. Armanios, E.A. and Rehfield, L.W., "Interlaminar Analysis of Laminated Composites Using a Sublaminate Approach," *Proceedings of the AIAA/ASME/ASCE/AHS 27th Structures, Structural Dynamics, and Materials (SDM) Conference*, San Antonio, Texas, 19-21 May, 1986. AIAA Paper No. 86-0969CP, Part 1, pp. 442-452.

2. Armanios, E.A. and Mahler, M.A., "Residual Thermal and Moisture Influences on the Free-Edge Delamination of Laminated Composites," *Proceedings of the AIAA/ASME/ASCE/AHS 19th Structures, Structural Dynamics and Materials (SDM) Conference*, Part 1, pp. 371-381, 1988.

3. Armanios, E.A. and Rehfield, L.W., "A Simplified Approach to Strain Energy Release Computations for Interlaminar Fracture of Composites," *Proceedings of the Fourth Japan-U.S. Conference on Composite Materials*, June 27-29, 1988, Washington, D.C., Technomic Publishing Co., pp. 285-296.

4. Armanios, E.A., Badir, A. and Sriram, P., "Sublaminate Analysis of Mode I Edge Delamination in Laminated Composites," *Proceedings of the AIAA/ASME/AHS/ASC 30th Structures, Structural Dynamics and Materials (SDM) Conference*, Mobile, Alabama, April 3-5, 1989, pp. 2109-2116.

5. Sriram, P., and Armanios, E.A., "Fracture Analysis of Local Delaminations in Laminated Composites," *Proceedings of the AIAA/ASME/ASCE/AHS/ASC 30th (SDM) Conference*, Mobile, Alabama, April 3-5, 1989, pp. 2109-2116.

6. Armanios, E.A. and Badir, A.M., "Hygrothermal Influence on the Edge Delamination in Composites," *Proceedings of the American Society for Composites Fourth Technical Conference*, V.P.I. Blacksburg, VA, October 3-5, 1989, pp. 944-950.

7. Armanios, E.A., Badir, A. and Berdichevsky, V., "Effect of Damage on Elastically Tailored Composite Laminates",Proceedings of the AHS International Technical Specialists' Meeting on Rotorcraft Basic Research, Atlanta, Georgia, March 25-27, 1991, pp. (48-1)-(48-11).

8. Badir, A. M., "Theory of Anisotropic Thin-Walled Closed- Section Beams with Hygrothermal Effects," *Proceedings of the 33rd AIAA/ASME/ASCE/AHS Structures, Structural Dynamics, and Materials (SDM) Conference*, San Antonio, Texas, 19-21 May, 1986. AIAA Paper No. 86-0969CP, Part 1, pp. 442-452.

Presentations:

1. Rehfield, L.W. and Armanios, E.A., "Sublaminate Analysis of Interlaminar Fracture in Composites," 1985 Grant and Contract Review Vol. II, NASA Langley Research Center, Materials Division, Fatigue and Fracture Branch, February 13-14, 1985.

2. Armanios, E.A., "Analytical Modeling of Interlaminar Fracture Behavior in the Edge Delamination Specimen (Extension)," NASA/AVSCOM/Bell Helicopter Meeting, Georgia Institute of Technology, Atlanta, GA, July 15-16, 1985.

3. Armanios, E.A., "Analytical Modeling of Interlaminar Fracture Behavior in the Edge Delamination Specimen (Bending and Combined Bending and Extension)," NASA/AVSCOM/Bell Helicopter Meeting, Georgia Institute of Technology, Atlanta, GA, July 15-16, 1985.

4. Armanios, E.A. and Rehfield, L.W., "Interlaminar Analysis of Laminated Composites using a Sublaminate Approach," *AIAA/ASME/ASCE/AHS 27th Structures, Structural Dynamics, and Materials(SDM) Conference*, San Antonio, Texas, May 19-21, 1986.

5. Armanios, E.A. and Mahler, M.A., "Residual Thermal and Moisture Influences on the Free-Edge Delamination of Laminated Composites," *Proceeding of the AIAA/ASME/AHS/ASC 29th Structures, Structural Dynamics and Materials (SDM)* Conference, Williamsburg, VA, April 18-20, 1988.

6. Armanios, E.A. and Rehfield, L.W., "A Simplified Approach to Strain Energy Release Computations for Interlaminar Fracture of Composites," *Fourth Japan-U.S. Conference on Composite Materials*, June 27-29, 1988, Washington , D.C.

7. Armanios, E.A., Badir, A., and Sriram, P., "Sublaminate Analysis of Mode I Edge Delamination in Laminated Composites," *AIAA/ASME/ASCE/AHS/ASC 30th Structures, Structural Dynamics and Materials (SDM) Conference*, Mobile, Alabama, April 3-5, 1989.

8. Sriram, P. and Armanios, E.A., "Fracture Analysis of Local Delamination in Laminated Composites," *AIAA/ASME/ASCE/AHS/ASC 30th Structures, Structural Dynamics and Materials (SDM) Conference*, Mobile, Alabama, April 3-5, 1989.

9. Armanios, E.A. and Badir, A.M., "Hygrothermal Influence on the Edge Delamination in Composites," *the American Society for Composites, Fourth Technical Conference*, V.P.I., Blacksburg, VA, October 3-5, 1989.

10. Armanios, E.A., "Analysis of Delamination Related Fracture Processes in Composites," *Review of NASA Langley Composites Grants*, NASA Langley Research Center, Materials Division, May 16-17, 1989.

11. Armanios, E.A., Sriram, P. and Badir, A., "Fracture Analysis of Matrix Crack-Tip and Free Edge Delamination in Laminated Composites," *Third Symposium on Composite Materials: Fatigue and Fracture*, Lake Buena Vista, Florida, November 6-7, 1989.

12. Armanios, E.A. and Parnas, L., "Delamination Analysis of Tapered Laminated Composites under Tensile Loading," *Third Symposium on Composite Materials: Fatigue and Fracture*, Lake Buena Vista, Florida, November 6-7, 1989.

13. Armanios, E.A. and Sriram, P., "Modeling of Transverse Cracks in Laminated Composites," *Fifteenth Southeastern Conference on Theoretical and Applied Mechanics (SECTAM)*, Atlanta, Georgia, March 22-23, 1990.

14 Armanios, E.A., Badir, A. and Berdichevsky, V., "Effect of Damage on Elastically Tailored Composite Laminates", *AHS International Technical Specialists' Meeting on Rotorcraft Basic Research*, Atlanta, Georgia, March 25-27, 1991.

15 Armanios, E.A., Badir, A. and Berdichevsky, V., "An Assessment of Thin-Walled Closed Sections Composite Beam Theories", *AIAA Aerospace Symposium*, Atlanta, Georgia, February 28-29, 1992.

16. Badir, A. M., "Analysis of Composite Rotor Blades," AIAA Southeastern Regional Student Conference, Orlando, Florida, April 11-13, 1991.

17. Badir, A. M.and Armanios, E. A. "Theory of Anisotropic Thin-Walled Opened-Cross-Section Beams with Hygrothermal Effects," To be presented *34rd AIAA/ASME/ASCE/AHS Structures, Structural Dynamics, and Materials (SDM) Conference*, Lajolla, California, April 19-21, 1993

M.Sc. Special Problems:

1. Mahler, M., "A Study on the Thermal and Moisture Influences on the Free-edge Delamination of Laminated Composites," Special Problem Report Submitted in partial fulfillment of the requirements for the M.Sc. degree, School of Aerospace Engineering, Georgia Institute of Technology, September, 1987.

2. Badir, A. M., "Hygrothermal Influence on Mode I Edge Delamination in Composites," Special Problem Report Submitted in partial fulfillment of the requirements for the M.Sc. degree, School of Aerospace Engineering, Georgia Institute of Technology, June, 1989.

Ph. D. Theses:

1. Parnas, L., "Failure Mechanisms and Prediction in Advanced Composite Materials," Ph.D Thesis, School of Aerospace Engineering, Georgia Institute of Technology, March 1991.

2 Badir, A. M., "Analysis of Advanced Thin-Walled Composite Structures". Ph.D. Thesis, Georgia Institute of Technology, February 1992.